A NUMERICAL MODEL FOR CHAR COMBUSTION IN PACKED BED REACTORS

Judy Cooper

A thesis submitted to the School of Graduate Studies and Research

in partial fulfilment of the requirements for the

degree of

MASTER OF APPLIED SCIENCE

in the Department of Chemical Engineering

University of Ottawa

July 1996

ISBN 0-612-16432-2

Canada

UNIVERSITÉ D'OTTAWA
UNIVERSITY OF OTTAWA

ABSTRACT

A numerical simulation of the combustion of centimeter-sized char particles in an overfeed fuel bed is presented. One-dimensional mass, species and energy balances for the reacting system are solved by finite volume discretization methods to predict operating curves and temperature and concentration profiles for char combustion under a variety of conditions. The simulation is unique in that it employs separate gas and solid phase energy balances with finite-rate CO kinetics and a particle number balance to account for the shrinkage of the char particles as they descend through the bed. All the major energy transport processes, such as particle-to-fluid heat and mass transfer, conduction, convection and radiation, are modelled.

The simulation was run for beds of 1-3 cm particles ranging from 30-60 cm in height. The range of air flow rates studied ranged from 0.036 to 0.87 m/s. Comparisons between predicted gas and temperature profiles and similar profiles obtained from the literature generally showed good agreement, indicating that the simulation was reliable enough for use as a design tool over the range of conditions that were studied. The simulation proved to be quite sensitive to choices of the heat and mass transfer coefficients and also to the CO_2 reduction rate expression, indicating that there is a need for more research on large-particle kinetics and high-temperature packed bed energy transport processes.

ACKNOWLEDGEMENTS

I would like to thank Dr. W. Hallett for the opportunity to work on this project and for his guidance and assistance throughout.

I would also like to thank NSERC for funding this research.

Additional thanks are given to Dr. D.Taylor for his advice on the some of numerical problems I encountered and to my fellow students at the University of Ottawa who add humour to the day and make this a pleasant place to work.

TABLE OF CONTENTS

LIST OF FIGURES

LIST OF TABLES

NOMENCLATURE

a_p - specific surface area (m^{-1})

C_P - heat capacity (J / kg K)

$\overline{C_P}$ - mean specific heat (J/ m^3 K)

d_P - effective particle diameter (m)

D_{eff} - effective gas diffusivity (m^2 s^{-1})

G - carbon consumption rate per unit area of particle surface (kg m^{-2} s^{-1})

h - particle-to-fluid heat transfer coefficient (W m^{-2} K^{-1})

h_G - gas enthalpy (J kg^{-1})

h_S - solid enthalpy (J kg^{-1})

k_{Geff} - effective gas thermal conductivity (W m^{-1} K^{-1})

k_{Seff} - effective solid thermal conductivity (W m^{-1} K^{-1})

k_y - particle-to-fluid mass transfer coefficient (kg m^{-2} s^{-1})

N_P - number of particles per unit volume of bed

$\dot{N}$ - particle number flux per unit area of bed

R - universal gas constant (kJ $kmol^{-1}$ K^{-1})

R_3 - CO_2 reduction reaction

R_4 - Carbon oxidation reaction

R_5 - CO oxidation reaction

r_i - species production rate per unit volume of gas (kg m^3 s^{-1})

T_G - gas temperature (K)

T_S - solid temperature (K)

v_S - average solid velocity (m/s)

v_G - average superficial gas velocity (m/s)

t - time (s)

x - vertical coordinate for the bed (m)

Y_i - mass fraction of species I (kg kg^{-1})

ϵ - bed void fraction

ρ_G - gas density (kg m^{-1})

ρ_S - solid density (kg m^{-1})

ΔH_R - heat release due to carbon oxidation (J kg^{-1})

ΔH_{RCO} - heat release due to CO oxidation (J kg^{-1})

Subscripts and superscripts

i - species i

eff - effective

G - gas

P - particle

S - solid

R - surface

O_2 - oxygen

CO - carbon monoxide

CO_2 - carbon dioxide

^{0} - previous timestep value

* - previous iteration value

∞ - free stream concentration

1.0 INTRODUCTION

Despite its antiquity, solid fuel bed combustion is still widely used in the supply of energy to industrial processes. Fuel beds, also referred to as packed bed combustors, derive their name from the fact that the solid fuel is stationary and supported by a grate while it burns. Air is supplied to the combustor from below at speeds well below the fluidization velocity. A schematic diagram of a typical packed bed combustor is shown in Figure 1.

The oldest applications for packed bed combustion are in wood stoves and fireplaces, whereas newer uses include municipal garbage incineration and the burning of pulp mill wood wastes to produce steam for other parts of the mill process. Recently, packed bed combustors have also been used as district heating boilers in small communities where isolation and a ready supply of wood waste make this an economical option. As these and other applications become more important, reliable computer simulations of the packed bed combustion of carbonaceous substances are expected to be in high demand.

An important factor in creating computer simulations of packed bed combustion processes is taking into account the nature of the char combustion mechanism. In packed bed combustion, particles of a combustible, such as coal or wood waste, are devolatilized in the top layer of the bed through rapid thermal decomposition of their constituent hydrocarbons, leaving carbonaceous solids (char) that burn far more slowly to release varying amounts of CO_2 and CO. The production of these gases occurs first by reduction of CO_2 to CO by carbon in the reduction zone, which is located in the middle of the bed where oxygen is scarce (see Figure 1), and then by oxidation of carbon to CO and CO_2 near the grate where oxygen

is readily available. CO_2 is also produced by a simultaneous reaction in the gas phase, where the CO produced in the oxidation zone reacts with O_2. The reaction of the solid fuel with its oxidants, CO_2 and O_2, (char combustion) is the rate-determining step in solid fuel combustion, taking approximately ten times as long as devolatilization and volatiles combustion, and therefore more directly affects fuel efficiency.

The difficulty in simulating char combustion processes lies in the need to represent complex interactions between mass transfer, heat transfer and reaction kinetics. At temperatures relevant to most combustion, the effect of reaction kinetics on both process efficiency and the concentrations of evolved gases is significant, requiring the model to predict the behaviour of several interdependent chemical reactions that may occur at the particle surface and in the bed interstices. Heat and mass transfer coefficients also become more difficult to predict because of uncertainties about their interaction with the flow field around the particles in the bed. Much of what is currently known about char combustion kinetics is drawn from studies of pulverized coal combustion, which involves the burning of fine particles ($d < 0.1mm$) in suspension rather than large, stationary particles. Unfortunately, the validity of extending these results to larger particles is unknown and requires investigation. The simulation developed for the purposes of this analysis employs rate equations from pulverized coal studies in an attempt to test their validity for large particle packed bed combustion and further the development of an accurate predictor of the progress of char combustion in packed bed reactors.

There are several types of packed bed reactors, which can be distinguished by the way in which the air and solid fuel are combined. Air is almost always supplied from below the

bed, but the solid fuel can be introduced into the reactor in a variety of ways. Fuel can be fed from above (overfeed combustion), from the side by gravity (inclined grates) or moving chain grates (side feed), or cocurrently with the air stream from below (underfeed combustion). Overfeed and side feed combustors have similar combustion zones (shown in Figure 1) and are therefore analogous in their functioning. They are also the most commonly used. Because of this, this study focuses on an analysis of overfeed char combustion because it represents the most basic form of combustion.

1.1 Objectives

The purpose of this work is to develop a one-dimensional computer simulation of overfeed char combustion that will predict the temperature and concentration profiles in beds of centimetre-sized particles with reasonable accuracy. Further objectives include using discretization techniques to produce a more detailed computer simulation than has been achieved in the past, verifying the results through comparison to published experimental data, and exploring the sensitivity of the model to various process parameters, such as transport and reaction rate coefficients.

In earlier work, the gas and solid phases in packed beds were usually treated as a single, composite phase, and the CO kinetics represented through an equilibrium relationship. These simplifications avoided the difficulty of representing complex heat and mass transfer phenomena and circumvented the numerical instability caused by the coupling of finite-rate CO kinetics and the gas phase energy balance. The model in this work solves separate,

transient gas and solid phase energy balances with finite rate CO kinetics in order to allow conclusions about the true magnitude of the temperature difference between the gas and solid phases. The model includes varying physical properties and all the transport phenomena believed to occur in packed beds, so that the relative importance of the aforementioned process parameters can be examined. The results of the model tests are used to set recommendations for future research on packed bed combustors.

In the following pages, a review of the literature on various aspects of packed bed combustion is given to summarize the ground covered by previous researchers. The nature of the physical processes relevant to packed bed combustion is discussed, along with the difficulties incurred in predicting them. This is followed by a section describing the equations representing the combustion process and the numerical method used to solve them. The unique numerical difficulties of this system and their management are discussed in detail here, as these subjects are of interest to many modellers. Finally, the results obtained from the model are presented and analysed as mentioned above, with a view to directing future research.

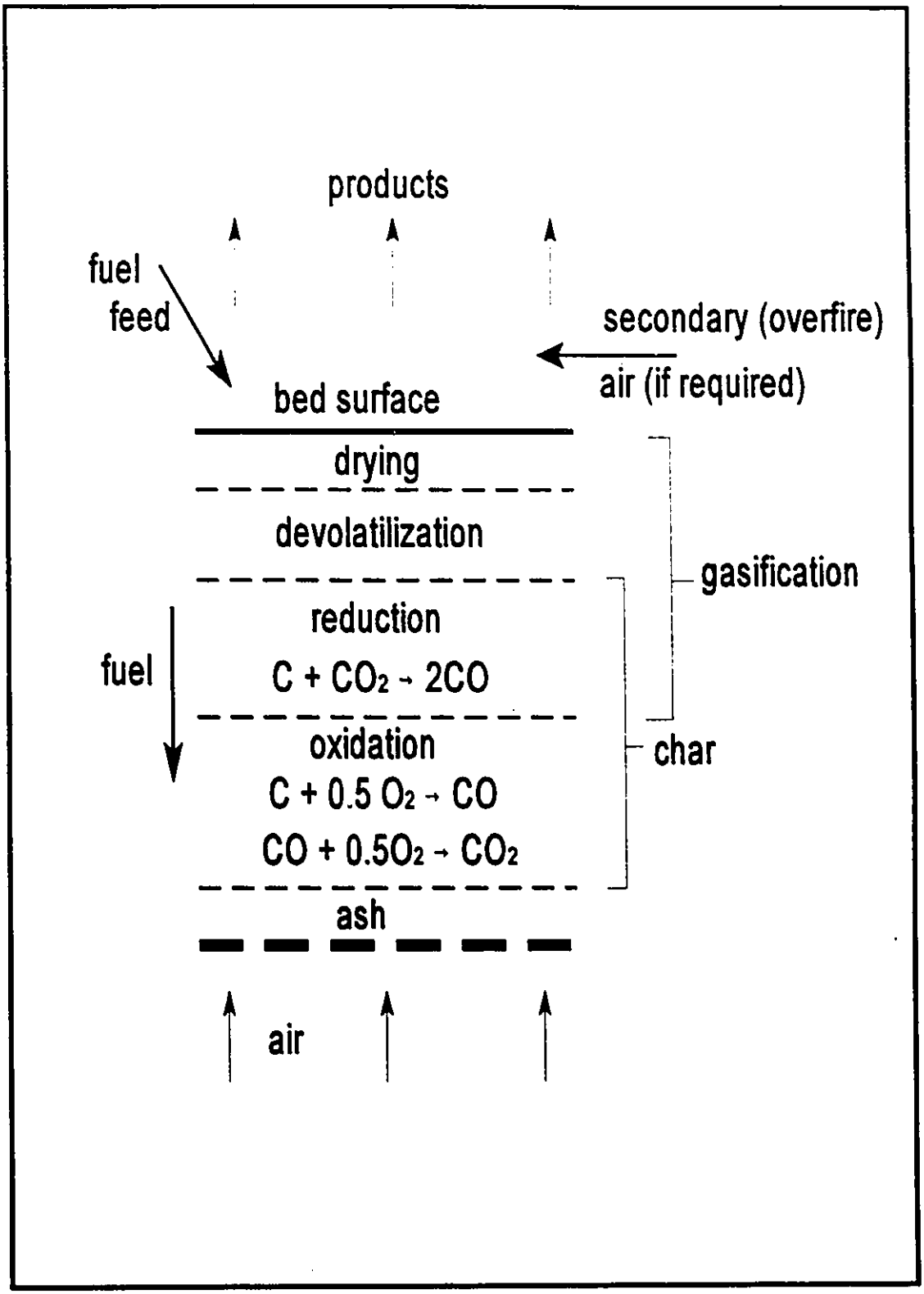

Figure 1: Schematic diagram of a packed bed combustor and its reaction zones

2.0 LITERATURE SURVEY

2.1 Background

A thorough simulation of any reactive packed bed process should include fluid-to-particle heat transfer, effective gas and solid conduction, species diffusion expressed as an effective gas diffusivity, and homogeneous and heterogeneous reaction kinetics. Properties should be modelled as realistically as possible and reflect sensitivities to operating conditions such as pressure, temperature and gas flow rate. For correct representation of energy transport through the bed, it is also essential that the simulation be *heterogeneous*, that is, contain separate gas and solid phase energy balances. *Homogeneous* simulations (those representing the two phases in a single energy balance) are inadequate for reactive flow because such simulations assume equal gas and solid temperatures. The latter assumption fails to hold for reactive flow because the phase temperatures are dictated by different chemical reactions and can thus be expected to differ substantially.

Unfortunately, creating perfect packed bed combustion simulations is often not as simple as it may appear. Packed-bed transport correlations are subject to varying magnitudes of error, depending on the design of the experiment used to obtain them. This means that the more desirable heterogeneous simulations, although more accurate in their treatment of the two phases, are nonetheless subject to error through the representation of particle-to-fluid transfer coefficients. This is because the characteristic behaviour of (packed-bed) reacting systems is very sensitive to values of these coefficients. Coefficients affecting the thermal behaviour of a system affect temperature profiles, and therefore also reaction rates and the

resulting concentration profiles. This is particularly true in the thin oxidation layer, where temperature and concentration gradients are large. Accurate reaction kinetics are important for similar reasons, particularly in the case of highly exothermic gas-phase reactions, where species and energy balances are strongly coupled.

Perhaps the largest impediment to simulating most reactive flow processes is the above-mentioned interdependence of the gas phase species and energy balances. In char combustion, the gas phase energy and species balances are coupled by the highly exothermic homogeneous (gas phase) CO oxidation reaction, and must be solved simultaneously. This creates an inherently unstable system of equations which usually requires the assumption of species equilibrium in the gas phase or the extensive employment of relaxation techniques to ensure convergence.

A review of the literature on coal conversion simulations is presented below, with emphasis on identifying the more successful simulations, followed by a summary of research on the various packed bed process correlations.

2.2 Review of existing coal conversion simulations

The coal conversion simulations in the literature fall into two broad categories, that of gasification and that of combustion. The numerical development in each category is generally the same; the distinction lies mainly in the thickness of the coal or char bed and the purpose of the process being simulated. In coal or char gasification, the bed can be up to several metres thick and the focus is on the product gas (mostly CO) emerging from the

gasifier; heat production is secondary. In coal or char combustion, the bed is much thinner and heat is the product, usually for the generation of steam. The primary effluent gas of combustors is CO_2, which serves no industrial purpose, but is simply released to the atmosphere with other combustion products. The study of combustion gases is thus usually confined to predicting the concentrations of various pollutants.

In the validation of either type of simulation, however, a full comparison of experimental and predicted temperature and concentration profiles should be conducted. Gasifier simulations are often tested by comparing predicted effluent compositions to experimental gasifier effluent data. This is sufficient to ensure reasonably accurate predictions of the product gases, but insufficiently rigorous to validate the simulation for details of the overall process, because the exit compositions of a gasifier are usually well defined by the equilibrium relations employed (Bhattacharya *et al.*, 1986). The latter is due to the thickness of gasifier beds and makes it possible to simulate gasifier effluents with very little information about the gas phase kinetics or the chemistry of the oxidation zone. In the much shallower beds of combustion simulations, the heat release of the CO oxidation reaction becomes very important to the accuracy of predicted concentration and temperature profiles. Gas phase kinetics are therefore very important in simulating a combustion process, and must be verified by profile comparisons along the entire bed.

Because most of the more recent simulations are for predicting the effluent compositions of char gasifiers rather than char combustors, a summary of some of the more recent gasification models is also included in the literature review. The corresponding combustion literature is scarce, somewhat out of date and seems to have been overlooked in

most surveys. Smoot (1984) and Hobbs *et al.* (1992) have done extensive reviews of packed bed coal conversion simulations and have identified thirty seven. None of the older combustion simulations were included in these reviews. Six of the simulations reviewed were simple unit type models (0-dimensional), 27 accounted for vertical variations in bed properties (1-dimensional) and 4 accounted for both vertical and radial property variations (2-dimensional). Only twenty-two were heterogeneous. All but two were of gasifiers, and most were tested only for their ability to reproduce effluent gas temperatures and compositions. Only 4 of the heterogeneous simulations included bed temperature and composition profiles. Since then, only one other relevant study has been found.

2.2.1 Char combustion simulations

Most of the combustion simulations found in the literature are relatively old, dating back to 1940-1950, and lack the sophistication of newer studies because of the absence (then) of detailed information on reaction kinetics and heat transfer and the limited availability of computers. All these early models contain the assumption that reaction rates and other physical properties in the bed are independent of temperature. This effectively uncouples the species and energy balances for the system and allows for analytical solution.

Mayers (1937) formulated a simplified one-dimensional model for combustion beds, using the assumptions of constant heat transfer, thermal conductivity and reaction rates. Reaction was assumed to occur only in the solid phase, with the surface carbon oxidation reaction proceeding directly to CO_2. The model for mass transfer was implicit, and assumed to be contained in the reaction rates. Thring (1952) and Silver (1953) developed combustion

models based on mass transfer, including both solid and gas phase reactions. The species concentrations were still treated as being independent of temperature, however, and in Silver's (1953) work, the thermal analysis of the bed was carried out on the basis of constant reaction heat releases and average heat transfer coefficients representing lumped conduction and diffusion processes.

The combustion study of Eapen *et al.* (1977) compared the results of a transient, 0-dimensional simulation with experimental data for changes in combustion rates with temperature and gas composition changes with time. The simulation proposed by the authors includes only the effects of the combustion reactions and predicts "local" concentrations of the principal combustion reactants, O_2, CO_2 and CO, based on their production or consumption by reaction. Models for carbon oxidation, CO_2 reduction and CO oxidation were included, but the latter model was simplified because of the fractional order dependency on oxygen. Transient gas composition profiles for O_2, CO and CO_2 were obtained from an experimental combustion "pot", but no attempt was made to simulate them.

A later study by Barriga and Essenhigh (1981) proposed a one-dimensional, steady-state simulation for the combustion pot described above. In this work, CO oxidation kinetics were lumped with carbon oxidation by assuming that only CO_2 was produced in the latter reaction. The particles of coke or coal simulated were assumed to be spherical and burn via surface reaction at constant solid density. Gas and solid temperatures as well as gas composition profiles were obtained and compared to those obtained from the combustion pot. Results of this comparison showed that the simulation tended to underpredict the reduction of CO_2 because of low predicted temperatures in the solid. This discrepancy was attributed

in part to the simplification of the CO oxidation kinetics.

The work of Arai and Hasatani (1987) was the most recent char combustion model found, and the only one absent from the review by Hobbs (1992). It was one-dimensional, transient, and featured 36 heterogeneous and homogeneous reactions, finite rate CO kinetics and balances for 16 chemical species. Its purpose was to predict the time traces of the concentrations of volatile nitrogen compounds over a bed of coal char burning in an NH_3-O_2-Ar atmosphere. The energy balances for the gas and solid phases were very similar to those in this study. Packed-bed particle-to-fluid heat transfer, mass transfer and effective thermal conductivity correlations were included and applied to particles with an average diameter of 2.6 mm for air flow rates of .03-.05 m/s. The model assumed spherical particles, plug flow, and a shrinking particle with no ash layer. The product for the primary surface reaction of C with O_2 was assumed to be CO at all reaction temperatures. Model discrepancies were attributed to flaws in the chosen char-N and char-NO reaction mechanism.

2.2.2 Char gasification simulations

Gasification has been studied far more often than combustion, despite the many industrial applications for the latter. Unfortunately, the results of char gasification and char combustion studies are rarely comparable because of the assumptions made for the oxidation zone in the former. Early gasifier simulations contain many simplifications which fail to hold for combustion and are often not valid for gasifiers either. Examples of these are: equal gas and solid temperatures, constant fluid-particle heat transfer coefficients or heat transfer coefficients adapted from single particle theory, gas phase equilibrium, negligible axial heat

conduction, negligible radiation effects and a constant CO/CO_2 product ratio for carbon oxidation. For reactors in which the fuel level is maintained by a feed of char or coal from above, there is a slow downward flux of fuel toward the grate which is neglected in almost all of the literature on char converters.

In the oxidation zone of a gasifier bed, there are significant temperature differences between the gas and the solid, and temperatures are higher than in the rest of the bed; homogeneous simulations which neglect radiation and heat conduction could therefore give a highly inaccurate description of the thermal behaviour in this zone. Heat transfer rates vary with Reynolds number, which in turn depends on factors such as particle diameter, gas density and mass velocity. Assumptions of constant heat transfer coefficients can therefore also be expected to lead to significant error, as can the adaptation of single particle heat and mass transfer theory (Bhattacharya *et al.*, 1986). The effect of the gas phase species equilibrium assumption on gasifier predictions has never been properly tested, as mentioned previously; yet it was employed in all the simulations that were found. For gasifiers, this assumption is probably reasonable since the thick fuel beds employed in gasification allow ample time for the gas phase to reach equilibrium. This is not true of the thinner beds of combustors, however; here, the use of finite rate gas phase kinetics is essential to accurate modelling.

Amundson and Arri (1978) developed a two-dimensional simulation for Lurgi gasifiers in which the gas and solid phases were considered separately. This resulted in a numerically complex system that required assumptions of water gas shift equilibrium and infinitely fast gas-phase kinetics to ensure stability. These assumptions were justified by the relative thicknesses of the reduction and oxidation zones (.95 and .05 m respectively). Radiation was

neglected in the model, and the heat/mass transfer analogy was adapted from that for single particles. Diffusion of gas into the solid was neglected despite the postulated formation of an ash layer on the particle during conversion. The effects of solid feed mass flow rate on the solid temperature profiles and the effect of changing the gas to solid feed ratio on the effluent gas species were studied. Temperature profiles were also obtained for varying feed gas temperatures, and coal reactivities were also varied, with a view to predicting the effects of these conditions in industrial gasifiers. No attempts were made to validate the predictions given by the simulation, confining the analysis to a purely theoretical one.

The simulation developed by Yoon *et al.* (1978) was also for Lurgi gasifiers, but was one-dimensional. Their assumptions included spherical particles, equal gas and solid temperatures, negligible axial conduction, constant wall heat transfer and negligible radial gradients. The CO oxidation reaction was neglected because of the short residence time of the gas in the combustion zone, and the water-gas shift reaction was assumed to be in equilibrium. Predicted effluent compositions for CO, CO_2, O_2, H_2 and CH_4 were computed and compared to plant data from several gasifiers. The agreement between predicted and experimental data was reasonable, in that the relative proportions of the effluent gases were well predicted. Other plant data was used to verify predictions of the magnitude and location of the maximum temperature in the gasifier, but this comparison was qualitative and examined only the shape of the temperature profiles. A quantitative comparison of the temperature profiles would have been a better measure of the validity of the energy balances used to simulate the system; thus the simulation was not completely validated.

Yu *et al.* (1983) used a two-dimensional gasifier simulation to examine radial effects

in Lurgi gasifiers operating under reduced loads (turndown). Their concern was primarily to provide information on the effect of wall cooling on the radial and axial temperature profiles, and on the performance of the reactor in terms of carbon conversion. The assumptions used in the model were basically the same as those employed in the simulation by Yoon *et al.* (1978) described above, which was a special case of the two-dimensional analysis applied to an adiabatic reactor. The predictions given by the two-dimensional simulation were compared to one-dimensional predictions to measure the deviations from adiabatic operation caused by wall cooling. The wall heat transfer coefficient was found to have a significant effect at turndown.

Goldman *et al.* (1984) produced the first validated char gasification simulation, in that a full comparison of temperature and gas concentration profiles was conducted. The work included separate gas and solid energy balances and finite kinetics for the carbon oxidation, CO_2 reduction and the water gas shift reaction. Although the authors describe the simulated process in terms of char combustion, the omission of CO kinetics limits the analysis to one of gasification processes. A bench-scale "combustion pot" was used to validate the predictions. In general, the predicted profiles were better when the char was gasified in the presence of significant amounts of water vapour (30% by volume); predictions for char gasified in air overestimated the temperatures everywhere in the gasifier and thus overestimated CO_2 reduction in the gasification zone. The predictions given by the simulation for gas and solid temperatures showed an average temperature difference of about 700 K between the two phases in the first 5 cm of the gasifier bed (oxidation zone), emphasizing the importance of separate phase energy balances for this zone. This difference was larger for

char gasified in the absence of water vapour.

Bhattacharya *et al.* (1986) developed a two-dimensional homogeneous simulation that predicted gasifier temperature profiles and histories. As with many gasifier simulations, the temperature difference between gas and solid in the oxidation zone of the reactor was deemed to be unimportant, and gas phase CO oxidation kinetics were neglected. The system was therefore modelled by a single energy balance, which avoided the uncertainty involved in predicting particle to gas heat transfer, but probably created larger errors in the representation of energy transport through the bed. Radial energy dispersion was included in the energy balances to account for any radial variations in temperature. The solid phase mass balance incorporated a transient term to permit prediction of temperature variations in the initial stages of gasification. Predictions of axial temperature profiles compared well with measurements obtained from a bench-scale gasifier. Comparison of predicted temperature histories showed a larger discrepancy, however, which increased with time. This effect was attributed to cumulative error resulting from poor modelling of reaction kinetics, specifically the assumption of a constant particle diameter, which was not in keeping with collapse of the bed observed during the experiment, and uncertainty in the mass transfer coefficient in the gas film surrounding the char particles.

The most recent char gasification simulation found in the literature was that of Hobbs *et al.* (1992). Although this work provided a good review on some of the literature on process parameters, the simulation presented here contained some unexpected simplifications. A two-zone, partial equilibrium model for the gasifier was developed which divided the reactor into an oxidation/gasification zone and a drying/devolatilization zone. This model

assumed that the oxidation/gasification zone was at an equilibrium temperature determined by the gas phase species equilibrium assumption, and that the temperature in the drying/devolatilization zone was equal to the gas exit temperature. Devolatilization was accounted for by a detailed mechanism, yet the more important gas phase kinetics were given only cursory treatment through the aforementioned water gas equilibrium assumption. Thirteen test gasifier cases were used to validate model exit gas compositions. The results showed consistent overprediction of the gas exit temperatures and underprediction of effluent CO concentrations. These discrepancies were attributed in part to the fact that the temperature assigned to the devolatilization zone was higher than the true exit temperature and led to a different coal volatiles distribution being predicted by the devolatilization model.

2.2.3 Conclusions

The preceding reviews of combustor and gasifier studies indicate that, although many numerical models have been produced, most concentrate on gasification and few include all the reaction kinetics and transport phenomena in packed beds. Finite rate CO kinetics, variation of physical properties, and separate gas and solid energy balances were omitted from most of the models. This was true of all the models that were reviewed, with the exception of that of Arai and Hasatani (1987). The latter, however, focused on pollutanant formation rather than the details of the combustion process. It can thus be concluded that few detailed models of char combustion have been developed and that a more detailed study of this process is required to test conclusions formed in simpler models.

2.3 Packed bed process correlations

2.3.1 Fluid-to-particle heat and mass transfer

The temperatures reached in all the packed bed heat and mass transfer experiments found in the literature (300 K) were far lower than those typically reached in combustion (700-2000 K) and none of the experiments were conducted in the presence of chemical reaction, so the applicability of the resulting transport coefficients to packed bed combustion may be limited. However, since no packed bed studies of heat and mass transfer at combustion conditions were found, these were assumed to be adequate for preliminary study.

Heat and mass transfer are often studied together because they are analogous processes. Both processes can be described by a transfer coefficient and a gradient, or driving force. For fluid-to-particle heat transfer, this driving force is the temperature gradient between the fluid and the particles in the packed bed reactor; in mass transfer, the driving force is the concentration gradient between the gas film at the particle surfaces and the gas in the interstices of the bed. The transfer coefficients are denoted by h and k_y respectively, and usually correlated in dimensionless form as Chilton and Colburn factors, j_H and j_D (see 3.3.3., Table I). Barker (1965) and Balakrishnan and Pei (1979) have done extensive reviews of the literature and summarized key studies in this area. The most relevant of these are discussed in more detail below.

Under ideal conditions, a direct analogy exists between heat and mass transfer such that $j_H=j_D$. Sen Gupta and Thodos (1963) quoted several experimental criteria that must be met for this analogy to hold, the most important of which were: no emission or absorption of

radiant energy, low rates of mass transfer and uniform bed temperature. Under conditions where these criteria were not met, the measurement of convective heat transfer would be confounded with other effects, such as the effect of the flow field produced by mass transfer from the particles on heat convection from the particle surface, the conduction of heat between particles of different temperatures, and radiative heat transfer.

Unfortunately, such ideal conditions are difficult to attain. Most of the experimental studies yielding correlations for both heat and mass transfer were conducted by drying water-saturated celite spheres with dry air and taking steady-state temperature measurements by means of thermocouples embedded in randomly situated particles. Uniform bed temperatures are difficult to obtain in such a setup, so the results most likely included the effects of conductive heat transfer, giving heat transfer coefficients that were too large.

Galloway *et al.* (1957) and McConnachie and Thodos (1963) studied the effect of different packing arrangements of celite spheres on the values of the heat and mass transfer coefficient. Both studies assumed the particle temperature to be uniform, so that the surface temperature of a given particle equalled that of its core, and that the bed temperature was uniform, an assumption which can easily be disputed by considering the effects of evaporative cooling. The steady-state assumption is also dubious, as drying is a transient process: a quasi-steady state would hold as long as the surface was wet, but, once the particle surfaces had dried, an additional diffusion resistance due to the pores of the particles would have to be considered. Wall effects were considered to be negligible for the temperatures under study. The ratios of j_H/j_D for these studies ranged from 1.058-1.128, indicating that the convective heat transfer coefficient may have been overestimated by confounding with conductive effects.

De Acetis and Thodos (1960) conducted similar experiments on fixed and extended beds of porous catalyst carrier. Here the surface temperature was assumed to differ from the wet-bulb temperature of the entering air, an assumption which had been omitted from previous studies. However, the j_H/j_D ratios were 1.51, indicating an even larger deviation from the direct analogy.

Some authors used pooled data from several similar studies to obtain their correlations. Sen Gupta and Thodos (1962) used the data of 8 studies to correlate j_H and j_D for Re > 20. Their correlations fitted the data to within 17% (at most) and gave a j_H/j_D ratio of 1.076. Yoshida *et al.* (1962), obtained a slightly different correlation from the data of three studies that exhibited a transition in the behaviour of j_D at packed bed Reynolds numbers of 50. (The authors attached no significance to this Reynolds number.) These correlations sometimes predicted lower j_D and j_H than those of individual studies, especially at Reynolds numbers greater than 100, indicating that pooled correlations may improve results because of the reduction in scatter produced by the increased number of data points (see Figure 3).

In other studies, attempts were made to eliminate the radiative and/or conductive modes of heat transfer. Sen Gupta and Thodos (1963) tried to minimize these effects by water-jacketing the walls of their apparatus so that its temperature could be kept equal to the average surface temperature of the spheres. Thermocouples were located at the surfaces of the spheres to allow direct measurement of surface temperatures. The experiment yielded a single correlation for ϵj_H. Chu *et al.* (1953) correlated expressions for the mass transfer coefficient arising from studies of naphthalene particles sublimating into air. This type of

study is generally more reliable, as sublimation generally occurs slowly and without the diffusive resistance present in evaporation studies. This makes the steady-state assumption more valid, therefore reducing measurement error due to transients.

The most recent study found was that of Bhattacharyya and Pei (1975), who used microwave heating in their experimental apparatus to allow them to obtain more accurate measurements of the heat flux to the bed. In their experiment, FeO_3 particles subjected to continuous microwave radiation were contacted with dry air. Steady-state inlet and outlet air temperatures were measured and the fluid-to-particle heat transfer coefficient calculated from a heat balance on the bed, resulting in a correlation for j_H that the authors believed could be used for j_D by direct analogy. The relationship developed in this study differed from previous relationships, in that j_H was correlated with the drag coefficient instead of the Reynolds number. This is an odd result, for which no details were given by the authors.

The heat and mass transfer studies outlined above were all conducted in packed beds where a certain amount of heat conduction was occurring. As this conduction heat transfer tends to become confounded with convective heat transfer and artificially inflate the convective heat transfer coefficient (as evidenced by the j_H/j_D ratios obtained), the heat transfer correlations developed by experimenters who attemped to reduce conductive effects (Chu et al. (1953), Bhattacharyya et al. (1975)and Yoshida et al. (1962)) are likely the most representative of the true heat transfer.

2.3.2 Effective thermal conductivities

In packed beds, or in any instance in which a solid and a fluid phase are involved in

the heat transfer process, defining thermal conductivities for the two phases becomes more complicated, requiring the use of "effective" values. Solid effective conductivities are influenced by the mechanisms of radiation between neighbouring particles, solid conduction, contact resistance, heat conduction through the stagnant layer of fluid surrounding each particle and radiant heat transfer between non-adjacent particles. Gas phase effective conductivities are a function of gas conductivity and turbulent mixing. The development of separate effective gas and solid conductivities is most critical in cases of vastly differing fluid and solid temperatures, in which fluid-to-particle heat transfer is significant. Expressions for the "effective" conductivity of each phase must then be developed by attributing the aforementioned mechanisms to the correct phase.

Because of the difficulty in isolating the various mechanisms for each phase, older packed bed effective conductivity studies lump the effects of the two phases in a single coefficient which is then defined as the overall effective thermal conductivity for the bed. Here, the two phases are considered to have parallel contributions to the overall effective thermal conductivity of the bed, and the bed is treated as a single phase with respect to conduction. This overall conduction process occurs separately from the aforementioned fluid-solid convective heat transfer process and requires the design of experiments that does not confound them.

(A) Solid Phase

Most of the early studies of effective conductivity concern themselves with radial heat conduction in beds with temperatures that are low enough so as not to require separate consideration of the phases. Gas-particle temperature gradients are generally small, and the radiative mechanisms insignificant, at these temperatures. In almost all of the cases, the experimental overall effective thermal conductivities, k_e, are deduced from radial temperature profiles in the bed under study. Stallings and Smith (1952) produced a correlation that combined five separate conduction mechanisms. Gas and solid phase molecular conduction, particle-to-particle radiation and turbulent diffusion were believed to occur in parallel with a solid convection-conduction mechanism. A breakdown of radial heat conduction in terms of the theoretical mechanisms was attempted. The same mechanisms were described by Argo and Smith (1953) in their correlation, which was tested for a wide range of experimental data and found to be reasonably accurate.

Yagi and Kunii (1957) and Kunii and Smith (1960) derived similar expressions for overall radial heat conduction in packed beds with stagnant gases, but described the mechanisms somewhat differently: heat conduction through the gas phase was deemed to occur via radiation between voids and by conduction, and solid conduction was thought to proceed by heat transfer through the particle contact points, conduction through the stagnant gas film about the particles, radiation, and conduction in the solid. Their correlation for overall effective radial conductivity, $k_{e,r}$ was tested on iron, cement clinker, glass and firebrick spheres in air for particle sizes of 0.01-11.0 mm, and found to give satisfactory results over a 300-1300 K temperature range. Further tests of this correlation with similar positive results

were done by Ofuchi and Kunii (1965) in their development of an expression for effective thermal conductivities at the walls of packed bed reactors.

Yagi *et al.* (1960) later studied non-stagnant effective axial thermal conductivities, $k_{e,a}$, and postulated a linear increase in overall bed conductivity with increasing particle Reynolds number. The stagnant $k_{e,a}$ obtained by extrapolation from values of $k_{e,a}$ to Re=0 were well predicted by the expressions for the stagnant radial effective conductivity ($k_{e,r}$) obtained previously by Yagi and Kunii (1957), indicating that the stagnant radial expression was also valid for stagnant axial heat conduction. This was later supported by Bischoff (1962) in his assumption of equal axial and radial overall thermal conductivities, which was used to develop an expression for effective overall axial thermal conductivity at high gas flow rates.

The need to separate gas and solid effective radial thermal conductivities by attributing a portion of the overall thermal conductivity to each phase was raised by De Wasch and Froment (1971). In their work, an adapted version of Yagi and Kunii's (1957) stagnant overall correlation was considered adequate for effective thermal conduction in the solid; gas conduction and void-to-void radiation were considered by the authors to be gas phase mechanisms and thus removed from Yagi and Kunii's (1957) original correlation to isolate the solid mechanisms. (This inclusion of radiation in gas phase mechanisms by DeWasch and Froment (1971) was however incorrect, as void-void radiation actually represents radiant exchanges between non-neighbouring *solids*) The effective gas diffusivity was also thought to play a role in heat conduction through the gas phase because of the effect of gas flow on mixing.

Dixon and Cresswell (1978), later repeated the above analysis in their consideration of a packed tubular heat exchanger. In this study, the defining differential equations for the reactor were presented, illustrating the proper use of effective thermal conductivities. Here, convection was a separate term in the energy balances, validating the use of stagnant (solid) effective thermal conductivities, such as those developed by Yagi and Kunii (1957) and Kunii and Smith (1960), to describe conduction in the solid. Some authors, such as Bhattacharyya and Pei (1975), believe that packed bed solid effective thermal conductivities are affected by gas convection, but the effect found by these authors appeared to be quite weak and can therefore be omitted.

(B) Gas Phase

A search of the literature revealed few applicable studies of gas axial effective thermal conductivity. Such studies are normally done by studying the dispersion of heat in a packed bed (by analyzing the progress of a temperature front through the bed in time). This, however, describes overall bed dispersion rather than isolating gas phase dispersion, because heat dispersion occurs via both phases, and is thus impractical for packed bed analyses in which the phases are considered separately.

An exception is the study of Edwards and Richardson (1968), in which a correlation for gas dispersion in packed beds was developed by examining the dispersion of a tracer gas through the interstices of a packed bed. Gas phase dispersion processes were thereby isolated because only gas particle motion was recorded. Analogy to heat transfer revealed a parallel dependency of effective gas phase conduction on gas conductivity and flow velocity. Such

a formulation is physically reasonable, as both gas conductivity and turbulent mixing would affect heat "conduction" through the gas phase. This correlation also agrees well with predictions obtained in a later theoretical study by Gunn (1986), who developed complex statistical models for axial and radial heat dispersion and used a variety of experimental and theoretical results from the literature to validate his results. Gunn's (1986) heat dispersion model was able to isolate heat dispersion due to the gas phase because it was based on gas (molecular) motion rather than experimental (overall) bed temperatures. The correlation of Edwards and Richardson (1968) compared well with Gunn's (1986) predictions for axial gas dispersion, showing that it is an adequate predictor of gas phase effective thermal conductivity despite its age.

A survey of effective thermal conductivities indicates that heat is "conducted" through each of the two phases in a packed bed via a variety of mechanisms which must be attributed to the correct phase to obtain the best energy balances. The works of DeWasch and Froment (1971) and Dixon and Cresswell (1978) both support the use of stagnant effective thermal conductivities in the species energy balances. The use of the effective stagnant thermal conductivity of Yagi and Kunii (1957) for the solid phase and that of Edwards and Richardson (1968) for the gas phase should therefore provide a reasonable representation of the conductive mechanisms at work in combustion beds.

2.4 Reaction kinetics

2.4.1 Heterogeneous kinetics

The term "heterogeneous" describes reactions occurring on the exposed surfaces of the particles in a packed bed. In char combustion, the reactions of primary concern are carbon consumption by oxidation with O_2 and by CO_2 reduction at the particle surface. The reduction of carbon dioxide is generally thought to occur once the local oxygen has been consumed, but these reactions can also occur simultaneously if the temperature at the particle-gas interface is sufficiently high. Char combustion proceeds by a series of steps, the first of which is gas diffusion to the particle surface. This is then followed by chemical reaction at the surface to generate heat and product gases, and the back-diffusion of those product gases. The rate at which the overall process occurs is therefore dictated by reaction kinetics and gas mass diffusion rates. If chemical reaction is much slower than diffusion, the rate is said to be *kinetically controlled*; if diffusion is slower than chemical reaction, the rate is said to be *diffusion controlled*. Diffusion control usually prevails at high temperatures, since the effect of temperature on the rate of reaction is much greater than its effect on the rate of diffusion.

2.4.2 Particle consumption model

Several different assumptions can be made about the behaviour of the char particles during reaction, and the chosen one must be built into the kinetic model for the surface reactions: the particle diameter can be assumed to stay constant as the density varies (internal burning), the outer diameter can be assumed to stay constant as the reaction front moves into

the particle, leaving an ash layer (shrinking core model), or the diameter can be assumed to vary at constant solid density as the carbon is consumed and removed to leave an ash particle (ash segregation or shrinking particle model). The former two are very difficult to model with any accuracy, as a great deal must be known about the internal structure of the char and its behaviour during burning, in the first instance, and the increased diffusion resistance posed by the ash layer, in the second. Little is known about the behaviour of ash in bed combustion, but large char particles have been shown to burn with a clearly defined unreacted core (Abdel-Hafez, 1987) and will have an insignificant ash buildup if the ash content of the parent fuel is low enough.

The ash segregation (AS) model is therefore the most practical, and is employed in this work, as there is no need to simulate the effect of char pores or an ash diffusion resistance. The heterogeneous reactions are assumed to occur only on the surface of the char, with a rate that is dictated by the available surface area and other factors, such as solid temperature and the partial pressure of oxygen or carbon dioxide (unless diffusion control prevails). The inside of the particle can therefore be assumed to remain unreacted and at its initial density, a simplification which has been examined by Abdel Hafez (1987) and found to be adequate for particles greater thatn 3.0 mm such as the ones modelled in this study.

2.4.3 Carbon oxidation

Many studies of carbon oxidation have been done, but few apply to larger particles. Thus, most of the kinetic data available is for pulverized coal, with typical particle sizes of 0.1 mm. The large majority of the correlations found in the literature expressed the C-O_2

reaction in the form of an Arrhenius relationship, with a first order power dependency on the partial pressure of O_2.

Several authors, however, state that the kinetics of this reaction are not critical to combustion simulations. Hobbs *et al.* (1992) believe that diffusion control dominates the oxidation process, and that reasonable predictions can be obtained despite the absence of precise kinetic data for this reaction. This idea is upheld in the earlier work of Lockwood and Salooja (1983), who ran computer simulations of pulverized coal flames in a furnace. They found almost no evidence of kinetic "influence" in the flames, which can be interpreted to mean that their simulation showed little sensitivity to variations in the kinetic expression used to represent this reaction. Patel *et al.* (1987) identified an experimental temperature of 700 K as marking the transition from kinetic to diffusion control. This temperature is much lower than temperatures found in the highly active regions of burning char beds; any errors arising from the assumption of diffusion control are therefore likely to be small. The kinetics found by Field (1969) for pulverized coal char are deemed to be satisfactory by most authors, and have been employed in the recent gasification model by Hobbs *et al.* (1992).

It is well accepted that carbon oxidation produces both CO and CO_2, and that CO is favoured at higher temperatures. The Arrhenius relationship developed by Arthur (1951) to correlate the ratio of CO/CO_2 produced by this reaction appears to be well accepted and is also cited in a more recent survey by Laurendeau (1978). The Arthur (1951) correlation is therefore also employed in this work.

2.4.4 CO_2 reduction

The CO_2 reduction reaction is somewhat slower than the carbon oxidation reaction, and endothermic rather than exothermic. It is therefore most active when solid temperatures are high and the local oxygen in the bed has been depleted. Because this reaction occurs more slowly than the carbon oxidation reaction, the rate of carbon consumption remains kinetically controlled at higher temperatures; correct kinetics are therefore expected to be more critical in obtaining accurate combustion simulations. The transition temperature to diffusion control has been identified through a large number of studies to be greater than 1100 K (Matsui *et al.*, 1986).

Many of the correlations developed for this reaction are derived from adsorption rate kinetics and contain a dependency on fractional carbon conversion that make them impractical in char combustion models, where rate is dependent on the effective surface area of the particle rather than on its mass. Von Fredersdorff and Elliot (1963) developed a rate expression for this reaction based on Langmuir-Hinshelwood kinetics. Rate was thought to be a function of CO_2 adsorption, CO desorption and the remaining mass of unconverted carbon. The authors concluded that different reaction mechanisms could share the same rate, and that comparison of predicted and experimental rates was an inconclusive test of kinetics. Dutta and Wen (1977) used thermogravimetric analysis (TGA) of a variety of coals and coal chars to obtain a similar correlation. An effectiveness factor was defined to account for the increased importance of intra particle diffusion resistance at higher reaction temperatures. Katta and Keairns (1981) defined reaction rate as the weight of carbon reacted per unit time per unit weight of carbon available for reaction. Rates for the C-CO_2 reaction were calculated

from a mass balance on their fluidized bed reactor, where the inlet and outlet gas concentrations were determined by gas chromatography. Rates were found to vary with carbon conversion, but not with particle size, a result which is questionable, since particle size is a function of conversion for shrinking particles.

Since many char combustion and gasification models employ shrinking particle or shrinking core assumptions, reaction kinetics based on surface area are far more practical. Smoot and Pratt (1986) have reviewed the literature and identify the correlations of Goetz *et al.* (1982) as being adequate for the purposes of most simulations. In their analysis, these authors studied the combustion behaviour of four different coal chars in a CO_2 environment and defined an Arrhenius rate coefficient for each type of coal. Coals of lower rank were found to yield more reactive chars, a fact that was associated with the higher initial pore surface area of these chars. The Goetz et al. (1982) correlation is employed in this work because of its compatability with the shrinking particle (char consumption) model.

2.4.5 Homogeneous kinetics

Reactions under the "homogeneous" category occur in the gas phase between CO or CO_2 and gases present in the free stream. In char combustion, the most important of these is CO oxidation, because it is highly exothermic and thus plays a large role in defining gas temperature profiles in the bed. Accurate modelling of homogeneous kinetics is therefore probably even more important than that of heterogeneous kinetics. Unfortunately, gas phase kinetic models are often simplified through the use of gas phase species equilibrium assumptions because of numerical instabilities arising from attempting to model finite rate CO

kinetics in conjunction with the gas phase energy balance. Such assumptions are inappropriate for char combustion. Beds typical of combustion are far thinner than gasifier beds, making gas residence times far too short for gas phase equilibrium to develop. Numerical difficulties must therefore be overcome, and finite-rate kinetics used, to obtain adequate combustion simulations.

The kinetics of CO oxidation have been well studied and most models represent a simplification of the actual multi-step mechanism for this reaction. It is widely accepted that the rate rises in proportion to the amount of CO present and the square root of the water vapour concentration. The power of the dependency on oxygen is less agreed upon, and has been found to range from 0.25-0.75 (Matsui et al., 1986). Westbrook and Dryer (1981) found a 0.25 power dependency on oxygen. The latter relationship was developed for fuel-lean conditions and has been found to give excessively high oxidation rates for fuel-rich conditions (Hautman *et al.*, 1981). Howard *et al.* (1973) believe that the power of the dependency on O_2 varies with the concentration of this gas, increasing from 0-0.2 for O_2 > 5% to about 1.0 for O_2 < 5%.

The largest source of variation in correlations for the CO oxidation reaction, however, is by far the temperature dependency, which takes the form of an Arrhenius relationship. The older correlation of Howard *et al.* (1973) purportedly results in a less active reaction for fuel rich conditions. This correlation was developed from the study of turbulent combustion of city gas (methane) in a flow reactor and from temperature and concentration traverses of a methane-air flame. An improved fit according to the accepted form described above was obtained by recorrelating the data from several other studies. A 0.5 power dependency on

O_2 was chosen to give reasonable CO oxidation rates for both fuel-rich and fuel-lean conditions.

The use of these correlations in combustion simulations has been rather haphazard; correlations are usually tailored to fit experimental results, indicating that additional factors, such as the concentrations of other hydrocarbons, may be influencing these kinetics. Hautman *et al.* (1981) developed a variable suppression factor for the reaction rate of Westbrook and Dryer (1981) that was dependent on the fuel-air ratio for CO oxidation in rich hydrocarbon environments. Lockwood and Salooja (1983) also suppressed the rate of Howard *et al.* (1973) for their prediction of pulverized coal flames, but did it by reducing the preexponential factor by a factor of 1000 instead. Both studies, however, involved CO oxidation in the presence of hydrocarbons, which are believed to suppress CO oxidation because of their consumption of OH radicals (Yetter and Dryer, 1992). Most char combustion and gasification models have failed to include finite homogeneous kinetics, so the validity of the proposed CO kinetics for char combustion is not known. In char combustion, the presence of hydrocarbons is curtailed by the low initial concentration of hydrogen in the char, making reaction suppression unnecessary. It is thus possible that the correlations would give better predictions for char combustion than other types of combustion. Arai and Hasatani (1987) used the relationship proposed by Howard *et al.* (1973) and obtained satisfactory predictions of the variations in CO output with time, indicating that this correlation is probably adequate for the purposes of most char combustion models, supporting its use in this work.

3.0 MODEL DEVELOPMENT

The char combustion simulation developed in this work is a one dimensional, transient, finite volume analysis of an overfeed packed bed reactor. The system is described by separate gas and solid mass and energy balances that include solid movement and full kinetic models for the three principal combustion reactions, as well as models for the solid-to-gas heat and mass transfer processes described above. The simulation is designed to track changes in the gas and solid temperatures and the concentrations of O_2, CO and CO_2 with bed height and give these as outputs along with particle diameters and fuel flow rates. The program code is written in Fortran and is shown in Appendix D.

3.1 Bed geometry and assumptions

For the purposes of analysing typical industrial applications of combustion, a vertical, overfeed reactor is considered and subjected to certain simplifying assumptions. The diameter of the bed is assumed to be very large, allowing for the elimination of radial temperature, velocity, concentration, and particle size gradients from the analysis. This reduces the problem to a one-dimensional one and makes it numerically more approachable. Bed pressure gradients are also neglected, since combustion beds are normally quite thin, which may limit the accuracy of the simulation for thicker (gasifier) beds.

The char bed is modelled as a stack of finite volume elements of thickness δx and assumed to consist of particles with similar geometries. The size of these particles varies with height in the bed, but is assumed to be constant with horizontal location. The volume of the

spaces between the particles is expressed in terms of the void fraction, ϵ, which is considered to be constant for the purposes of this analysis. The entering air is assumed to be uniformly distributed over the bed and is characterized by the superficial, or empty column, velocity, v_G. A transient solution is developed to allow for the consideration of bed behaviour during startup. A diagram of the processes occurring in and on the boundaries of a single slab of the bed is shown in Figure 2 below. The flow directions of both phases with respect to the positive vertical coordinate are shown to establish the sign conventions employed in the numerical analysis.

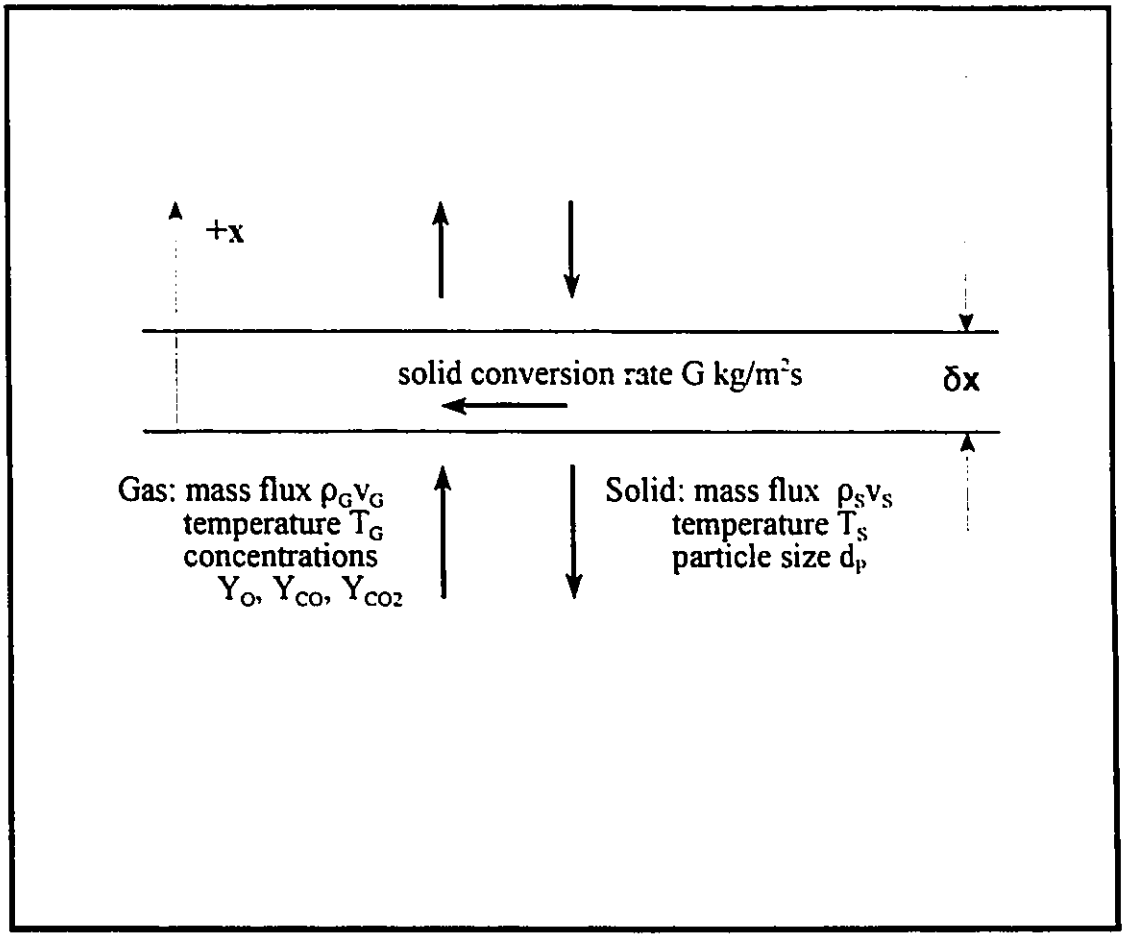

Figure 2: Schematic diagram of the processes occurring in and across the boundaries of a differential slice of the char bed (horizontal arrow indicates transfer of carbon from solid to gas phase)

The reacting char in each slab of the bed as depicted above is assumed to obey the shrinking particle model and burn with constant density as described previously (Section 2.4.2). The particle surface area available for reaction is a_B, and increases with decreasing particle size. Bird *et al.* (1960) give the following correlation, which is developed from the geometry of the particles in the bed :

$$a_B = \frac{6(1-\epsilon)\psi}{d} \qquad (3\text{-}1)$$

where d is the effective particle diameter in m. The variable ψ is a shape factor that depends on particle geometry and has a value of 1.0 for spheres. The void fraction in the above expression was assumed to be 0.33, which is a typical void fraction for packed beds of spherical particles.

3.2 Governing differential equations

The equations required to describe the temperature and gas concentration changes in the system are the mass, species and energy transport equations for the gas and solid phases. Note that the possible occurrence of a pressure drop along the bed has been neglected. A solid mass balance on a volume element of the bed gives the relationship between the carbon consumption rate by the surface reactions and the velocity of the fuel moving down through the bed, v_S :

$$\frac{\partial}{\partial t}[(1 - \epsilon)\rho_S] + \frac{\partial}{\partial x}(\rho_S v_S) = -Ga_B \qquad (3\text{-}2)$$

where ρ_S is the density of the char and G is the rate of carbon consumption per unit surface area of the char particles in kg m^{-2} s^{-1}. Since v_S is opposite to the positive x direction, it will be negative. A similar balance can be done on a volume element of the gas phase :

$$\frac{\partial}{\partial t}(\epsilon\rho_G) + \frac{\partial}{\partial x}(\rho_G v_G) = Ga_B \qquad (3\text{-}3)$$

where v_G is the superficial gas velocity. The net mass gained by the gas phase per unit surface area of particle is equal to the rate of carbon consumption per unit surface area G in (3-2) and

thus also appears in the above balance.

A transport equation for each of the species is required to describe the changes in gas composition occurring in the system and can be written for each of the species *i* as follows:

$$\frac{\partial}{\partial t}(\rho_G \epsilon Y_i) + \frac{\partial}{\partial x}(\rho_G v_G Y_i) = \frac{\partial}{\partial x}(\rho_G D_{eff_i} \frac{\partial Y_i}{\partial x}) + \epsilon r_i \qquad (3\text{-}4)$$

where Y_i is the mass fraction of species *i*, D_{eff} is the effective diffusivity of species *i* in the bed, and r_i is the rate of production of species *i* by chemical reaction per unit volume of gas phase. One such equation must be written for each of O_2, CO and CO_2. The last term in the above equation is the species source term stemming from the three combustion reactions and requires special numerical treatment during discretization because of the non-linear nature of the reaction rate expressions involved. This will be discussed in more detail in a later section.

The energy equation for the solid phase is

$$\frac{\partial}{\partial t}[(1-\epsilon)\rho_S h_S] + \frac{\partial}{\partial x}(\rho_S v_S h_S) = \frac{\partial}{\partial x}(k_{S\,eff} \frac{\partial T_S}{\partial x}) + h a_B (T_G - T_S) - G a_B \Delta H_R \qquad (3\text{-}5)$$

where h_S is the solid enthalpy, T_S the solid temperature, k_{Seff} the effective thermal conductivity of the solid, h the fluid-to-particle heat transfer coefficient, and the last term is an abbreviated expression for the net heat release due to all the surface reactions. (The expanded version is given in Appendix B.3). This equation assumes that all of the heat produced by the heterogeneous reactions is deposited in the solid phase. The gas phase energy equation is:

$$\frac{\partial}{\partial t}(\epsilon \rho_G h_G) + \frac{\partial}{\partial x}(\rho_G v_G h_G) = \frac{\partial}{\partial x}(k_{G\,eff}\frac{\partial T_G}{\partial x}) - h a_B (T_G - T_S) - \epsilon r_{CO}\Delta H_{RCO} \qquad (3\text{-}6)$$

where k_{Geff} is the effective thermal conductivity of the gas and r_{CO} is the rate of CO "production" in kg m^{-3} s^{-1} (this will be negative, since CO is consumed). Only one reaction occurs in the gas phase, so ΔH_{RCO} in this case represents only the heat of combustion of CO.

A further balance equation is required to model the shrinking of the char particles as they move downward through the bed. This is derived from a particle number balance on each differential slice of the bed as follows:

$$\frac{\partial N_P}{\partial t} = - \frac{\partial \dot{N}}{\partial x} \qquad (3\text{-}7)$$

where N_p is the number of particles per unit bed volume, given by

$$N_P = 6(1 - \epsilon)/\pi\, d_P^3 \qquad (3\text{-}8)$$

and $\dot{N}$ is the particle number flux per unit bed cross-section:

$$\dot{N} = 6 v_S/\pi\, d_P^3 \qquad (3\text{-}9)$$

Substituting (3-8) and (3-9) into equation (3-7) yields

$$(1 - \epsilon)\frac{\partial d_P}{\partial t} + \frac{\partial (v_S d_P)}{\partial x} = \frac{4}{3} d_P \frac{\partial v_S}{\partial x} \qquad (3\text{-}10)$$

The last term can be substituted for from equation (3-2) :

$$\frac{\partial v_S}{\partial x} = -\frac{1}{\rho_S}\left[\frac{\partial}{\partial t}[(1-\epsilon)\rho_S] + v_S\frac{\partial \rho_S}{\partial x} + (ia_B)\right] \qquad (3\text{-}11)$$

Assuming constant solid density (shrinking particle model) and substituting for a_B from (3-1), equation (3-10) then simplifies to :

$$(1-\epsilon)\frac{\partial d_P}{\partial t} + \frac{\partial}{\partial x}(v_S d_P) = -\frac{8G}{\rho_S}(1-\epsilon) \qquad (3\text{-}12)$$

This development assumes that the particles maintain their identity throughout the bed; (3-7) implies that no breakage of the particles occurs, but that they are steadily consumed in accordance with the shrinking particle model as described previously.

Equations (3-2)-(3-6) and (3-12) are the defining equations for the system and are solved numerically using finite volume techniques that are described in more detail elsewhere. A description of the system transport coefficients, reaction kinetics and physical property correlations is given below.

3.2.1 Boundary conditions

The boundaries of the system are defined by the bottom surface of the grate and the surface of the char bed. Integration of the defining differential equations required the development of several boundary conditions, which are given below.

(A) Mass balances

Each mass balance required the definition of one boundary condition. For the gas

phase, no special boundary condition was necessary because the mass flux of air entering through the grate was defined by temperature and velocity of the air stream entering the bed. The solid mass flux boundary condition at the top of the bed is the fuel feed rate, which is determined by the carbon consumption rate in the bed and the ash exiting the bed:

$$\rho_S v_S|_{x=h} = \int_0^h Ga_B \, dx - \rho_S v_S|_{x=0}$$

where all variables are as previously defined (note that v_S is a negative quantity, since the x coordinate for the bed is positive in the upward direction -see Figure 2). This assumes that the ash has the same density as the char and that the bed void fraction is constant.

The inlet and outlet mass fluxes of fuel are related by :

$$\rho_S v_S|_{x=0} = \zeta \rho_S v_S|_{x=h}$$

where ζ is the mass fraction of ash present in the char. This assumes that all the carbon in the char is consumed and only ash remains. (Note that the above assumes complete conversion of the char entering the bed. In reality, this would be controlled by the size of the holes in the grate and the diffusion resistance posed by the ash in the bed. The latter might result in the extinction of the reactions at the particle surface, especially in the very bottom portion of the bed where the cooling effect of the entering gas is still relatively high and the solid temperature therefore too low to sustain surface burning.)

(B) Gas phase species and energy balances

The solution of the gas phase species and energy balances required that two boundary conditions be defined. As with the mass balances, the (x=0) boundary conditions were

defined by gas temperature and inlet concentration. The (x=h) boundary was defined by assuming

$$\left.\frac{\partial T}{\partial x}\right|_{x=h} = 0$$

and

$$\left.\frac{\partial Y_i}{\partial x}\right|_{x=h} = 0$$

This is a standard outflow boundary condition, and assumes that diffusion and heat conduction are negligible at the boundaries, a reasonable assumption as long as flow velocities are fairly high.

(C) Solid energy balance

Since the solid was discontinuous at the boundaries, it could only lose heat by radiation. Heat *losses* across the bottom boundary of the bed were therefore expressed in terms of the radiant heat exchange between the bottom of the grate and the ash hopper assumed to be situated below the bed and solid convection in or out of the bed:

$$\dot{q}_R = \epsilon_C \sigma_B (T|_{x=0}^4 - T_{ash}^4) - (\rho_S v_S h_S)|_{x=0}$$

where T_{ash} is the temperature of the ash hopper (input), σ_B is the Boltzman constant, ϵ_C is the particle emissivity (assumed to be 0.8) and $T|_{x=0}$ is the temperature of the bottom of the bed. (Note that v_S is a negative quantity.)

Since the grate portion of the bed consists of three phases (ash, the entering air and

the grate material), the exact modelling of which would have required excessively complex heat transfer and effective thermal conductivity relations, the solid structure of the grate was approximated by spherical particles of the size originally fed to the top of the bed. These particles were assumed to have an effective solid conductivity calculated in the same manner as that for the rest of the bed, but based on solids composed of the grate material (see Section 3.3.1 (A)). The thermal conductivity of the gas phase between these particles was calculated from the expression for effective gas thermal conductivity used for the rest of the bed, with no change (see Section 3.3.1 (B)). Since the mass flux of the ash leaving the bed was very small and therefore practically negligible in the solid energy balance (in comparison with the radiation heat flux shown above), the ash was assumed to have the same temperature and properties as the large particles making up the grate and assumed to pass between them as it would have passed through the grate.

The heat loss boundary condition for the top of the bed was similar to that at the bottom, but without the complications represented by the grate structure:

$$\dot{q}_R = \epsilon_C \, \sigma_B \, (T|_{x=h}^4 - T_{boiler}^4) + (\rho_S v_S h_S)|_{x=h}$$

where $T|_{x=h}$ is the temperature of the top of the bed and T_{boiler} is the temperature of the boiler being radiated to.

(D) Particle number balance

The top boundary for the particle number balance was dictated by a specified particle feed size, whereas the particle diameter of the exiting fuel was dictated by the fraction of ash

in the original char and therefore controlled by the solution of the solid mass balance.

3.3 System transport coefficients

The transport coefficients for the system are the effective thermal conductivities and heat capacities of the gas and solid, the effective gas diffusivity, D_{eff}, and the heat and mass transfer coefficients h and k_y between the gas and the solid. Because of the uncertainty associated with some of these coefficients, particularly the mass and heat transfer coefficients between the two phases, the simulation was run with several different models for these coefficients to examine their relative importance. The selection of models for the effective solid and gas conductivities in the literature was relatively limited, making the choice there more straightforward. All of the models in the literature were developed for packed beds of uniform sizes, but are assumed to hold for the particle size ranges and particle size variations with bed height encountered in combustion problems.

3.3.1 Effective conductivities and diffusivities

(A) Effective solid conductivity

Most of the effective solid conductivity studies found were related to, or cited, the works of Yagi and Kunii (1957) and Kunii and Smith (1960). Effective solid thermal conductivities differ from pure solid thermal conductivities in that they account for conduction mechanisms that arise from the discontinuous nature of the solid phase in a packed bed. The model used for this transport coefficient was based on the relation for solids in stagnant air

as expressed by Yagi and Kunii (1957) for the four principal solid phase conduction mechanisms. These were: bulk solid conduction, conduction through the stagant gas films around the contact points between solids, radiation between non-adjacent solids and radiation between adjacent solids. A fifth mechanism, conduction through the contact point between solids, was considered by the authors to be negligible in most cases and was omitted from their final correlation, which is given by:

$$k_{Seff} = \frac{\beta(1 - \epsilon)}{(\gamma/k_S) + 1/(k_G/\varphi + h_{RS}d_p)} + \epsilon\beta d_p h_{RI'} \qquad (3\text{-}13)$$

The above expression reflects the operation of the first three mechanisms in parallel with the fourth, where k_{Seff} is the effective solid thermal conductivity of the bed in W m^{-1} K^{-1}; k_S is the solid thermal conductivity in W m^{-1} K^{-1} ; k_G is the gas thermal conductivity in W m^{-1} K^{-1} ; γ is the dimensionless effective length of solid relating to conduction and has a value of 0.67 obtained through geometrical arguments (Kunii and Smith, 1960); φ is the dimensionless gas film thickness near the particle contact points and has a value of approximately 0.25 for void fractions typical of spheres (Yagi and Kunii, 1957), and β is the dimensionless effective path length between particle centres, which is 1.0 for relatively loose packing (Kunii and Smith, 1960). The quantities h_{RS} and $h_{RI'}$ are the radiation heat transfer coefficients for non-adjacent and adjacent particles and are given by Yagi and Kunii (1957) as

$$h_{RI'} = \frac{0.2268}{1 + [0.5\epsilon/(1 - \epsilon)]\,[(1 - \epsilon_C)/\epsilon_C]} \left[\frac{T_M}{100}\right]^3$$

and

$$h_{RS} = 0.2268\ [\epsilon_C/(2 - \epsilon_C)] \left[\frac{T_M}{100}\right]^3$$

where ϵ_C and T_M are respectively the particle emissivity and average temperature in K.

The results of Merrick's (1983) study on the thermal conductivity of solid coal, k_S, were used in the study by Hobbs (1992) and seem to represent the most recent model for this property. According to this work, the thermal conductivity of coal or char varies with particle density and solid temperature as

$$k_S = \left[\frac{\rho_S}{4511}\right]^{3.5} \sqrt{T_S} \qquad (3\text{-}14)$$

where k_S is in W m^{-1} K^{-1}.

The thermal conductivity of the gas phase, k_G, can be described by the Eucken equation for energy exchange in polyatomic gases as given by Bird *et al.* (1960):

$$k_G = \left[C_{pg} + \frac{5}{4}\frac{R}{M}\right]\mu \qquad (3\text{-}15)$$

where C_{PG} is the specific heat of the gas in J kg^{-1} K^{-1}, R is the gas constant in kJ $kmol^{-1}$ K^{-1} and M is the molecular weight of the gas mixture. The quantity μ is the dynamic viscosity of the gas in kg m^{-1} s^{-1} and is given by the Chapman-Enskog theory (Bird *et al.*, 1960):

$$\mu = 2.6693\ X\ 10^{-6}\ \frac{\sqrt{MT_G}}{\sigma^2\Omega} \qquad (3\text{-}16)$$

where M and T_G are as defined previously, σ is a Lennard-Jones parameter for N_2 in Å (equal

to 3.681 for temperatures over 100 K) and Ω is a slowly varying function of temperature, which was assumed to remain constant at 0.8, the value for N_2 at about 1200 K (Bird *et al.*, 1960). (A temperature of 1200 K was chosen here because it was expected to represent an approximate average of the gas temperatures encountered in combustion.) In cases of gas mixtures involving a wide range of molecular weights, the use of a mixing formula is recommended for gas viscosities, but this was omitted here due to the similar molecular weights of combustion gases, and the properties for the most abundant species, N_2, were used.

The solid effective conductivity for the grate is also calculated from (3-13), but with the conductivity of the grate material taking the place of k_S. In most cases, the value of k_S required was that of nickel steel, which has a thermal conductivity of about 35 W m^{-1} K^{-1}.

(B) Effective gas thermal conductivity

The effective gas thermal conductivity model developed by Edwards and Richardson (1968) was deemed sufficient for heterogeneous packed bed analyses by Dixon and Cresswell (1978) and appeared to be the only model in the literature that expressed the conductivity of the gas separately from that of the solid. The correlation seems to have been omitted from other major combustion simulations, but was used here to obtain the effective heat conduction through the void space of the bed. The latter is given by a sum of the two conductive heat transfer mechanisms for the gas phase in packed beds:

$$k_{Geff} = 0.73 \epsilon k_G + \frac{0.5 v_G d_P C_{PG}}{1 + 9.7 \epsilon k_G / v_G d_P C_{PG}} \qquad (3\text{-}17)$$

where the first term represents conduction through the bulk gas phase under stagnant conditions, and the second the increase in conduction with gas flow rate due to turbulent mixing ($W\ m^{-1}\ K^{-1}$).

The gas conductivity in the grate section of the bed is calculated from (3-17) so that it remains consistent with the assumption that the grate behaves like a packed bed of steel spheres. The actual gas thermal conductivity in this area may actually be lower than that predicted by (3-17), however, because the flow through the grate is is less likely to be turbulent; thus, laminar values of the gas thermal conductivity may be more appropriate. Because the interest of the study lay in simulating the portion of the bed that lay above the grate, however, refinements to the grate model were deferred to future studies.

(C) Effective gas diffusivity

The gas effective diffusivity can be derived from (3-17) by making use of the analogy between heat and mass transfer:

$$D_{eff} = k_{Geff} Le_{eff} / (C_{PG} \rho_G) \qquad (3\text{-}18)$$

where D_{eff} is in $m^2\ s^{-2}$. This effective diffusivity is used for all gas species. This simplification is reasonable because of the similar molecular weights of the gases (CO_2, O_2, CO and N_2) in question. The effective Lewis number, Le_{eff} is the turbulent Lewis number. A value of 1.0 for Le_{eff} is reasonable in instances where the gas flow is known to be turbulent.

3.3.2 Fluid-to particle heat and mass transfer

Fluid to particle heat and mass transfer is an area of uncertainty in the simulation of packed-bed systems, particularly in cases where such systems are undergoing reaction (Pathengey and Kovenklioglu, 1989). Because of this, the simulation was run with several different correlations for these transport coefficients. The changes in heat transfer rate with Re for various correlations found in the literature are shown in Figure 2.

The packed bed Reynolds number employed in Figure 2 is based on the specific surface for the packed bed, a_B, and is given by:

$$Re = \rho_G v_G / \mu a_B = \rho_G v_G D_p / 6(1-\epsilon)\mu \qquad (3\text{-}19)$$

This form of the Reynolds number is most often used to correlate packed bed processes. Occasionally, however, the factor 6 is included in the correlation itself, requiring that the Reynolds number be adjusted by appropriate factors of 6 (see Table I). Bird *et al.* (1960) indicate a transition to turbulent flow at Re=2 for this Reynolds number (deduced from a transition value of Re=10 for packed bed Reynolds numbers defined without the factor 6 in the denominator).

With the exception of that of Galloway (1957), most of the correlations in Figure 2 show similar trends for Re, but give different magnitudes of heat transfer coefficients. Since many of these were developed from experimental data for low temperatures, or for extended beds (McConnachie and Thodos, 1963, Sen Gupta and Thodos, 1963) their validity for packed bed combustion was questionable. The choice was therefore restricted to correlations valid for the packed bed Reynolds number ranges of about 2-100 expected in combustion

beds and those applying to beds with appropriate void fractions (0.30-0.44). Those predicting lower heat transfer rates were favoured because of the greater possibility that conductive heat transfer effects were excluded (see Section 2.3.1.). The heat and mass transfer models of Chu *et al.* (1953), Yoshida *et al.* (1962) and Bhattacharyya and Pei (1975) were selected because they best fitted this criterion for the expected packed bed Reynolds numbers (see Figure 3). These are expressed in the form of j_H and j_D and are tabulated below. The correlation of Bhattacharyya and Pei (1975) was extended beyond the experimental conditions quoted by the authors (see Table I) to examine its validity for low gas flow rates.

Table I: Heat and mass transfer submodels

Submodel	Source
$j_D = \frac{k_y}{\rho_G v_G} Sc^{2/3} = 0.91\ Re^{-0.51} \quad (1<Re<50)$ $j_D = j_H = 0.61\ Re^{-0.41} \quad (50<Re<10{,}000)$	Yoshida *et al.* (1962)
$j_D = 5.7 Re^{-0.78} \quad (1<Re<10{,}000)$ $j_H = \frac{h}{\rho_G C_{PG} v_G} Pr^{2/3} = 1.77\ Re^{-0.44}$ $Re = 6\rho_G v_G / \mu a_B$	Chu *et al.* (1953)
$j_H = j_D = 0.018(Ar/Re^2)^{0.25}$ $(4.2< Ar/Re^2 <103)$ $Ar = d_P^3 g\ \rho_G(\rho_S - \rho_G)/\mu^2$ $Re = 6\rho_G v_G / \mu a_B$	Bhattacharyya and Pei (1975)

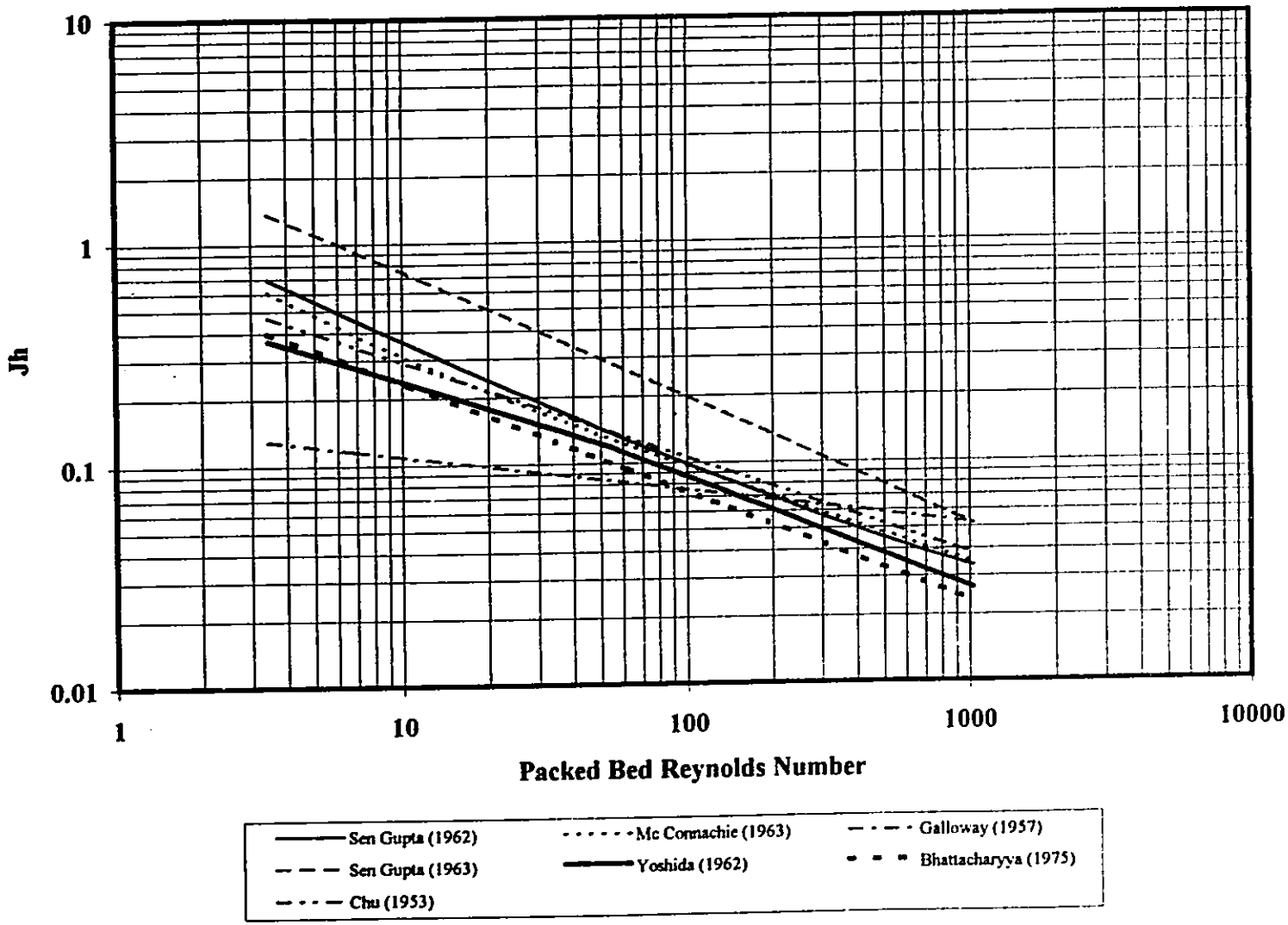

Figure 3: Effects of Reynolds number on predicted heat transfer rates for various heat transfer correlations in the literature at 1000 K

The packed bed Reynolds number given by (3-19) applied only to the correlation of Yoshida and Wen (1962) and was multiplied by 6 for use in the other two heat and mass transfer correlations (see Table I). Pr and Sc are respectively the Prandtl and Schmidt numbers and are assumed to be equal because of the turbulent nature of the flow in packed bed combustors.

The above heat and mass transfer correlations apply in instances where there is little or no mass flux from the surfaces of the particles in the packed bed. In char combustion, however, the diffusion of product gases from the surface of the char particles pushes the boundary layer outwards, resulting in lower concentration and temperature gradients between the particle surface and the free stream. The effect is a reduction in the heat and mass transfer rates.

For mass transfer, this can be developed using the "film" theory of mass transfer (Bird *et al.*, 1960) and is expressed in terms of the Spalding transfer number for diffusion B_M as follows (Hallett, 1994):

$$k_y = k_{y_o} \frac{\ln(1 + B_M)}{B_M}$$

where k_{y_o} is the uncorrected mass transfer coefficient and B_M is given by (Hallett, 1994):

$$B_M = \frac{Y_{O_{2_\infty}} - Y_{O_2}}{S_{CO} + Y_{O_2}}$$

where Y_{02_∞} is the free stream concentration of oxygen, Y_{O2} is the surface concentration and S_{CO} is the oxygen to carbon mass ratio required for combustion to CO (50% air deficit). The quantity B_M is a measure of the ease of mass transfer and increases with mass flux from the

particle surface (reaction rate). In the correction for the mass transfer coefficient given above, the numerator increases more slowly than the denominator, resulting in a decrease in mass transfer rate as mentioned previously. This increase is expected to be small because the value of B_M is generally small : it reaches a maximum value of 0.174 in atmospheric air when Y_{O2R} approaches 0, corresponding to only an 8% decrease in k_y.

A similar argument can by developed for heat transfer by analogy to mass transfer. The correction to heat transfer takes the same form as that for mass transfer (Hallett, 1994):

$$h = h_o \frac{\ln(1 + B_T)}{B_T}$$

where h_o is the uncorrected form of the heat transfer coefficient, and the thermal transfer number B_T is developed from the transfer number for diffusion by analogy (Hallett, 1994):

$$B_T = (1 + B_M)^{Le_{eff}} - 1$$

where Le_{eff} is the effective Lewis number at the particle surface and is assumed to equal 1.0.

A further effect that can be included is energy transport by interdiffusion. As one species, such as O_2 or CO_2, diffuses in to the surfaces of the char particles, another species, such as CO may be diffusing out. If the enthalpies of these species are different, a net energy flux results. It can be shown (Appendix C) that this is equivalent to defining an effective heat capacity for heat transfer to the particle surfaces:

$$C_{PGeff} = (1 + S_{CO})\, C_{PCO} - S_{CO}\, C_{PO_2}$$

where C_{PCO} and C_{PO2} are the heat capacities for pure carbon monoxide and oxygen. The

latter stems from a derivation involving the species interdiffusion term in the energy balance on a single char particle (Appendix C) and was estimated to have only a small effect (less than 1%) on heat transfer rates.

3.3.3 Gas and solid heat capacities

The specific heat for the gas mixture was calculated from a mixing formula of the form

$$C_{PG} = \Sigma Y_i C_{P_i}$$

where the C_{Pi} are the specific heats of the individual gas species. The latter were taken from Smith and Van Ness (1987) and were of the form:

$$C_{P_i} = \frac{R}{M_i} (A_i + B_i T_G + D_i T_G^{-2}) \qquad (3\text{-}20)$$

where the A_i, B_i and D_i for each gas are shown in the first data file for the program (Appendix D).

The specific heat for the solid was taken from Merrick (1983). This correlation was chosen because of its simplicity and because it reflected a variation in solid thermal conductivity with temperature as well as the relative amounts of carbon and ash present in the char. The Merrick model operates with a mixing formula similar to that described above, except that for the solid :

$$C_{PS} = \Sigma\ w_i C_{P_i}$$

where the w_i and C_{Pi} are the mass fractions and specific heats of the "as fired" char and its

ash. The specific heat of the char in J kg^{-1} K^{-1} is given by

$$C_{P\,char} = \frac{R}{1000\ a}\left[g_1(380/T_S) + 2g_1(1800/T_S)\right] \qquad (3\text{-}21)$$

where a is the average molecular weight of the char, which was approximated as 12 kg $kmol^{-1}$ for pure carbon , and g_1 is a function derived from the Einstein specific heat theory for the vibrational modes of the molecules in the solid that operates on the ratios of the char temperature to the Einstein characteristic temperatures of 380 and 1800 K:

$$g_1(z) = \exp(z) \,/\, ((\exp(z) - 1)/z)^2$$

where z is a dummy variable representing the temperature ratios.

The specific heat of the ash is a linear function of solid temperature:

$$C_{P\,ash} = 754 + .586\ T_S \qquad (3\text{-}22)$$

Also calculated for use in the transport equations were the mean specific heats of the two phases for the purposes of estimating the enthalpies h_S and h_G in equations (3-5) and (3-6) as:

$$h = \overline{C_P}\ T = \frac{1}{T}\int_0^T C_P\ \partial T \qquad (3\text{-}23)$$

where T is in K. These were calculated from equations (3-20), (3-21) and (3-22) by performing the operation indicated in (3-23) above to yield:

$$\overline{C_{pi}} = \frac{R}{M}\left(A_i + \frac{B_i}{2}T_G - D_i T_G^{-2}\right)$$

and

$$\overline{C}_{p_{char}} = \frac{R}{1000\ a\ T_S}\ [380g_0(380/T_S) + 3600g_0(1800/T_S)]$$

where g_0 is the integral of g_1, and

$$\overline{C}_{p_{ash}} = 754 + .293\ T_S$$

3.4 Reaction kinetics

The char combustion process was simulated by two surface reactions and one gas phase reaction. At the particle surface, carbon oxidation and CO_2 reduction were assumed to occur by the following reactions:

$$C + S_{CO}\ O_2 \rightarrow (1+S_{CO})\ CO \qquad \text{(R1)}$$

$$C + S_{CO_2}\ O_2 \rightarrow (1+S_{CO_2})\ CO_2 \qquad \text{(R2)}$$

$$C + S_2\ CO_2 \Rightarrow (1+S_2)\ CO \qquad \text{(R3)}$$

where S_{CO}, S_{CO2} and S_2 are mass stoichiometric coefficients with values of 1.332, 2.664 and 3.667 respectively.

Reactions R1 and R2 are assumed to occur simultaneously to produce CO and CO_2 in a ratio that varies with temperature according to the relationship developed by Arthur (1951). From the latter, the mass of carbon dioxide per kg of product ($CO+CO_2$), χ, for these reactions can be expressed as :

$$\chi = \frac{1}{1 + [2500\ \exp(-6240/T_s)(M_{CO}/M_{CO_2})]} \qquad \text{(3-24)}$$

where M_{CO} and M_{CO_2} are the molecular weights of CO and CO_2.

Equations R1 and R2 can therefore be rewritten as:

$$C + S_1 O_2 \rightarrow (1+S_1)(CO + CO_2) \qquad \text{(R4)}$$

where S_1 is a mass stoichiometric coefficient that is dependent on temperature through χ and given by:

$$S_1 = \frac{(1+S_{CO_2})(1+S_{CO})}{\chi(1+S_{CO}) + (1-\chi)(1+S_{CO_2})} - 1 \qquad \text{(3-25)}$$

The rates of the particle surface reactions R3 and R4 were modelled as having an Arrhenius temperature dependency. For the oxidation of carbon, the rate expression of Field (1969) was used. This is given by:

$$G_1 = A \exp(-E/RT_S) P_{O_2} \qquad \text{(3-26)}$$

where G_1 is the rate of carbon consumption in kg m^{-2} s^{-1}, A is the preexponential factor, equal to 860 kg m^{-2} s^{-1} kPa^{-1}, P_{O2} is the partial pressure of oxygen at the particle surface in kPa, and R is the universal gas constant in kJ $kmol^{-1}$ K^{-1}. E is the activation energy for the reaction and is equal to 149.6 kJ mol^{-1}. Field's (1969) expression, like most in the literature, was derived from experiments on pulverized coal char; however, as mentioned in Section 2.4.3, char oxidation is expected to be diffusion controlled, so that the actual kinetic expression used will have little effect.

The rate of CO_2 reduction is given by a similar expression, developed by Goetz *et al.*

(1982). As mentioned previously, this was the most recent CO_2 reduction model found in the literature and preferred because of its compatibility with the shrinking particle model:

$$G_2 = A \exp(-E/RT_s)\, P_{CO_2} \qquad (3\text{-}27)$$

Here P_{CO_2} is the partial pressure of CO_2 at the particle surface in kPa and G_2 represents the carbon consumption rate in kg m^{-2} s^{-1}. The activation energy and preexponential factor vary with char type and are tabulated below.

Table II: CO_2 reduction Arrhenius rate coefficients

Parent Coal Type	A	E
	(kg m^{-2} sec^{-2} kPa^{-1})	(kJ mol^{-1})
Lignite	65	165.2
Subbituminous	103	177.7
Pittsburgh #8	137	224.7
Illinois #6	128	235.8

For the experiments conducted in this work, the expression for subbituminous coal char was found to best represent CO_2 reduction in the beds being simulated. The difference in the reaction expressions for the chars listed in the table above is believed to be due to differences in surface structure produced by the devolatilization of the parent coal types.

In the gas phase, CO oxidation with oxygen was assumed to occur via a simplified one-step mechanism:

$$CO + S_3\, O_2 \rightarrow (1+S_3)\, CO_2 \qquad (R5)$$

where S_3 is a mass stoichiometric coefficient equal to 0.571. The available rate models for this reaction all had a similar form, but because of the apparent controversy surrounding the oxygen dependency of this reaction, the models of Howard *et al.* (1973) and Westbrook and Dryer (1981) were both employed in the simulation to examine the effect of gas phase rate kinetics on the predicted profiles. The general form of the rate model for CO oxidation is:

$$r_{CO} = A\ \rho^{1+m+n}\ Y_{CO}\ Y_{O_2}^{\ m}\ Y_{H_2O}^{\ n}\ \exp(-E/RT_g)$$

where the values of the parameters m, n, A, and E are tabulated below.

Table III: CO oxidation Arrhenius rate coefficients

	A	E	m	n
Units	**(kg m^{-3} s^{-1})**	**(kJ mol^{-1})**	-	-
Westbrook and Dryer (1981)	2.218×10^{11}	167.3	0.25	0.5
Howard *et al.* (1973)	5.417×10^{9}	125.5	0.5	0.5

The mass fraction of water vapour, Y_{H2O} in the gas phase was assumed to be .007 kg/kg, corresponding to 50% relative humidity at 20 °C.

3.5 Particle Surface Conditions

Because of the reactions occurring at the particle surface, the concentrations of gases in the boundary layer around the particle differ from those in the bulk gas phase (free stream). This concentration difference is the driving force for mass transfer. Since the only mass being added to the free stream is that of oxidized carbon, the net mass flux issuing from the particle

surface can be described by the total carbon consumption rate G, equal to the sum of G_1 and G_2 as developed above. This flux can be attributed to convection and mass transfer of each species by the following :

$$G = \sum_{i=1}^{N} G_i = \sum_{i=1}^{N} [\, GY_{iR} + k_y\,(Y_{iR} - Y_{i\infty})\,]$$

where the first term in parentheses represents mass transport of species *i* by convection and the second mass transfer of species *i* to or from the particle surface by diffusion. $Y_{i\infty}$ is the concentration of species *i* in the free stream and Y_{iR} its concentration at the particle surface. The mass transfer coefficient is denoted by k_y, which is assumed to be the same for all species, and is given in Section 3.3.3. (Note that the quantity G is defined as positive when it represents mass leaving the particle surfaces.)

Each of the terms in the summation above may then be equated with its reaction source term as per the mass stoichiometry given in 3.4:

$$G_{O_2} = -S_1 G_1 = GY_{O_2R} + k_y(Y_{O_2R} - Y_{O_2\infty})$$

$$G_{CO_2} = -S_2 G_2 + \chi(1+S_1)G_1 = GY_{CO_2R} + k_y(Y_{CO_2R} - Y_{CO_2\infty})$$

$$G_{CO} = (1-\chi)(1+S_1)G_1 + (1+S_2)G_2 = GY_{COR} + k_y(Y_{COR} - Y_{CO_\infty})$$

The expressions given above can then be solved for the Y_{iR} as, where G_{O2}, G_{CO} and G_{CO2} represent the rates of generation or consumption of O_2, CO and CO_2 respectively:

$$Y_{O_2R} = \frac{Y_{O_2\infty}}{1 + (1/k_y)\,(G + S_1 G_1 / Y_{O_2}^{*})} \qquad (3\text{-}28)$$

$$Y_{CO_2R} = \frac{\chi(1+S_1)(G_1/k_y) + Y_{CO_2\infty}}{1 + (1/k_y)(G + S_2G_2/Y_{CO_2}^*)} \quad (3\text{-}29)$$

$$Y_{COR} = \frac{(1+S_2)G_2 + (1-\chi)(1+S_1)G_1 + k_yY_{CO\infty}}{G + k_y} \quad (3\text{-}30)$$

Note that in (3-28) and (3-29) above, G_1 and G_2 are as defined by (3-26) and (3-27) and therefore change with the surface concentrations Y_{iR} being calculated. The forms of (3-28) and (3-29) reflect the assumption that G_1 and G_2 change negligibly with temperature, so that the S_1G_1/Y_{O2R} and S_2G_2/Y_{CO2R} are essentially constant. The "predicted" surface concentrations (from the previous iteration), Y^*_{O2R} and Y^*_{CO2R} approach Y_{O2R} and Y_{CO2R} respectively, so their substitution for the current values in the above-mentioned terms "corrects" these terms suffficiently to still give an accurate solution for the Y_R at convergence. Equations (3-28) and (3-29) thus represent "predictor-corrector" forms and were solved before (3-30) for each iteration to ensure that the expressions for G_1 and G_2 in the latter were correct.

4.0 NUMERICAL METHOD

4.1 Finite Volume Discretization Techniques

4.1.1. Background

The discretization of differential equations leads to a system of linear algebraic equations which can be solved far more easily than the original system, often with minimal loss of accuracy. In the discretization approach, the system to be modelled is discretized in time and space into time steps and control volumes. Each control volume contains a node, to locate the solution. The values of the dependent variables at each node over each time step, Δt, can then be expressed as functions of values at the neighbouring nodes through algebraic equations that contain the same information as the original differential equations. The linear nature of these equations allows previously non-linear systems to be solved by relatively simple matrix methods.

The governing partial differential equations outlined in Section 3.0 were solved simultaneously using standard discretization techniques. Such techniques are well covered in the literature on computational fluid flow. Readers wishing to obtain the background for developments given in this section are referred to the work of Patankar (1980).

4.1.2. Grid generation scheme

A diagram of the discretized (gridded) char bed is shown in Figure 4. The size of control volumes depends on the amount of resolution desired. In the transient char combustion simulation of this work, the oxidation zone was expected to experience the

largest temperature and concentration changes, thus the control volumes are smallest at the grate surface and increase exponentially up the bed. The nodes are situated in the centers of the control volumes, as shown in Figure 4.

The control volume grid was generated by a scheme that allowed prespecified bed heights to be divided into a known number of exponentially increasing slices, or control volumes. The distance of each control volume interface from a defined starting point was calculated as:

$$x_i = A\,(\exp(\delta\,(i-1)) - 1)$$

where i represents the the ith interface height being calculated, A is a constant with dimensions of m, and δ is a spacing that is determined by the desired number of divisions and the bed height to be subdivided as follows:

$$\delta = \frac{1}{N-1} \ln\left(\frac{h}{A} + 1\right)$$

where h is the desired bed height in m and N-1 is the desired number of control volumes.

4.1.3. Discretization of governing equations

The governing equations were then transformed into a set of discrete, algebraic equations according to the grid defined above. Each algebraic equation was written in terms of a central node, P, and involved the "north" and "south" neighbours of this node, denoted by N and S respectively. Thus, for each of the six defining differential equations given in Section 3.0, an algebraic equation of the form

$$a_P\phi_P = a_N\phi_N + a_S\phi_S + b \qquad (4\text{-}1)$$

was written, where ϕ is the dependent variable being solved for and a_N, a_P and a_S are its coefficients at each of the nodes N, P and S. The term **b** in the equation represents the source term for the dependent variable and involves reaction, transient or heat transfer terms. The physical and transport properties at each node P varied with its height in the bed and were thus calculated separately. Coefficients as shown in (4-1) arise from the discretization process and were developed for each of the governing equations (3-2)-(3-6) and (3-12). The general forms of these coefficients are shown in Appendix A.

Equation (4-1) represents a fully implicit solution, which means that the values of the dependent variables at node P are linked to the *current* values (as opposed to values from the previous time step) of the dependent variables at nodes N and S. In this type of approach, the values of ϕ_P are not *explicitly* obtainable from discretized equations of the form (4-1), and thus the latter must be solved simultaneously. Where possible, implicit solutions are preferred to explicit solutions because the emergence of physically unrealistic results is prevented by their form (Patankar, 1980). For this reason, the implicit solution method is employed in this work.

A further method that avoids the emergence of unrealistic results is the use of power-law differencing schemes (Patankar, 1980) in the representation of the combined effects of convection-diffusion and convection-conduction in the species and energy balances respectively. These are employed in the discretization of the above-mentioned balances and detailed in Appendix A.

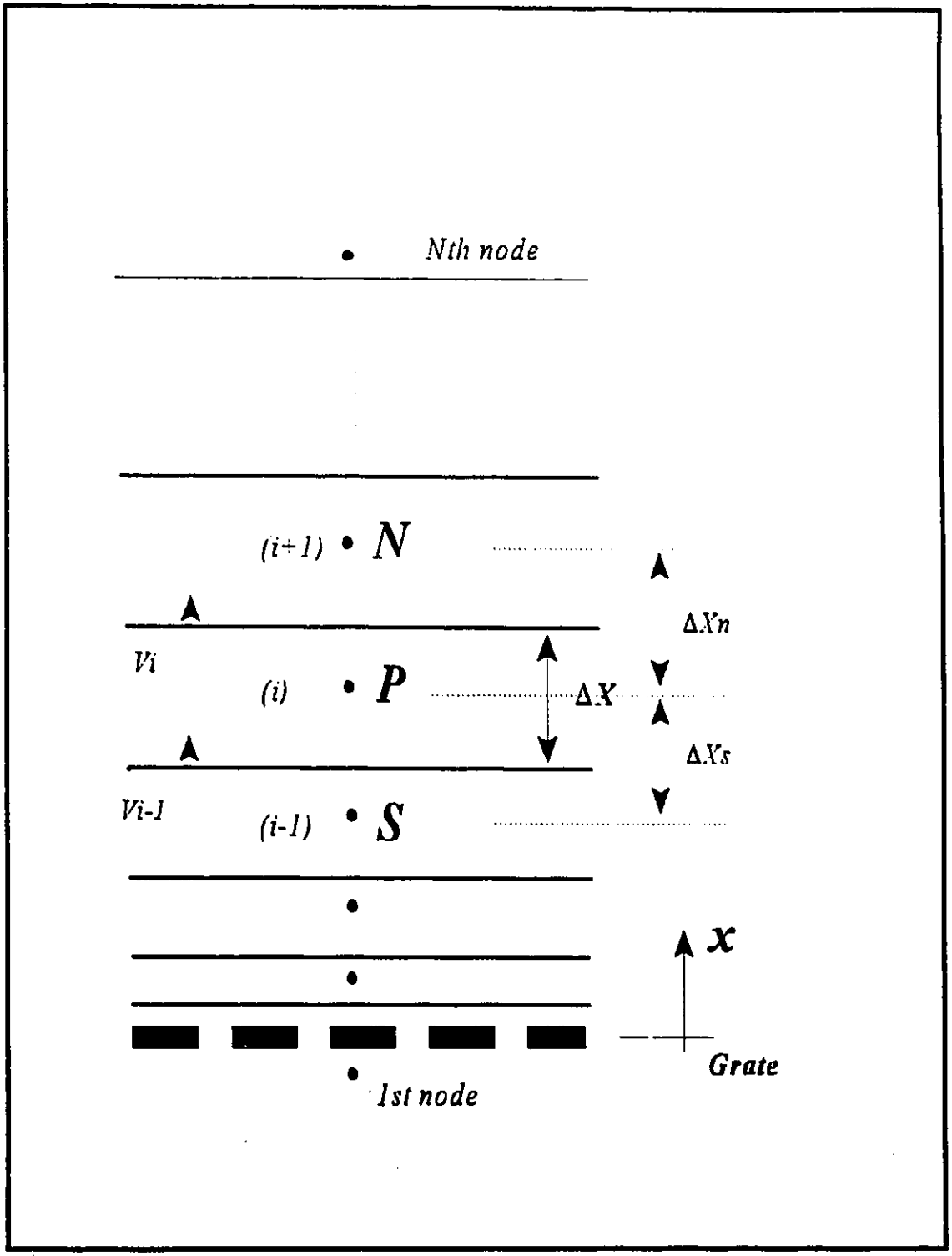

Figure 4: Diagram of the discretized combustion bed showing control volumes, three neighbor nodes and velocity subscript conventions

4.2 Solution Technique and Algorithm

Because the numerical problem of packed bed combustors as specified above involved transport equations that were coupled by velocities, reaction and heat transfer terms, an iterative procedure was used to solve the discretized governing equations for each dependent variable ϕ (shown in Appendices B and C). The equations for particle surface conditions were solved in conjunction with the governing equations, because of their effect on free stream species concentrations through the surface reaction rates G_1 and G_2.

The timescale of the problem was divided into time steps of uniform length Δt and a converged solution obtained for each of the nodes in the bed shown in Figure 4 over each time step. A converged solution for a given timestep was considered to have been reached when the gas temperatures obtained at each node in the bed were equal to within 0.1 °C for 2 consecutive iterations. The progress toward steady state was checked by both a steady state energy balance on the entire bed and the time derivative of the gas temperatures. The latter was considered to be the best indicator of steady state because the energy balance seemed more subject to machine error and small steady-state oscillations. Steady state was thus reached when the average temperature change at each of the nodes was less than 0.1 °C over one time step.

Solution of the species, particle number and energy balances required a tridiagonal matrix algorithm (TDMA), the details of which are given in Patankar (1980). The solution of the mass balances was simpler because of the unidirectional nature of convective mass fluxes; here, each node was solved for in sequence, starting from the bottom of the bed. The

order of solution of the equations was dictated primarily by the variables required to fully define the conditions for each and is given by the flow diagram in Figure 5. No particular attempt was made to optimize the solution algorithm.

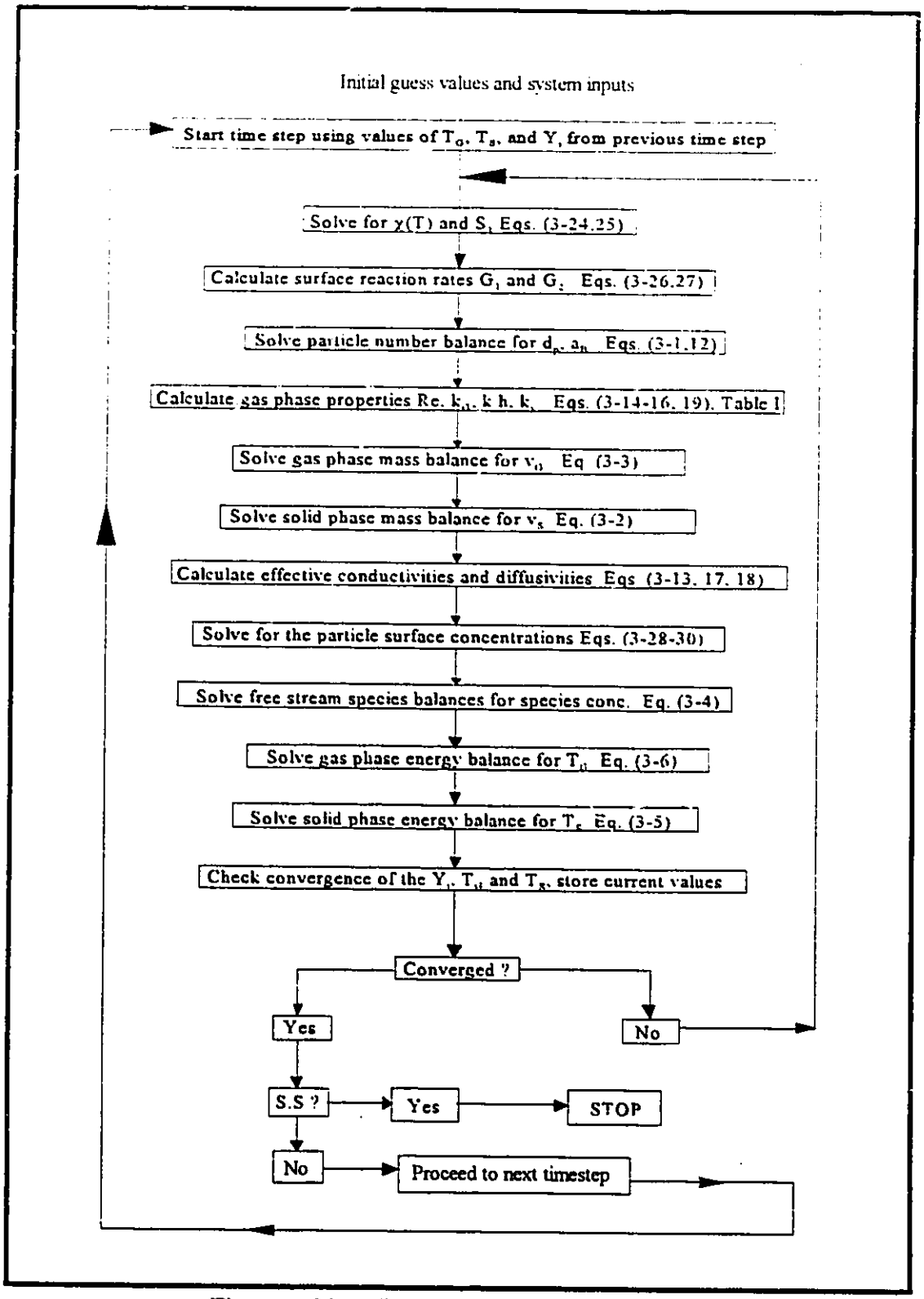

Figure 5: Flow diagram of the solution algorithm

The primary inputs to the simulation were the system constants such as the void fraction of the bed, molecular weights, the ambient pressure, coefficients for the calculation of heat capacities, initial estimated temperatures, initial surface reaction rates and gas concentration profiles (by mass) for the bed, stoichiometric coefficients, and heats of reaction. Also required were the temperatures of the radiative boundaries at the bottom and top of the bed, representing the ash hopper and the heat transfer surfaces above the bed respectively. These constants and estimated inputs were the same for each run of the simulation.

For the purposes of simplicity, and because little was known about the effect of alternative guess values on the progress of the iterations, the initial gas concentration profiles in the bed were assumed to be flat and equal to the atmospheric levels for each gas. The initial total reaction rate, G at the surface of the particles was set to zero and the gas and solid temperatures were initially assumed to be uniform and equal to a temperature sufficient to allow ignition of the bed (about 1500 K). The top and bottom radiative boundaries of the bed were assigned temperatures of 300 K and 350 K based on the estimated temperature of surfaces above the bed and the estimated temperature of the ash hopper. These input parameters are shown in Appendix D in the first data file of the program listing.

The input variables for the simulation consisted of the velocity and temperature of the entering air, the diameter, density, ash content and temperature of the char particles being supplied to the bed, the desired height of the bed, the thickness of the grate, the number of control volumes in the bed and the length of the time step. These were changed to match the conditions of the bed being simulated and are given in the second data list in Appendix D.

The above mentioned inputs were used to begin the iterative loop shown in Figure 5. In general, the order of execution of the steps in this loop was determined by the variables required for each step. The reaction rates at the surface of the particles, for instance, were required before the new particle diameters could be determined; these, in turn, were required for the calculation of the gas phase properties shown in step 5. The order of execution of certain steps is rather arbitrary, such as the placement of the surface stoichiometry step (step 2) before the calculation of the surface rates. Step 2 is required only in the solution of the species and solid phase energy balances and could just as easily have preceded step 10. Likewise, the particle surface gas concentrations are only used in the calculation of surface rates, and could thus have been solved at any point in the loop without adverse effect on the iterations.

Many of the steps shown in Figure 5 also included the calculation of the gas and solid properties required to execute them. Where convenient, the calculations of these properties were included in the subroutines for those steps. More lengthy calculations, however, were relegated to function subroutines that calculated gas densities, specific heats and mean specific heats. These excursions from the principal solution path are not shown for the purposes of simplicity. Readers requiring greater detail are referred to the program listing contained in Appendix D.

4.3 Numerical Stability

4.3.1 Requirements for reaction source terms

One of the characteristics of reactive flow is its inherent numerical instability. Highly exothermic reactions such as the CO oxidation reaction in the gas phase of packed bed char combustors cause large temperature and concentration transients that can wreak havoc on the iterative progress of any solution. Several numerical approaches, such as operator splitting methods (Radhakrishnan and Pratt, 1986) and quasi-steady state solutions, are possible in this instance, but were found to be impractical in this study because they gave inaccurate results and required excessive computer time. Previous works of this nature have assumed equilibrium to prevail in the gas phase and have thus skirted the difficulties arising from the use of finite-rate kinetics. Such an assumption is inappropriate for packed bed combustion because of the greater importance of the oxidation zone, as previously mentioned.

(A) Linearization

The key to ensuring stability in the solution of discretized equations lies in the handling of the overall reaction source terms for the chemical species, which must first be linearized. This must be done in a way that ensures that a_P, a_N and a_S remain positive. Patankar (1980) recommends grouping the source terms for each species in ϕ- independent and dependent parts of an overall source term:

$$S = S_C + S_P\phi_P \qquad (4\text{-}2)$$

where S represents the overall source term. S_C is then assigned to the **b** term in (4-1), and S_P to the coefficient a_p. Since the overall reaction source term S originally appears on the right side of the discretization equation, S_P must be negative to ensure a positive a_p. This general approach was used for all the chemical species (O_2, CO_2 and CO) being tracked by the simulation.

(B) Ensuring always-positive variables

Most reaction rates involve Arrhenius expressions, however, and are therefore linearized by making the rate independent of current values of ϕ, where ϕ represents temperature or concentration. This puts the entire source term S into S_C, which can cause problems in cases where (4-1) is dominated by negative reaction sources for a certain species. Negative sources make it possible to obtain negative concentrations, which can corrupt the solution.

This gives rise to a further stability criterion, which is that S_C must always be positive when the values of the dependent variable ϕ are known to be always positive. Occasionally, however, such an arrangement is impossible because of the nature of the source terms making up the overall source term S, as mentioned above. In char combustion, O_2 has only negative source terms, since O_2 is consumed by carbon and CO in the oxidation zone. The other species, CO and CO_2, have both positive and negative source terms. To ensure always-positive species concentrations and mass fractions, an artificial S_P term must be created from the negative source terms (originally in S_C) as follows :

$$S_P = \frac{S_C}{\Phi^*_P}$$

where Φ^*_P represents the value of Φ_P from a previous iteration. This then creates a negative S_P as desired by the first criterion and leaves the remaining (positive) source terms in a positive S_C. As convergence is reached, Φ^*_P approaches Φ_P, and thus the final solution involving (4-2) is unchanged.

This above technique was applied to the CO consumption term, which exhibited a tendency to drive the CO concentrations in the bed to negative values when temperatures in the oxidation zone became sufficient to activate the highly exothermic CO oxidation reaction. The temperature source term for the endothermic CO_2 reduction reaction in the gasification zone was given a similar treatment, but this was of less importance because of the considerably lower solid temperatures and reaction rates in this zone. All the transformed source terms used in this work are shown in Appendix B.

(C) Constraining variables according to physical limits

The value of putting part of the reaction source term into S_P is twofold: it ensures positive values of Φ, and it damps out oscillations in the progress toward a converged solution. The latter characteristic of S_P is useful in cases where the reaction source term dominates to the point where overly large species concentrations are obtained. In this case, the source term can be linearized in such a way that the magnitudes of S_P and S_C change to

keep ϕ within physically reasonable limits.

This can be achieved by the linearization:

$$S_C = \frac{S^* \tilde{\phi}_P}{\tilde{\phi}_P - \phi^*_P}$$

and

$$S_P = - \frac{S^*}{\tilde{\phi}_P - \phi^*_P}$$

where $\tilde{\phi}$ represents a physically-imposed limit for ϕ_P, always 1.0 or less for species concentrations, the ϕ^*_P are previous iteration values of ϕ_P, and S^* is the value of the reaction rate corresponding to ϕ^*_P.

This linearization was applied to CO_2, which is produced exothermically in the gas phase of the oxidation zone. The iterations for this species frequently became unstable in instances of low gas flow rates to the reactor, because the increased residence time of the gas in the oxidation zone accelerated the CO oxidation reaction to the point where unreasonable CO_2 concentrations developed before they could be checked.

Since CO_2 had no consumption term in the gas phase, the creation of an S_P term in this linearization produced a much-needed stabilizing effect. As in the linearization for always positive variables, as the converged solution is reached, ϕ^*_P approaches ϕ_P, and

$$S = S_C + S_P\phi_P = \frac{S^{\cdot}(\tilde{\phi}_P - \phi_P)}{(\tilde{\phi}_P - \phi^{\cdot}_P)} \cong S^{\cdot}$$

Thus the overall representation of the rate is unchanged. The specific treatment of this term in the combustion simulation is shown in Appendix B.

The physical limit for CO_2, was defined by stoichiometry and varied along the bed. This limit was therefore unknown, but expected to be somewhat less than 1.0. A more conservative limit was therefore applied where:

$$\tilde{\phi}_P = (\phi_P^{\cdot} + 1)/2$$

The latter ensured that ϕ_p only progressed halfway toward a physical limit of 1.0 in one iteration, and was sufficient to allow convergence in the cases tested. In cases of severe instability, the upper limit of 1.0 above could be reduced to 0.5, which is still reasonable in terms of the observed maximum (about .20-.25), and would create a larger damping effect.

4.3.2 Requirements for particle to gas heat transfer source terms

This term was linearized in the gas and solid energy balances by making the heat transfer rate h dependent on the previous iteration values of Re and Ar as required and then separating it into ϕ-independent and dependent terms as shown above. The main requirement in performing this separation was to ensure equal heat gain and loss terms in the gas and solid energy balances. This was achieved by first solving the gas phase energy balance with

$$S = S_C + S_P\phi_P = h^* a^o_B \, (T^*_S - T_G)$$

where a^o_B is the previous time step value of the specific surface area, a_B, ϕ_p represents T_G, and h^* is the heat transfer coefficient based on the previous iteration values of Re and/or Ar. T^*_S is the previous iteration value of the solid temperature.

The solid phase energy balance was then solved with :

$$S = S_C = h^* a^o_B \, (T_G - T^*_S)$$

where the gas temperature T_G represents the current gas phase temperature as obtained from the solution of the gas phase energy balance and T^*_S is the previous iteration value of T_S as used in the heat source transfer term for the gas phase above. This procedure ensured that the same amount of heat was transferred in both energy balances and met all stability requirements for S_C and S_P.

4.3.3. Time step and control volume requirements

The choice of time step and the size of the chosen control volumes were found to affect stability. Control volumes that were too thick often spanned concentration and temperature gradients that were too large for the simulation to handle and caused the iterations to diverge. This was prevented by increasing the number of control volumes for thicker beds.

The opposite was found for the choice of time step. For very thick beds, small timesteps (1-3 s) failed to lead to convergence, indicating that longer time steps actually *increased* stability. This was attributed to the fact that large time steps increased the importance of the transient with respect to the other terms in the discretized equation, which may have damped out any instabilities generated by the source terms.

The length of the time step and the number of control volumes used for each run of the simulation were established by trial-and error based on successful convergence to a steady state solution; generally 40 control volumes and 5 s time steps were allowed for beds over 0.6 m in height, 30 control volumes and 3 s time steps for beds over 0.3 m and 20 control volumes and 2 s time steps for beds under 0.3 m. These choices resulted in adequate resolutions of the oxidation zones for the runs without consuming excessive amounts of computer time. It should be noted here that the predictions obtained from the model were surprisingly insensitive to both the control volume size and the length of the timestep. Since these parameters are most relevant in solving the equations for the relatively fast-moving gas phase, this indicates that the time scale of the bed as a whole is probably controlled by the thermal inertia of the solid.

5.0 RESULTS AND DISCUSSION

The predictions obtained from the char combustion simulation were analysed for sensitivity to different reaction rate kinetics and heat/ mass transfer correlations as obtained from the literature. A comparison of these predictions with results of appropriate experiments documented in the literature was also done to verify their reliability. Most of the experimental combustion contained inadequate information to enable a study of all the variable parameters (heat and mass transfer coefficients, effective thermal conductivities and reaction rate constants) in the model. This was particularly true when it came to distinguishing between the two phases, since the thermocouples in the experimental beds could only yield a single temperature. Thus, no attempts were made to "fit" the predictions to the data.

5.1 Sensitivity Analysis

Several options existed in the choice of heat and mass transfer coefficients and reaction rates for the simulation, requiring that a sensitivity analysis be done first to gain an understanding of the effects of these parameters and allow for an informed selection. This was achieved by superimposing the predictions obtained for each combination of parameters on the most reliable experimental curves and choosing the parameters that resulted in the best approximations to those curves. The packed bed coke combustion experiments of Nichols (1935) were chosen as the reference for the sensitivity analysis because they represented the most recent study found in the literature to give both temperature and gas concentration profiles. The configuration of the packed bed in these experiments best matched that of the

simulation, in that both involved beds with of constant height (maintained by a top feed of fuel) and both involved steady state conditions.

The graphical output from a typical model run is shown in Figure 6. The solid lines represent the predictions of the simulation and the overlaid data points were extracted from Nichols' (1932) experimental data. The graph essentially represents the bed lying on its side, so that the top surface of the grate falls along the vertical axis, followed by the oxidation zone (0-4 cm) and then the gasification zone (from 4-60' cm). The boundary between the oxidation and gasification zones is marked by the complete disappearance of oxygen and the beginning decline of the CO_2 concentration. The temperatures peak in the oxidation zone, where a maximum temperature difference of about 500 K is observed between the gas and solid phases, supporting the earlier argument that assumptions of equal gas and solid temperatures are invalid for this zone.

The effects of different surface reaction kinetics, gas phase reaction kinetics and particle-to-fluid transfer rates on predicted profiles of the type shown in Figure 6 are summarized below. The effects of bed depth, particle size, air flow rate and fuel ash content on bed performance were also examined and are included in the analysis to illustrate possible design applications.

5.1.1. Effects of surface kinetics

(A) Carbon oxidation

The rate of surface oxidation of C to CO and CO_2 (R4) was increased by a factor of 10 and the resulting predictions were compared to those obtained with the original rate (given

by equation 3-26) to verify that this reaction was diffusion controlled. Under diffusion control, the general shape and magnitude of the profiles and the location of the various maxima and minima were expected to be the same, regardless of the kinetics of R4. As expected, no significant differences (ones visible from an overlay of the resulting curves) were observed between the two sets of predictions. Thus, the surface oxidation of C to CO and CO_2 was shown to be diffusion controlled, and the rate expression of Field (1969) to be adequate as stated before.

(B) CO_2 reduction

Figures 6 and 7 show predictions obtained from the simulation for two different rates of the CO_2 reduction reaction (R3) under identical conditions for an air inlet temperature of 300 K. These are superimposed on the experimental values obtained by Nichols (1935) obtained for similar conditions. The (R3) reaction occurs primarily in the gasification zone of the bed (0.04-0.7 m), so its effect on bed temperature and gas concentration is greatest there. Decreasing the rate increased solid temperatures, because of the endothermicity of this reaction, and decreased the CO production in the top portion of the bed, but had no effect on the position of the maxima and minima of the profiles. Changes to the preexponential factor of the (R3) rate expression had nearly the same effect as changes to the activation energy because of the isothermal nature of the gasification zone.

Figure 6 shows predictions obtained with the rate for subbituminous coal char as correlated by Goetz *et al.* (1982). The rates given by this author for chars derived from higher rank coals proved to be too slow, and that given for the lower rank coal chars too fast,

hence the rate for subbituminous coal chars was chosen as best representing the reaction. The predictions obtained from the simulation were best in the oxidation zone of the bed (0~0.04 m), showing greater deviations from experiment with increasing bed height. The overprediction of CO concentrations and underprediction of solid temperatures in this zone indicated that the endothermic CO_2 reduction reaction was proceeding too quickly. The rate of this reaction is known to proceed at different rates for different chars according to their structure (Goetz *et al.*, 1982). Thus, the structure of the subbituminous char modelled by the given rate expression may well have differed from that of the coke being burned in the experiments. This theory was tested by successive reductions of the preexpeonential factor for the reaction and led to results shown in Figure 7. Here, with the preexponential factor reduced from 103 to 34.5 kg m^{-2} s^{-1} kPa^{-1}, predictions of CO and CO_2 concentration are much improved and the solid temperatures more closely approach those observed in experiment. Because of this improved agreement, Figure 7 was made the base case for future tests and subsequent runs were all done with the reduced preexponential factor.

5.1.2 Effects of gas phase kinetics

A comparison of Figures 7 and 8 demonstrates the effect of changing the CO oxidation rate. The base case, Figure 7 was generated with the rate kinetics of Howard *et al.* (1973), whereas the kinetics employed in Figure 8 were those of Westbrook and Dryer (1981). All other conditions for the two runs were the same. Contrary to statements made in the literature, the difference between the two CO oxidation rate expressions was not great and restricted to the oxidation zone. The Westbrook and Dryer (1981) rate had a much

higher preexponential factor, and an only slightly higher activation energy, which caused CO to be oxidized more rapidly at low temperatures for this rate expression. This is evident from the more rapid consumption of the CO peak in the oxidation zone in Figure 8 and the zero CO concentration in the last half of this zone. Once the CO is consumed, however, there appears to be no difference in the concentration profiles. In fact, the gasification zone concentration and temperature profiles in Figures 7 and 8 are virtually identical. This was attributed to the lower activation energy of the Howard *et al.* (1973) rate, which doubtless compensated for higher preexponential of the other rate at high gas temperatures. Because the Westbrook and Dryer (1981) rate is believed to overpredict CO oxidation rates for fuel-rich conditions (Hautmann *et al*, 1981,), such as those found near the end (top) of the oxidation zone, where the O_2 is nearly depleted and there is an "excess" of fuel, the Howard *et al.* (1973) rate of Figure 7 was preferred and used to conduct the remaining tests.

5.1.3 Heat and mass transfer effects

Figures 7, 9 and 10 show the predicted curves given by the simulation for different particle-to-fluid heat and mass transfer correlations. All other conditions for the bed were kept constant for these trials in order to isolate the effects of heat and mass transfer. Overall, variations in the heat and mass transfer coefficients had the greatest and most complex effects on the bed because their influence on gas and solid temperatures also affected the progress of reactions. It was found that these variations mainly affected the oxidation zone, where they had a marked effect on the position of peak temperatures and concentrations in the bed. High heat and mass transfer rates tended to accelerate processes in the bed, causing peak

temperatures and concentrations to occur closer to the grate, whereas low heat transfer rates had the opposite effect.

Figures 7 and 9 are essentially the same, implying that similar heat and mass transfer rates were predicted by Yoshida *et al.* (1962) and Chu (1953) for the conditions of the bed under study (see Figure 3), and show good agreement with the experimental CO and CO_2 concentrations obtained by Nichols (1935). The predicted oxidation zone (0-0.04 m), however, appears to be 2-3 cm too thin and temperatures in the gasification zone (0.04-0.7 m) of the bed are underestimated.

The latter problems were improved in Figure 10 with the use of the Bhattacharyya and Pei (1975) heat and mass transfer relationship, which predicted lower heat and mass transfer coefficients because of the reduced contribution of conductive heat transfer mechanisms in the experiments. The reduced rate of heat transfer is evident in the larger difference between gas and solid temperatures in the bed and the higher overall bed temperatures. The main result of this reduced heat transfer was that the hot solid (heated by the exothermic oxidation (R4) of carbon to CO and CO_2) lost heat more slowly, delaying the heating of the gas phase and the onset of CO oxidation. The gas phase temperature reached a higher and later maximum because of this delay (2300 K as opposed to 2200 K), because a higher concentration of CO was present to activate the reaction. Thus, both the solid and the gas maintained higher average temperatures throughout the bed with the use of the Bhattacharyya and Pei (1975) heat transfer relationship, improving the agreement with the experimental temperature profiles. The latter was deemed to be less of an indicator of model accuracy, however, because temperature measurements obtained in packed beds represent some sort

of average of the gas and solid temperature and are thus less reliable than concentration measurements.

Evidence of a reduction in mass transfer rate is more difficult to observe from Figure 10, but can be seen in the increased spread of the CO peak in the oxidation zone and the increased thickness of the oxidation zone. In Figures 7 and 9, CO is produced almost instantaneously. Since the only significant CO-producing reaction occurring at this point in the bed is (R4), which is diffusion-controlled, the sharpness of the peak in these figures indicates a high diffusion rate of oxidant (O_2) to the particle surfaces. In Figure 10, this peak develops a little further up the bed, showing that diffusion rates are reduced, and reaches a greater maximum because of the delay in CO oxidation to CO_2. This reduction in diffusion rate, combined with the delay in CO oxidation described above, increases the thickness of the oxidation zone to agree with the experimental profiles; the CO oxidation reaction is inactive in the first 1-2 cm of the bed because of the low gas temperatures and therefore fails to consume the oxygen that bypasses (R4).

The predictions shown in Figure 10 for the oxidation zone concentrations of CO and CO_2, however, showed a greater deviation from experiment than those observed in the runs represented by Figures 7 and 9, thus the merit of using the lower heat and mass transfer coefficients was uncertain. The failure of the Bhattacharyya and Pei (1975) coefficients to perform well may have been related to the somewhat different from of this correlation, which included a dependency on the Archimedes number, Ar, and may have resulted in a dependency of heat transfer on factors other than the Reynolds number. The use of this correlation for packed bed combustion also extended it to gas flow rates that were lower than

those for which it was intended (.1-.9 m/s as opposed to 1-2.5 m/s), which may have resulted in further discrepancies. The heat transfer relationship of Yoshida *et al.* (1962) was therefore chosen to simulate the remaining experiments because of its better performance in the oxidation zone, and Figure 7 was considered to represent the best prediction. All subsequent runs of the simulation were therefore executed with the adjusted rate for subbituminous coal char recommended by Goetz *et al.* (1981), the CO kinetics of Howard *et al* (1973), and the fluid-to-particle transfer coefficients derived by Yoshida *et al.* (1962).

5.1.4. Other effects

There are a number of other factors that could have affected the accuracy of the predicted profiles, particularly in the oxidation zone, where high temperature and concentration gradients prevail. The use of accurate correlations for the effective gas and solid thermal conductivities is crucial in such instances, as is an accurate representation of the effective species diffusivity, because the strong role of conduction and diffusion in this zone. However, since none of the experimental data found in the literature provided detailed temperature and concentration measurements for the oxidation zone, the possible magnitude of errors stemming from these sources could not be ascertained.

5.2 Comparison with Experimental Data - Validation

The reliability of the char combustion simulation was tested by comparing its prediction to sources of experimental data in the literature. Only three sources giving gas species and temperature profiles applicable to large particle char combustion were found, but these covered a sufficient range of conditions to verify the trends predicted by the simulation. The first of these was a series of overfeed coke combustion experiments conducted by Nichols (1935), which examined the effects of air preheat on combustion in 60 cm beds of 3 cm coke particles. The second, a transient experiment (Eapen, 1977), covered a smaller particle size and bed thickness (1 cm and 40 cm respectively) and was used to validate the transient behaviour of the simulation. The third source of data, a set of experiments conducted by Kreisinger and Augustine (1916) which examined overfeed combustion of 3 cm coke particles in 30 cm beds, was deemed to be somewhat out of date, but was included because of the rarity of such experimental data.

5.2.1 Comparison with Nichol's experiments - effect of air preheat

Figures 7, 11, 12 and 13 show the relationship between predicted and experimental gas concentrations and temperatures for air inlet temperatures of 300, 478, 589 and 700 K respectively. The predicted curves were obtained with the "optimal" transport coefficients and rate expressions as chosen in the sensitivity analysis above. In general, the simulation reproduced the experimental results quite well. In most cases, the deviations from the experimental data had physical causes, or could be attributed to known limitations in the

transport coefficients. These points are outlined in more detail below.

Despite these hindrances, the effects of air preheat were well predicted by the simulation. The experiments indicated that gas preheat had little effect on the average temperature in the bed, and this result was also obtained in the simulation. The reason for this was that higher initial gas temperatures caused a proportional increase in the endothermic reduction reaction (R3) through heating of the solid. This kept solid temperatures low and allowed for cooling of the gas by heat transfer. Both the experiments and the simulation also predicted higher exit CO concentrations for higher gas preheats. This appeared to be the most significant effect of preheating the air supply, and was due to the slightly higher solid temperatures in the bottom half of the gasification zone (as a result of heat transfer from the preheated gas) which resulted in faster reduction of CO_2 to CO by (R3). The experimental results seemed to indicate a slight shift in the curves toward the grate at higher preheat temperatures, and this was matched by the simulation, although not to the same degree.

Many of the deviations from the experimental oxygen concentrations could be attributed to faulty sampling techniques on the part of the experimenters, and the use of outdated equipment. In the experiments, the sampling of the bed was conducted by inserting a 1.3 cm diameter sampling probe horizontally into the bed at various heights via ports in the side of the reactor. Since the probe insertion was perpendicular to the direction of flow and a vacuum was applied to withdraw the gas samples from the bed, such sampling failed to represent point measurements. Instead, the resulting sample probably represented concentrations upstream as well as downstream of the actual insertion point, with the upstream concentrations being favoured because of the direction of flow.

This possible experimental smearing effect may explain the results shown in Figures 7 and 11, where a net reduction of CO_2 to CO can be seen to occur in the oxidation zone. This was not predicted by the simulation and is unlikely, as CO_2 reduction is not expected to occur until all the O_2 has disappeared. The error was therefore attributed to the experimental oxidation profiles. Samples taken in the oxidation zone are the least reliable because of the large concentration gradients there. This is particularly true of oxygen concentrations, which are reduced from atmospheric levels to zero in the first 2-3 cm of the bed. The oxygen concentrations in such samples are likely to be too large because of the formation of channels in the bed during gas extraction by the probe, which would allow oxygen to reach the probe before it had time to react with the char in the bed and give rise to the overly thick oxidation zone observed in Figure 7.

Temperature was consistently underpredicted by the simulation for this set of experiments. The experimental temperatures, however, reflected processes in the solid as well as the gas; thus the possibilities for comparison were limited. The method used to obtain these temperatures may also have been subject to error, since this was done by sighting an optical pyrometer down the channels left by the probes. Such channels are constantly collapsing as the bed settles, and consistent measurements are difficult to obtain. It is also very difficult to define the precise location of such measurements. No experimental errors for these measurements were stated by the authors. From the appearance of the experimental and predicted profiles in the oxidation zone (Figures 11-13), however, it appears that the temperatures obtained by such measurements are closer to those of the solid than the gas.

The deviation of the predicted CO and CO_2 concentrations from the experimental

values in Figures 11-13, however, could not be explained by the trends arising from the sampling error postulated above and were thus believed to be indicative of faulty reaction kinetics. The discrepancy in the shape of the CO and CO_2 curves seemed to indicate that the activation energy for reaction (R3) was too high, (or that the CO_2 reduction rate was too low). When further tests were conducted, it was found that lower activation energies improved the predictions for the cases with high preheat, but gave excessively fast rates for the cases with low preheat temperatures. This was expected, as the activation energy of 177.7 kJ mol^{-1} used previously had given good predictions for the 300 K case. This failure of the rate to match all the cases seemed to indicate that pulverized char combustion kinetics of Goetz *et al.*(1982) did not extend very well to the combustion of larger char particles.

There are several other possible reasons for this discrepancy in CO and CO_2 concentration: the accuracy of the heat transfer coefficient and the gas effective conductivity are also suspect, as they were derived for non-reactive beds and for temperatures for below those of combustion beds. Since these discrepancies grew with increasing preheat temperature, a consistent problem may have existed in the correlation of one or both of these coefficients.

The discrepancies observed in Figures 11-13 are very similar to those in Figure 10, where the heat and mass transfer coefficients were too low. In the present work, the magnitudes of all known corrections to heat and mass transfer coefficients, such as that for the effect of mass transfer to and from the particle surface, and that for the effect of species interdiffusion, have been investigated and found to be quite insignificant. It was therefore assumed that the discrepancies stemmed from some other (possibly unknown) problem, such

as the failure of heat transfer coefficients developed for non-reactive, low temperature packed beds to hold for reactive, high temperature beds. Pathengey and Kovenklioglu (1989) have studied the effects of endothermic and exothermic reactions on the particle-to-fluid heat transfer coefficient in packed bed reactors and found this coefficient to increase in the presence of exothermic reactions and decrease in the presence of endothermic reactions. The reason for this, however, has not yet been ascertained. (This study was done for catalytic reactors, but it possible that similar effects exist in packed-bed combustion.) If the simulation had been able to incorporate such a variation, the temperature in the gasification zone would have been higher and the CO_2 reduction rate would have increased -a requirement indicated by the discrepancy in the predicted and experimental CO curves.

An increase in the gas effective conductivity would also improve the predictions of the simulation; high effective thermal conductivities cause sharp temperature peaks such as those observed in the gas phase to flatten out, reducing the peak temperature, but resulting in a higher overall temperature for the gas and thus the bed. The gas phase effective conductivities used in this study may have been too low, or have increased too slowly with temperature, resulting in lower temperatures for the gasification zone, which would in turn have decreased the local rate of (R3) and caused the predicted CO curves to undercut the experimental ones as shown in Figures 11-13.

The inability of the simulation to handle particle size distributions may also have contributed to deviations from the experimental profiles: the surface kinetics are quite sensitive to particle size, as previously mentioned, and might have yielded considerably different results if the effects of non-monosized particle size had been accounted for. (To the

best of the author's knowledge, the literature contains no treatments of beds with non-monosized particles.)

5.2.2 Comparison with Eapen's transient profiles

Figures 14 and 15 show predicted and experimental gas concentration profiles for the transient combustion of 1 cm coke particles in a 0.38 m bed at intervals of 1 and 3 hours. The air velocity for these experiments was unusually low (0.036 m/s), making it possible to examine the performance of the simulation for a quite different set of operating conditions. A disadvantage of these conditions was that this flow rate gave rise to packed bed Reynolds numbers as low as the transition value of 2, which may have invalidated some of the assumptions based on turbulent flow, such as the assumption of an effective Lewis number of 1, on which some of the heat and mass transfer developments are based.

The experimental bed was contained in a sealed reactor and allowed to burn down over the time of the runs (decreasing bed height, no fuel feed). This effect could not be accounted for in the simulation because the latter was designed for open beds of constant height. The experimental and predicted concentrations for the shortest time period (1 hr) were therefore expected to be most comparable, because the experimental bed would be closest to its original height. The original (R3) rate for subbituminous coal char prescribed by Goetz *et al.* (1982) seemed to yield the best results for this run and was therefore used to simulate both of the transient runs in this comparison.

Except for the gas concentrations at 0.02 and 0.04 m, the predictions for the 1 hour case (Figure 14) were very good. At 0.02 m, the experimental CO and CO_2 concentrations

are lower than the predicted values, whereas the O_2 concentration is higher. This discrepancy is likely due to smearing effects similar to those described in the previous section. In the experiments, a single probe was inserted vertically down into the bed to obtain measurements. A diaphragm pump was used to extract the gas samples. Near the grate, the vacuum created by the probe may have formed channels in the bed, allowing upstream gases to enter the probe before they could react with the surrounding fuel. The slightly higher predicted CO and lower CO_2 values obtained near the top of the bed were attributed to the fact that the experimental bed was probably thinner than the simulated bed by this time, and thus had a lower gasifying capacity.

Slight deviations in the predicted results due to the burnout of the experimental bed are somewhat visible in Figure 15, where the experimental CO concentrations exceed the predicted values by almost 5%. This was unexpected, since thinner beds usually result in lower exit CO concentrations. Since the experimental bed was covered by a refractory-lined hood, however, the temperatures at the top of this bed could have been considerably higher than those in the simulated bed because of the lower radiative losses. This would have resulted in the higher CO_2 reduction rate observed in the experiments.

The predicted oxidation zone remains unchanged over the two hours between the tests, indicating that profiles here are rapidly established, whereas the gasification zone takes much longer to reach equilibrium. This failed to occur in the experimental bed, because the oxidation zone collapsed with the rest of the bed. The experimental oxidation zone in Figure 15 should therefore have been thinner than the predicted one. This, however, was not observed, possibly because of the sampling errors mentioned previously.

Figure 15 represents the steady-state conditions for the bed being simulated (if it had been open and supplied with fuel). These were reached a short time before the 3 hour marker for this run. The long time taken for the gasification zone to reach steady state is indicative of the high thermal inertia of the char particles.

Figures 16 and 17 below show gas and solid temperature transients from the bed modelled above. These figures clearly show that many of the thermal changes occurring in the gas phase are either not transmitted to the solid phase at all, or delayed. The initial solid temperatures of 1500 K required for ignition (see Section 4.2.) are not exceeded in the course of the run represented by Figure 17, whereas the gas phase temperatures shown in Figure 16 reach a peak of 1850 K at t=30s during gas phase ignition. The gas temperature peaks in the oxidation zone are not reflected in the solid until much later (t=10' min).

The bulk of the time taken to reach steady state can be attributed to the slow cooling of the char particles via radiative losses from the top of the bed, contact with cold, entering char particles and the progress of the endothermic CO_2 reduction reaction. As such, the length of the transient could be expected to scale with bed depth (because shallower beds would experience higher radiative losses relative to their volume) but not directly, since other factors, such as the reduced turbulence expected in shallow beds, are probably also involved.

5.2.3. Comparison with the experiments of Kreisinger - effect of gas velocity

Figures 18-21 show predicted and experimental profiles for the combustion of a 0.3 m bed of 3 cm metallurgical coke particles at inlet air velocities of 0.14, 0.44, 0.64 and 0.87

m/s. The inability of the simulation to reproduce the experimental results for this set of tests was attributed in part to the sampling method used, and the possible failure, on the part of the experimenters, to completely remove accumulated ash from the bed during testing. The effect of the latter was probably quite significant, as the ash content (16.6%) of this fuel was the highest encountered. The general trends with increasing flow rate predicted by the simulation, however, were physically reasonable and were thus accepted as correct.

The most significant difference between the experimental bed and that modelled in the simulation was the possible presence of ash in the former. This seems to have remained in the bed for the duration of the tests. Ash is inert, and its accumulation in a bed of constant height reduces the volume of bed available for chemical reaction. The results of tests on such a bed would yield profiles equivalent to those observed in thinner beds, but stretched over the height of the thick bed. This trend was observed by Nichols (1935) who ensured that all ash was removed from his experimental bed by agitating it between tests, and is visible in some of the discrepancies between the predicted and experimental results in Figures 18-21. The predictions for the oxidation zones are the worst, which can be explained by the fact that the amount of accumulated ash would be greatest at the bottom of the bed, where combustion has progressed the farthest.

The sampling technique for the experimental bed contained several uncertainties, which may have affected some of the test results. The largest of these was an uncertainty in the flowfield and local temperatures due to the presence of multiple probes. The test points in the bed were sampled simultaneously via probes inserted horizontally into the bed as in Nichol's (1935) experiments. These probes were distributed radially around the furnace at

planes about 4 cm apart and had an outer diameter of 1.6 cm. Since these probes were rather large, and resident in the bed during the tests, they probably had a significant effect on the flow field during gas extraction. This could have caused the distortion in the experimental concentration profiles that can be observed in Figures 18-21. Local temperatures may also have been affected, as each probe was water-cooled.

According to the profiles generated by the simulation, an increase in the air supply rate to the bed causes the profiles to shift away from the grate and allows the gas and solid temperatures to increase. These shifts and increases are proportional to the change in air flow rate. As the gas residence time in the bed decreases, there is less opportunity for heat transfer between the two phases; thus the gas-solid temperature difference also increases. This increase is also roughly proportional to the change in gas flow rate. The gas concentrations exiting the bed stay approximately the same, however, because the increase in solid temperature compensates for the shorter gasification zone and speeds up reaction (R3).

Some of these effects could be observed from the experiments, but, in general the experimental curves were too distorted to be comparable. The order of the test results shown in Figures 18-21 was also random, as several of the runs had to be repeated by the authors. Different runs may therefore have represented different amounts of accumulated ash, which would have confounded the shift in the profiles caused by increasing air flow rates with profile changes caused by ash accumulation.

5.3 Design Applications

5.3.1. Effects of bed depth

Simple analyses of packed bed char combustors that consider only fluid-to-particle mass transfer and do not model the heat transfer processes in the bed, lead to the conclusion that events in the bed scale with particle size, that beds with the same particle size to depth ratio will behave identically and that combustion rates rise linearly with air flow (Spalding, 1955). These conclusions are also approximately true when all bed processes are included, as is shown in the discussion below.

(A) Scaling depth with particle size

Under complete diffusion control, the simple analyses described above predicts that beds of different depths but having the same ratio of particle size to bed depth (the same number of particles) will have very similar steady state temperature and concentration profiles. This is because combustion rates in diffusion-controlled beds depend mostly on the physical process of mass transfer, which are the same on any scale. Combustion rates in kinetically controlled beds, however, depend on the particle surface area per unit volume available for reaction, which varies greatly with particle size. Since the fuel being supplied to commercial combustors is rarely of constant size, it is useful to understand the effects of such size variations on combustor performance.

A comparison of Figures 22 and 23 demonstrates that the conclusions derived from simple packed bed combustor analyses are good descriptors of overall reactor behaviour.

Figure 22 shows the predicted profiles obtained from the simulation with 0.02 m diameter particles stacked to a height of 0.2 m; the predictions in Figure 23 were obtained by replacing the 0.02 m particles with the same number of 0.05 m particles for a bed height of 0.5 m. The same air inlet velocity was used in each case. The profiles in each case are quite similar, and the solid temperature profiles are almost identical. These results were expected, as the most significant solid reaction (R4) is diffusion-controlled, and a fair amount of kinetic control existed in the gas phase. The similarity of the solid temperatures for the two runs further supports the notion that highly accurate rate expressions for the carbon oxidation reaction are not crucial in simulating combustion (Lockwood and Salooja, 1983). This reaction exerts the greatest influence over solid temperatures in the oxidation zone and also dictates the temperature of the gasification zone, since the latter is almost isothermal.

The other profiles only show small differences that can be explained by a reduction in the kinetically controlled rates for larger particle sizes (because of the reduced surface area per unit volume of bed) and a small departure from diffusion control for (R4) at solid temperatures below 700 K. The oxidation zone in Figure 23 occupies a larger proportion of the bed than in Figure 22, (over 1/6 as opposed to 1/8 of the bed), reflecting the slightly reduced rate of oxygen consumption due to larger particles. The use of larger particles therefore shifts the profiles slightly to the left and increases the CO_2 output of the bed somewhat because of the shorter gasification zone, but these differences are really quite small given that the bed scale was increased by a factor of 2.5.

(B) Changing depth only

In beds of different thicknesses where the particle size is constant, the primary factor of interest is that of combustion efficiency. For char combustion processes, 100% efficiency is defined by complete combustion of the char to CO_2, which recovers the maximum heating value of the fuel. In thin char beds, oxygen penetrates far into the bed, and the gasification zone is very thin, allowing a large amount of CO_2 to leave the bed before it can be endothermically converted to CO by (R3). Thus, the fuel is converted primarily to CO_2 and high temperatures are generated, denoting an efficient combustion process. Such a bed is shown in Figure 24. This bed is operating under the same conditions as that in Figure 22, except that its depth is reduced by a factor of 10. Note that almost no CO is produced from CO_2 because of the deep penetration of oxygen into the bed. Relatively thick beds, such as those represented in Figures 22 and 23 have thicker gasification zones, which results in lower CO_2 yields, temperatures and efficiencies.

To predict the performance of a given bed, an operating diagram for a range of bed thicknesses (for beds with the same particle size), such as the one shown in Figure 25, can be generated. Figure 25 shows the relationship between char conversion rates and air supply velocity as generated by the simulation for 2.0, 3.0, 5.0, 25.0 and 55.0 cm beds of 1 cm particles, and the position of these performance curves with respect to stoichiometric combustion (all carbon converted to CO_2) and 50% air deficit (all carbon converted to CO) lines that define the operating range. From this diagram, combustion beds can be seen to be self-regulating; char conversion proceeds at a rate that increases linearly with increasing air supply until the convective losses created by the airstream passing through the bed are such

that the bed is literally "blown out". The latter phenomenon can be observed in the thinnest beds for air velocities of approximately 0.4 and 1.2 m/s. The thickest beds lie very close to the 50% air deficit line, and are thus shown to be quite inefficient, whereas the 5.0 cm bed lies in the centre of the operating range (50% efficiency), and the 3.0 and 2.0 cm beds exhibit efficiencies of approximately 80% and 100 % respectively.

From this diagram, it can be concluded that thin beds are more desirable because of their greater efficiency, but that their operation is limited to low air flow rates because of the potential for extinction. It is also evident from the constant slopes of the operating "curves" on this diagram that the stoichiometry of combustion can only be controlled by adjusting the bed depth and that the combustion rate for a given bed depends solely on airflow. The latter two conclusions are unique to packed bed combustion, as most other combustion systems allow independent control of stoichiometry and burning rate. Through the use of diagrams such as Figure 25, however, an optimal bed thickness and range of air feed rates can be found for the packed bed combustion of particles of any size.

5.3.2 Effects of fuel ash content

The effect of the fuel ash content (by mass) input to the simulation relates to the boundary condition prescribed for the solid mass balance in Section 3.2.1. The particles were assumed to be consumed until only ash remained, and this ash was assumed to emerge from the bottom of the bed as appropriately sized particles. This effect is shown in Figure 26, where the final, steady state particle sizes of 30% and 0% ash chars are compared. The final diameter of about 1.33 cm for the 30% ash char represents about 0.3 of the original volume

as expected, whereas the final diameter for the 0% ash char clearly approaches zero. Any amount of ash in the particles also translates to a cooling effect because of the convective heat loss created by ash leaving the bed, but this is not shown here because the difference for the range of ash contents studied was insignificant.

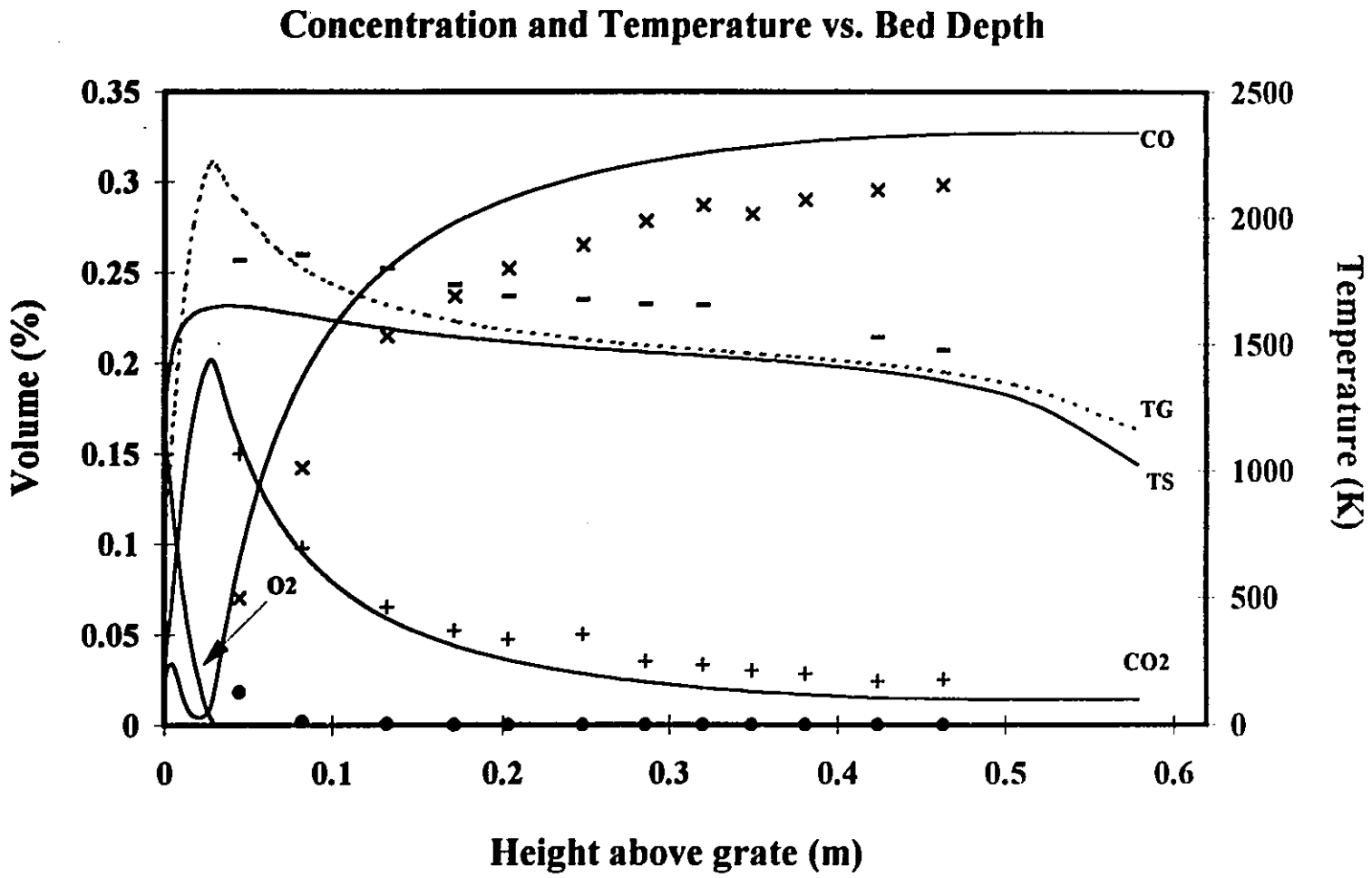

Figure 6: Predicted and experimental profiles for 61 cm bed of 3 cm coke particles with 300K, .203 kg/m^{2}s air (Data from Nichols (1935), CO oxidation rate: Fine (1973), CO_2 reduction rate: Goetz (1982), Heat and mass transfer: Yoshida (1962)

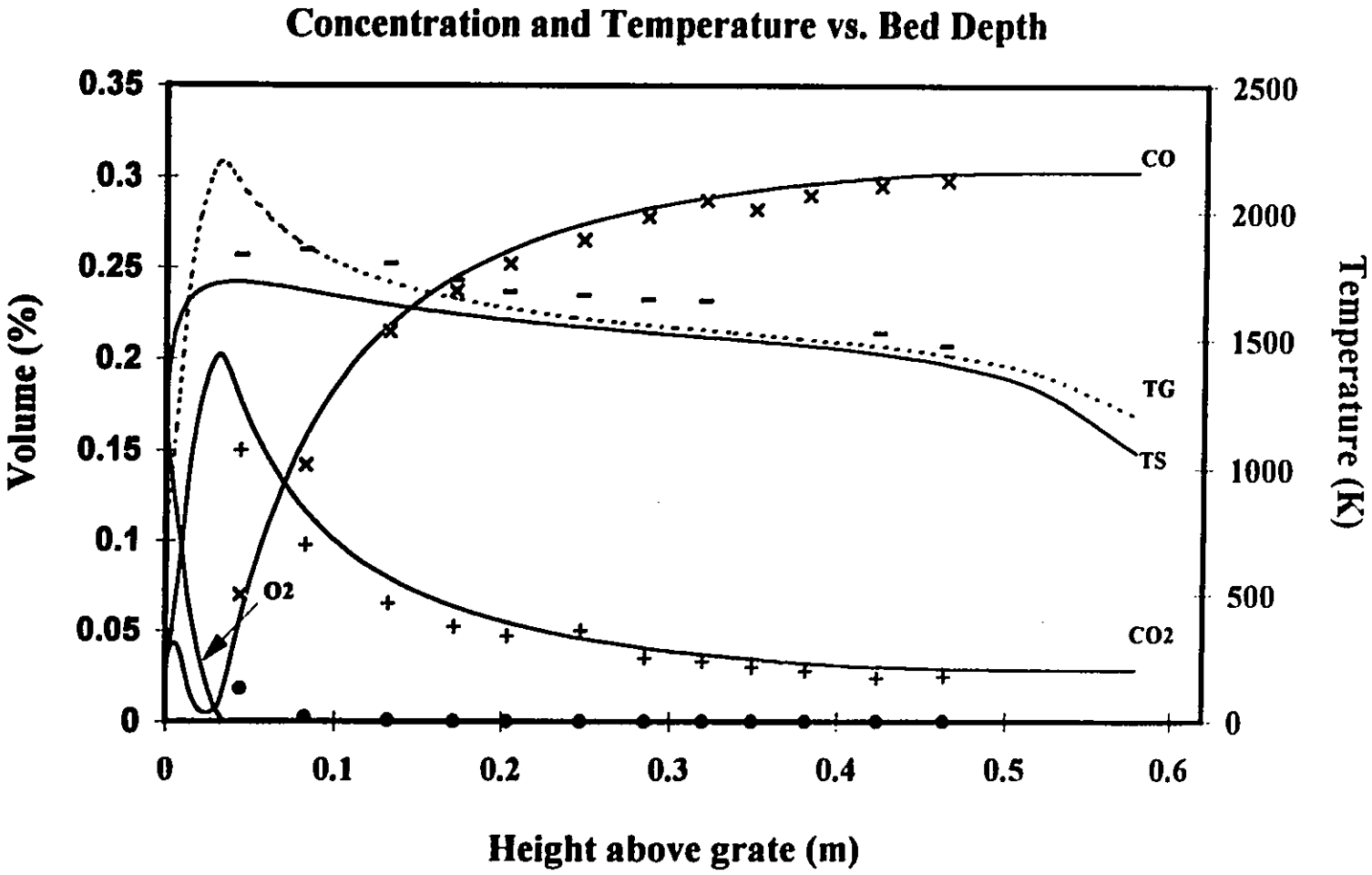

Figure 7: Predicted and experimental profiles for conditions of Fig. 6 except with CO_2 reduction rate reduced by a factor of 4 (experimental points from Nichols, 1935))

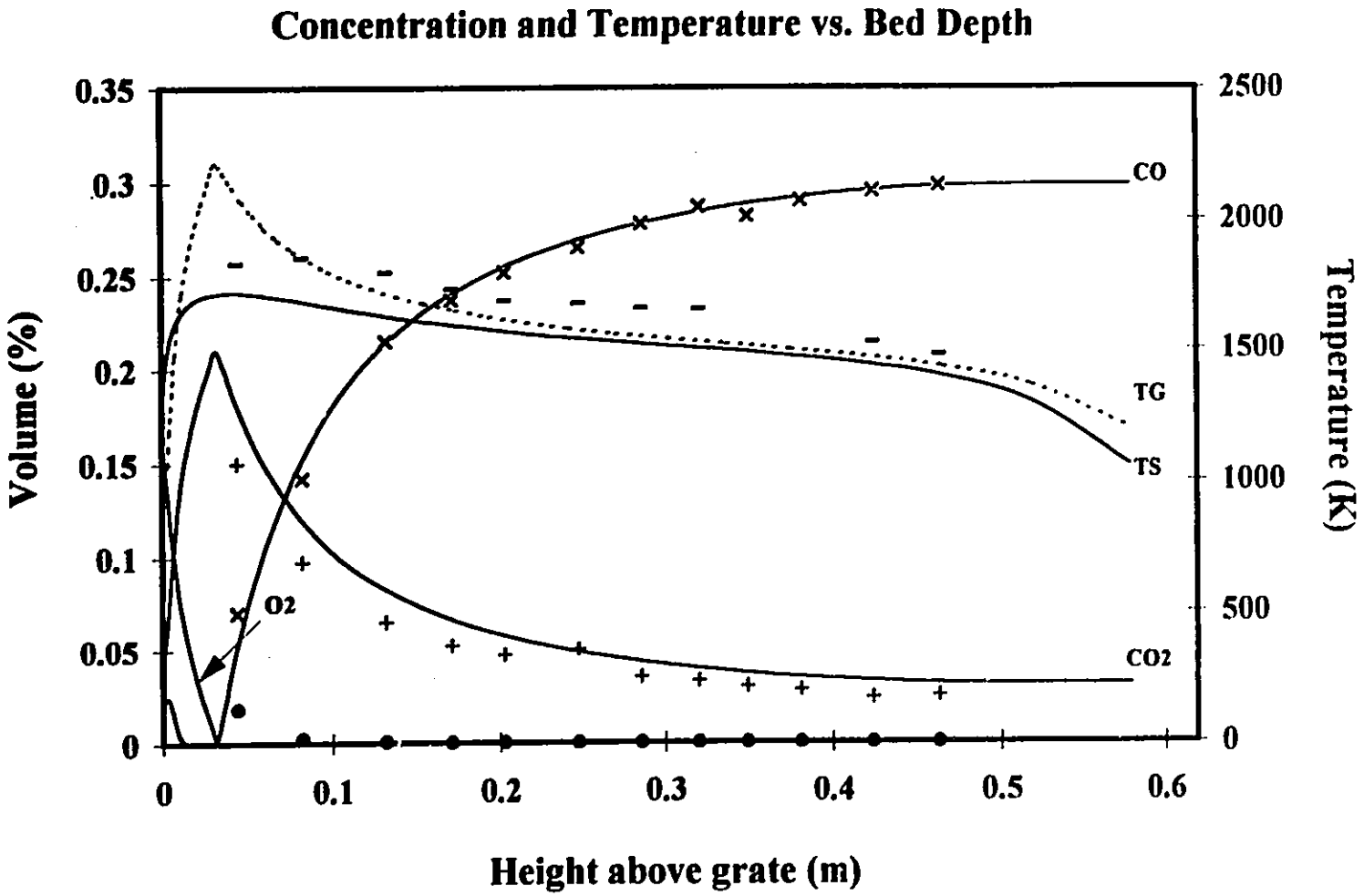

Figure 8: Predicted and experimental profiles for conditions described in Fig. 7 except with Fine's (1973) CO kinetics replaced by those of Westbrook and Dryer (1981)

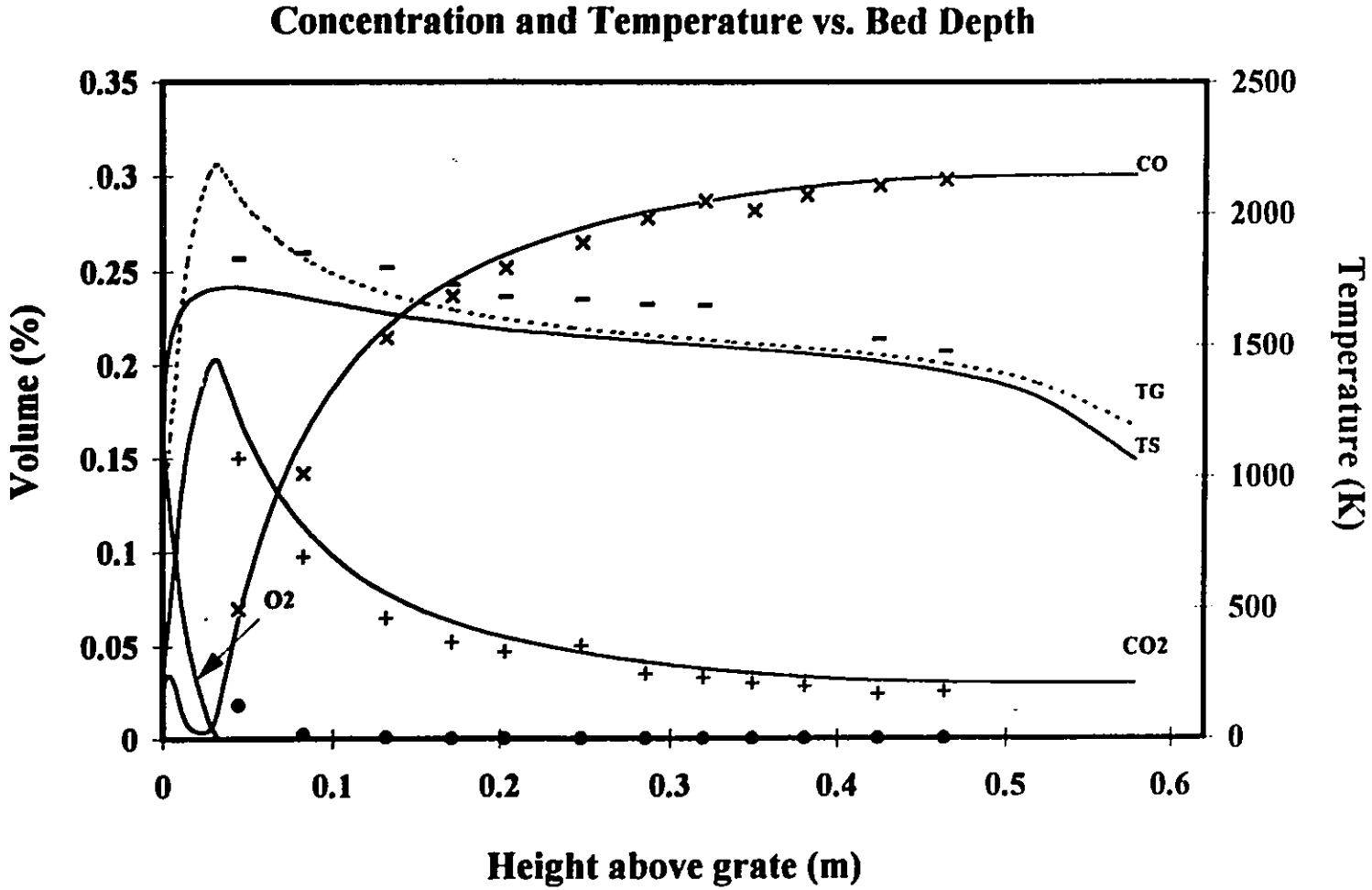

Figure 9: Predicted and experimental profiles for conditions of Fig. 7 except with Yoshida (1962) heat and mass transfer correlation replaced by that of Chu (1952)

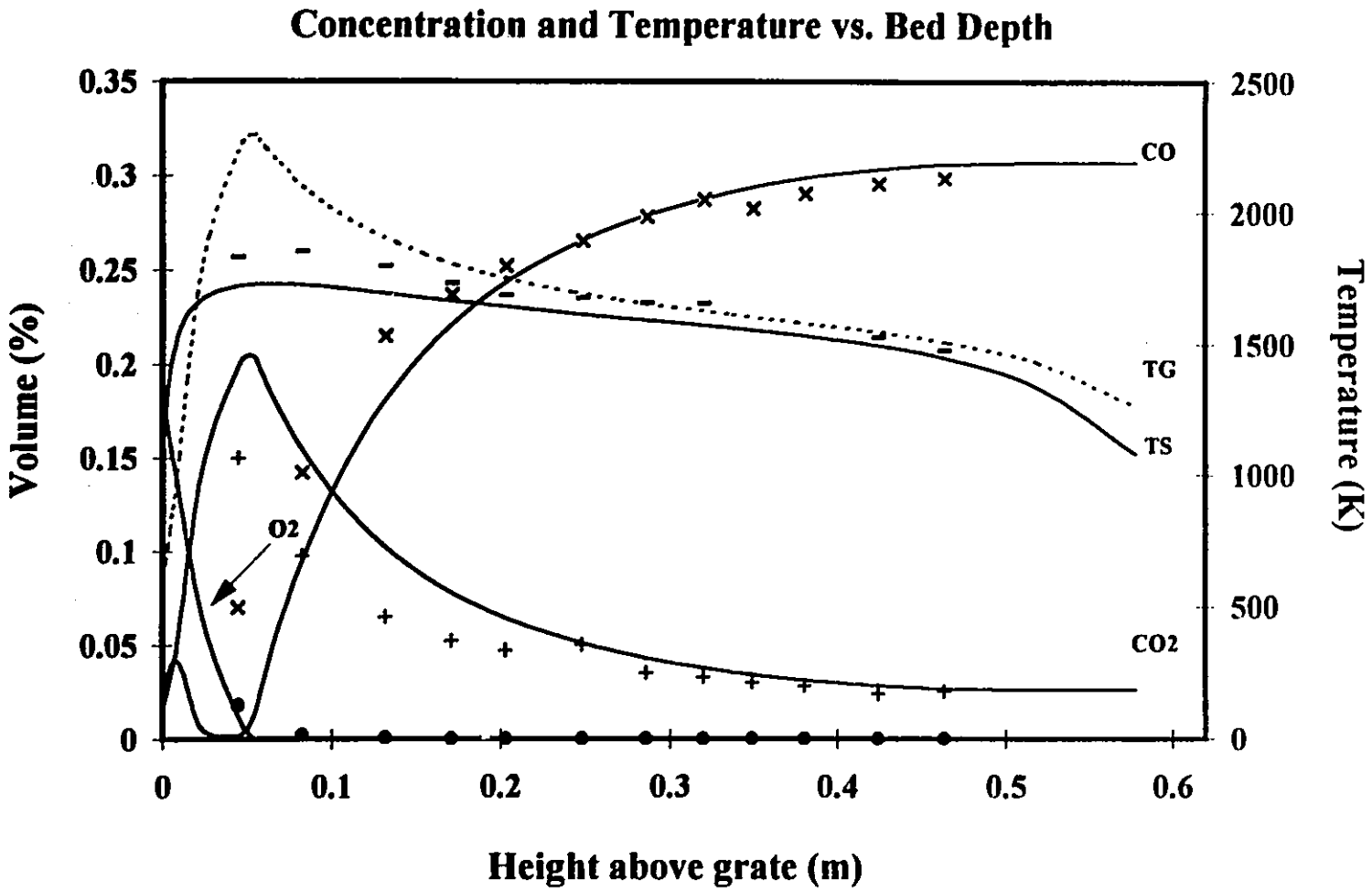

Figure 10: Predicted and experimental profiles for conditions of Fig. 7 except with heat and mass transfer correlation of Yoshida (1962) replaced with that of Bhattacharyya and Pei (1975)

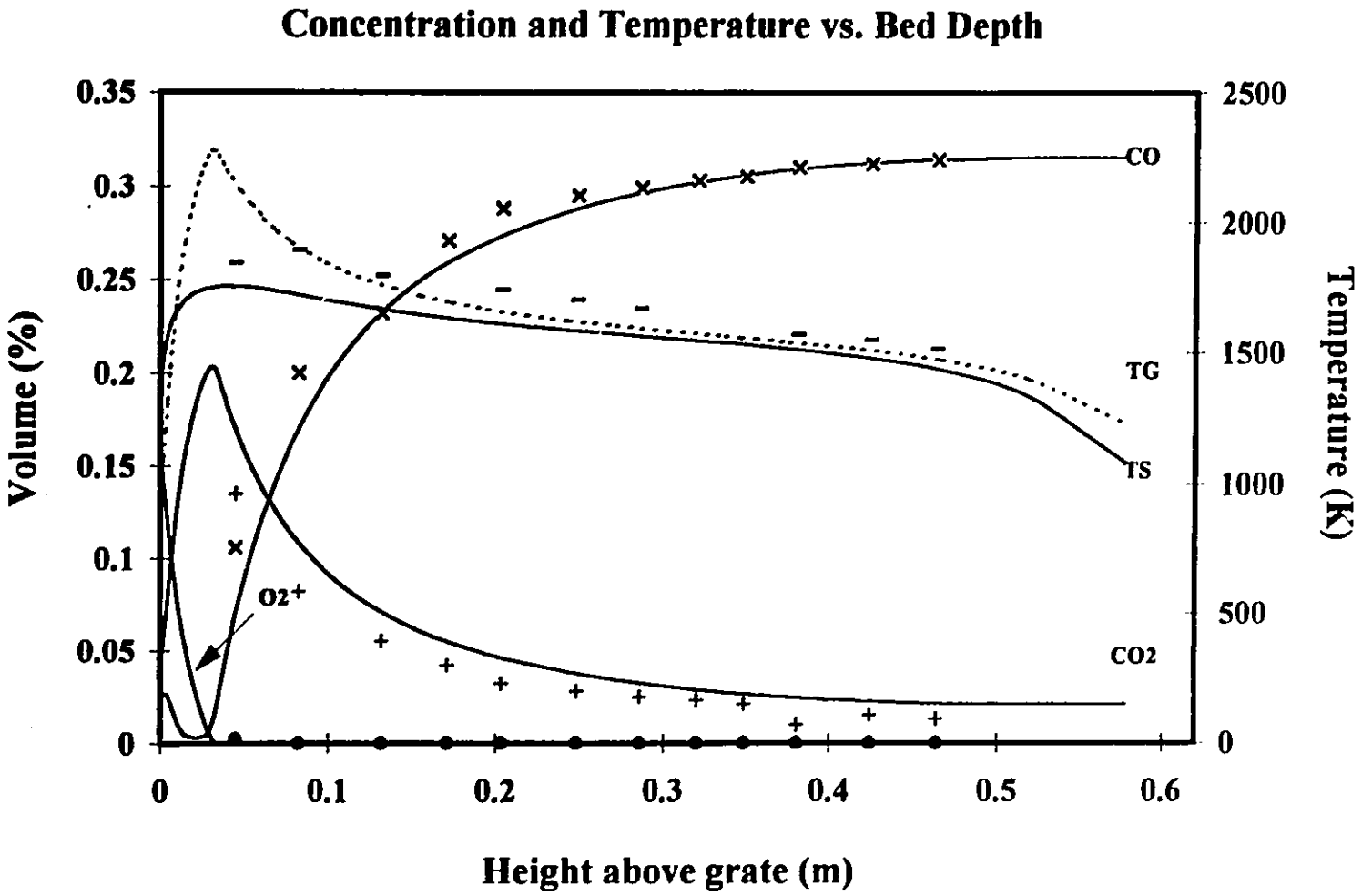

Figure 11: Predicted and experimental profiles for conditions of Fig. 7 except with air inlet of 478 K (experimental data from Nichols, 1935)

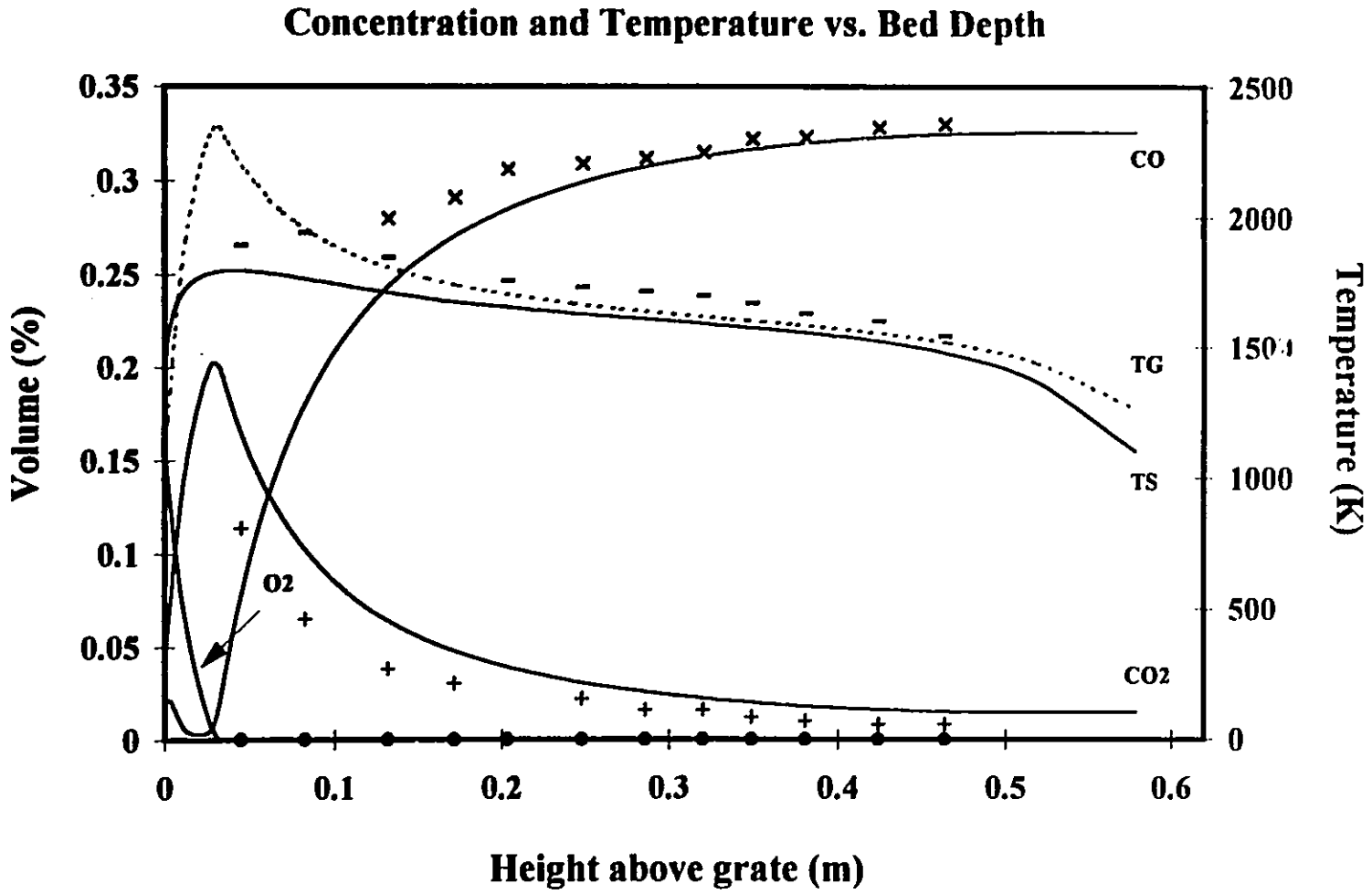

Figure 12: Predicted and experimental profiles for conditions of Fig. 7 except with air inlet of 589 K (experimental points from Nichols, 1935)

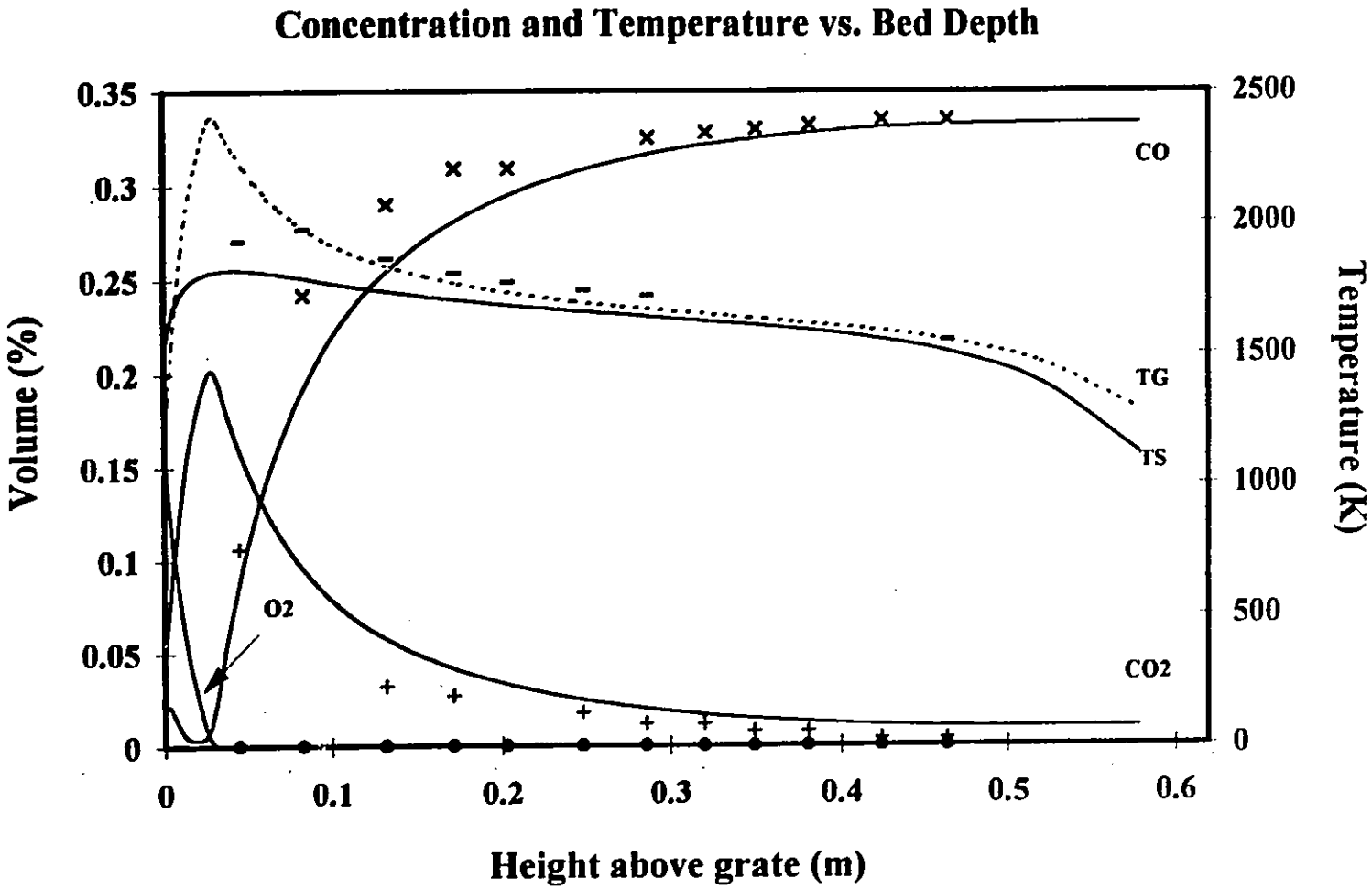

Figure 13: Predicted and experimental profiles for conditions of Fig. 7 except with air inlet of 700 K (experimental points from Nichols, 1935)

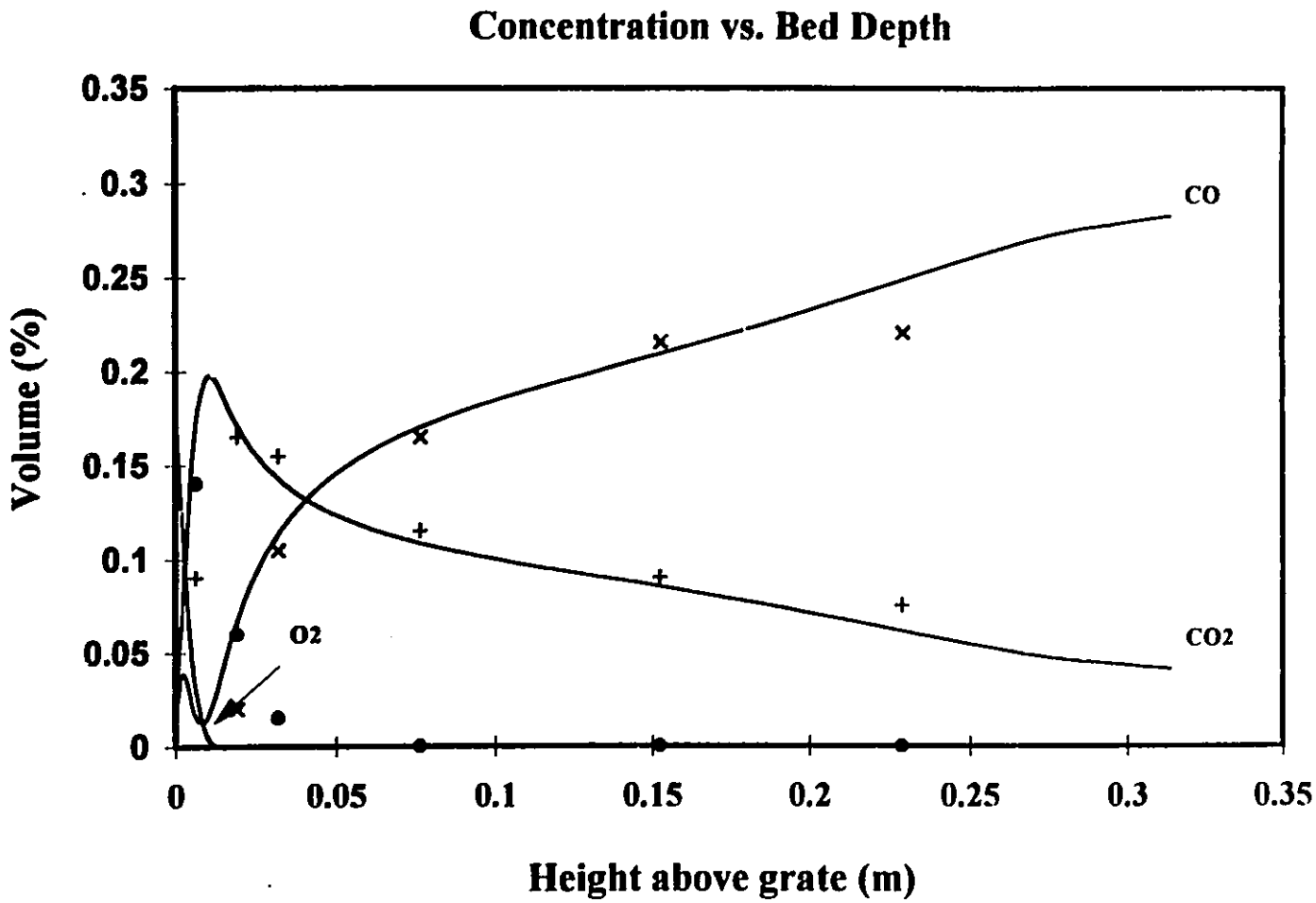

Figure 14: Predicted and experimental profiles for transient combustion of 38 cm bed of 1 cm coke particles after 1 hr with air at .036 m/s (correlations as in Fig.6, data from Eapen, 1977)

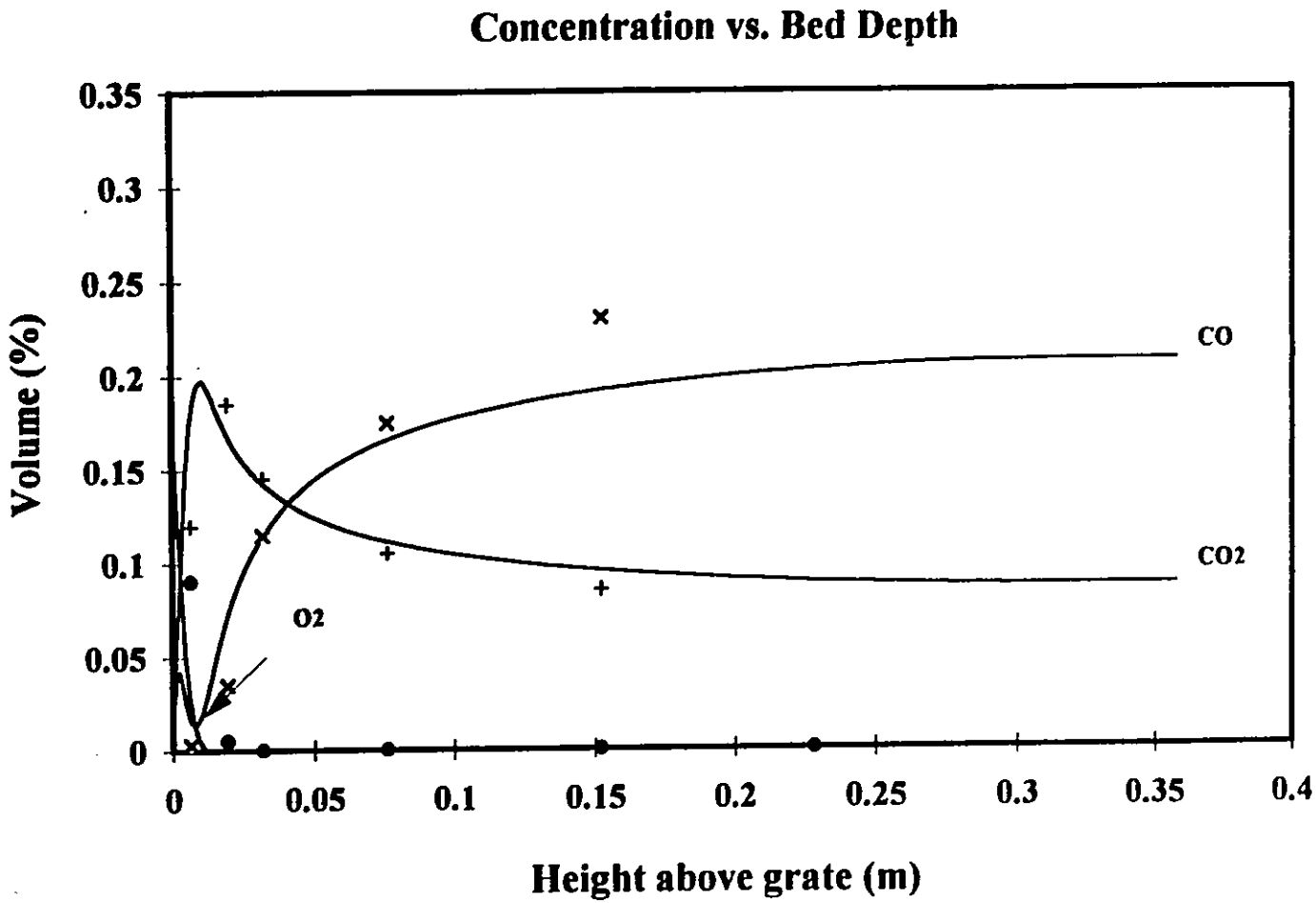

Figure 15: Predicted and experimental profiles for transient combustion as described in Fig. 14 after 3 hrs. (experimental data from Eapen, 1977)

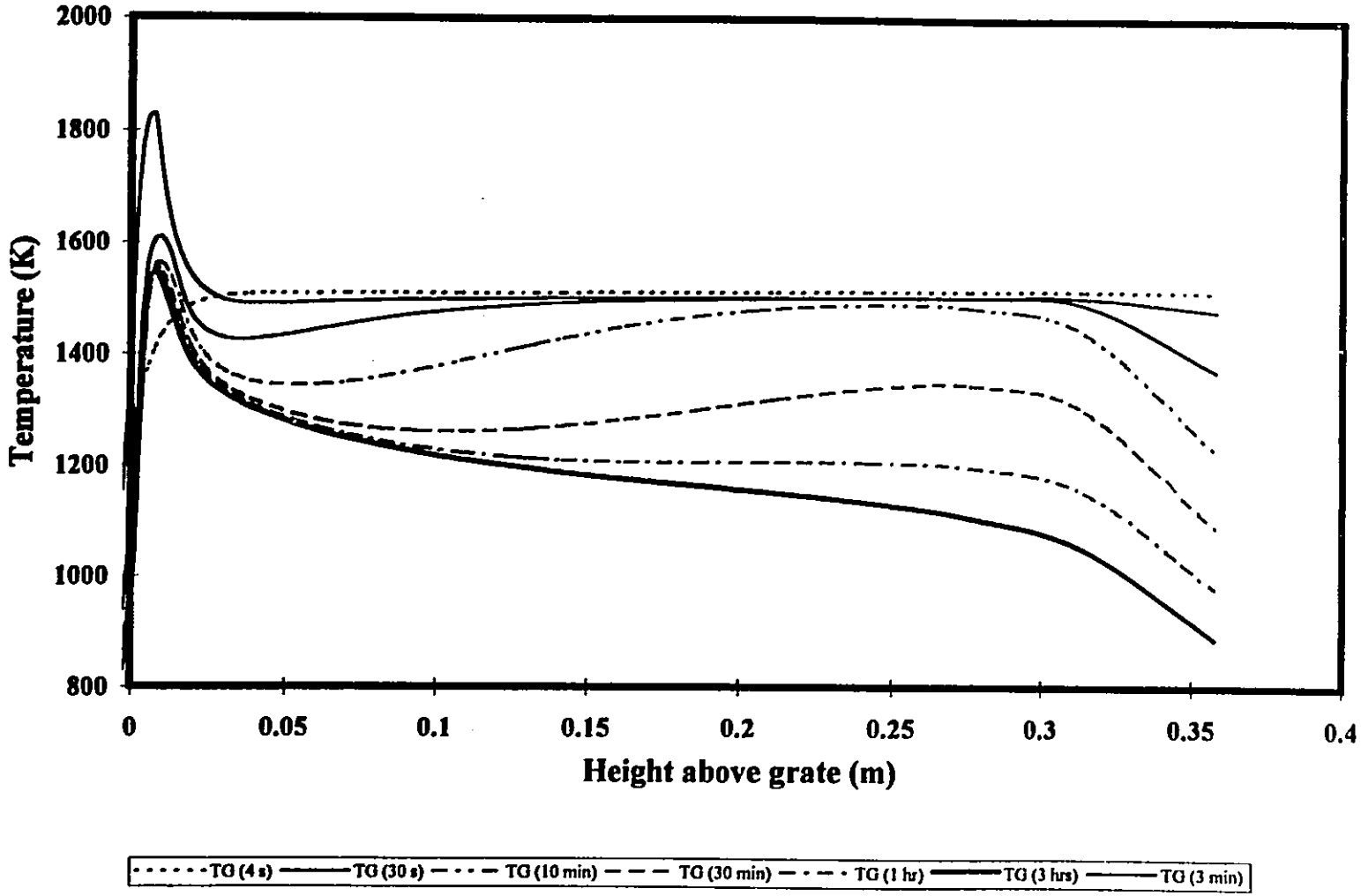

Figure 16: Predicted transient gas temperature profiles for the bed described in Fig. 14 showing ignition event at t=30 s

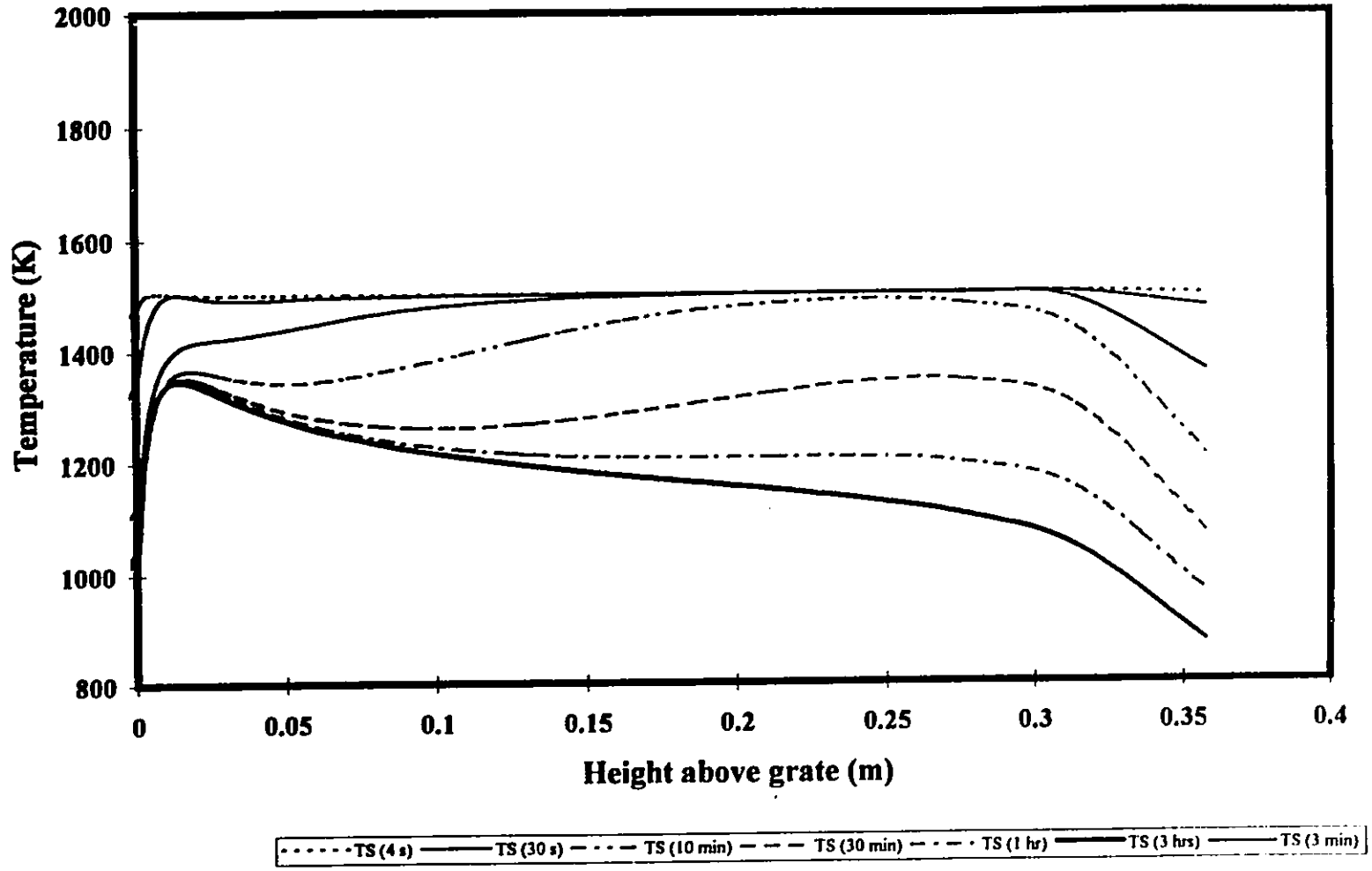

Figure 17: Predicted transient solid temperature profiles for the bed desribed in Fig. 14

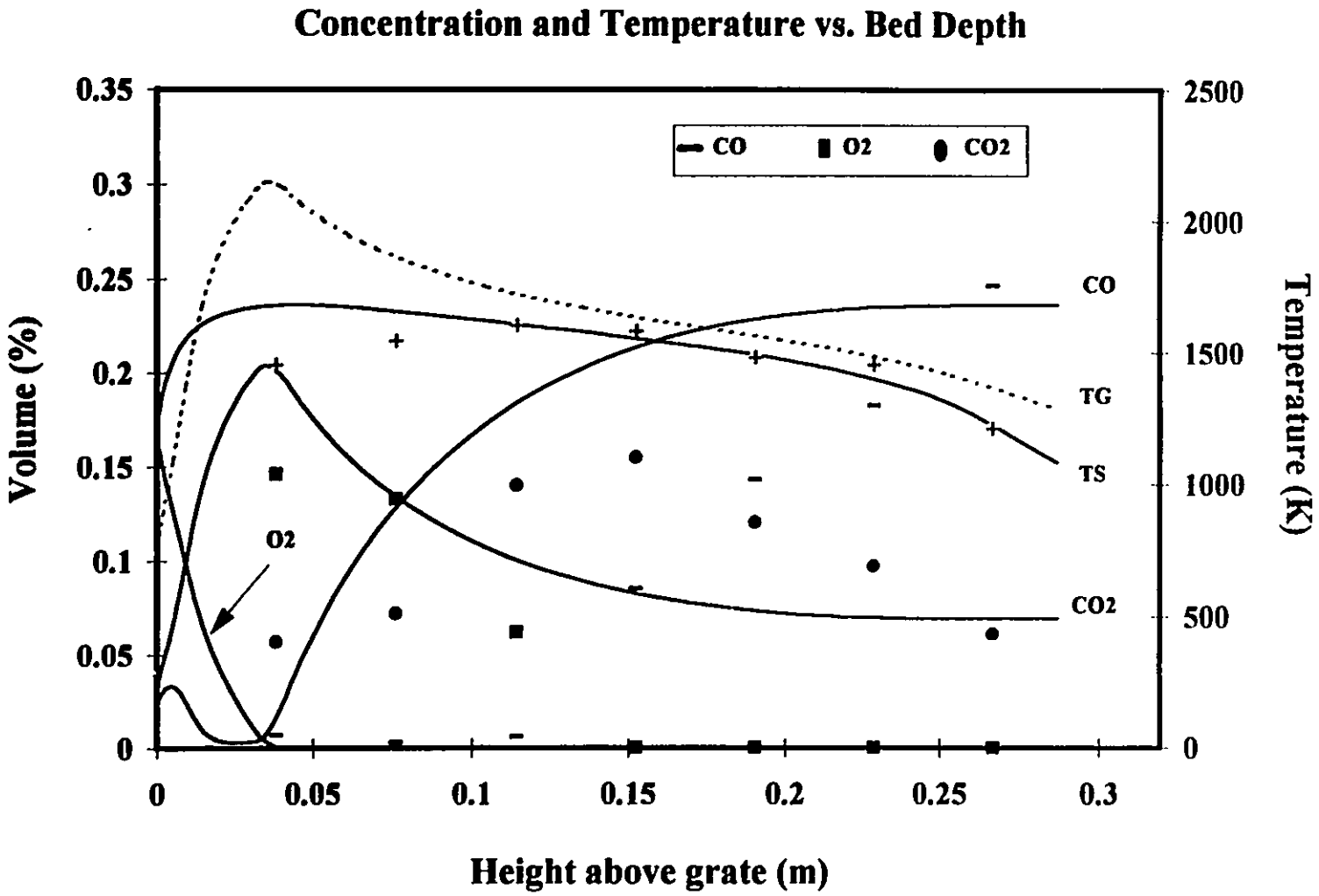

Figure 18: Predicted and experimental combustion profiles for 30 cm bed of 3 cm coke particles at air inlet velocities of 0.15 m/s (correlations of Fig. 7, data from Kreisinger, 1916)

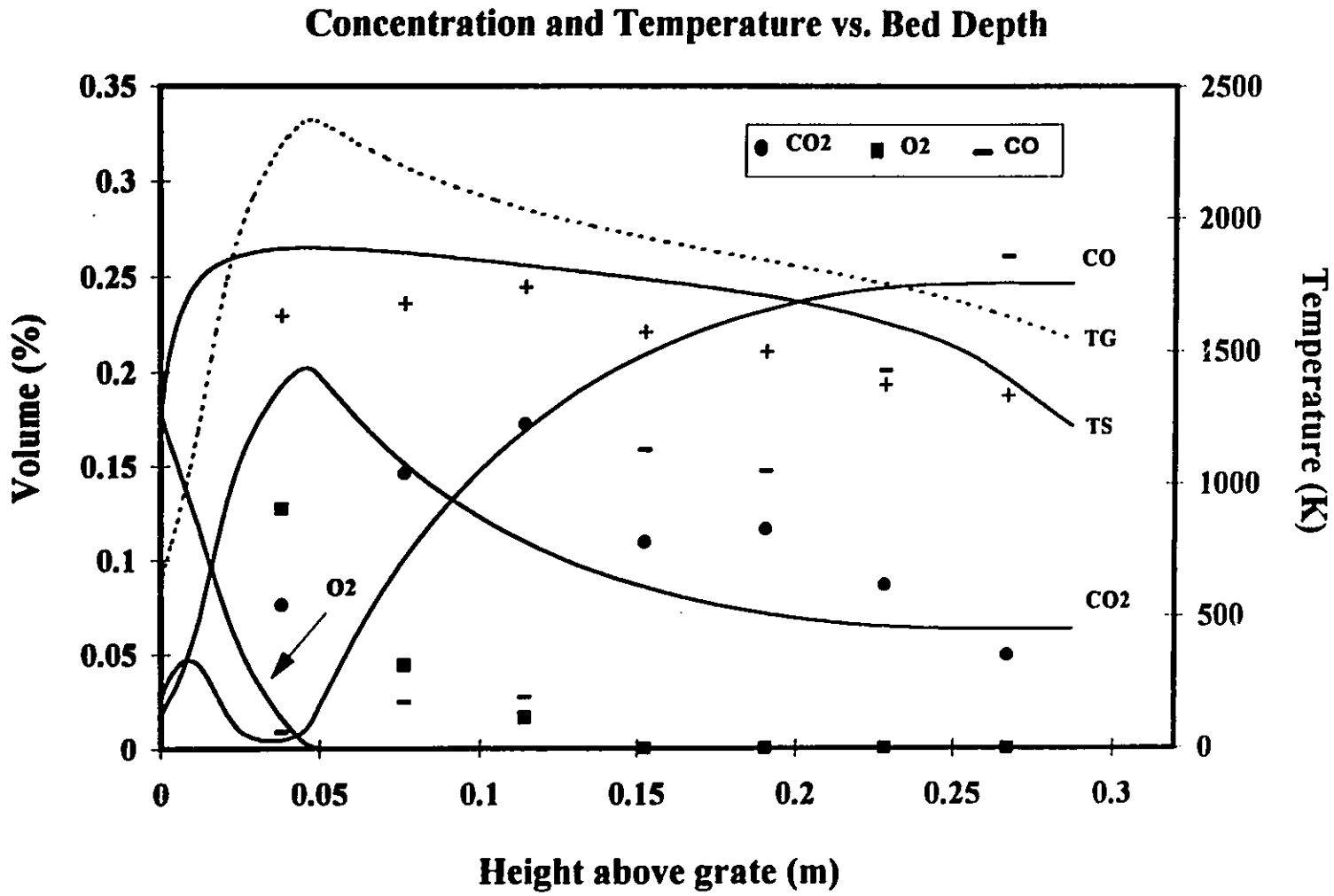

Figure 19: Predicted and experimental combustion profiles for the bed described in Fig. 18 except at air inlet velocities of 0.44 m/s (experimental data from Kreisinger, 1916)

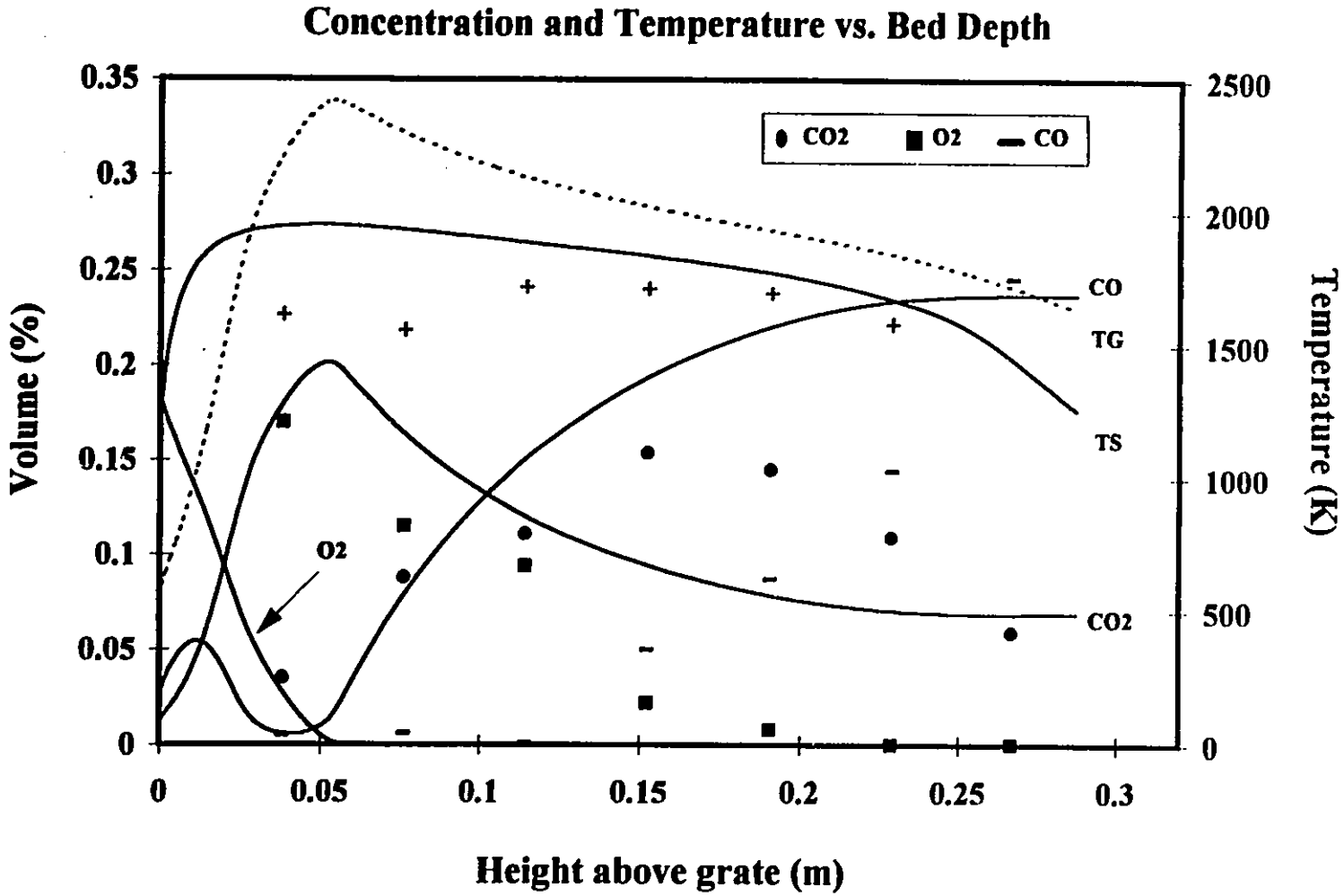

Figure 20: Predicted and experimental combustion profiles for the bed described in Fig. 18 except at air inlet velocities of 0.64 m/s (Kreisinger, 1916)

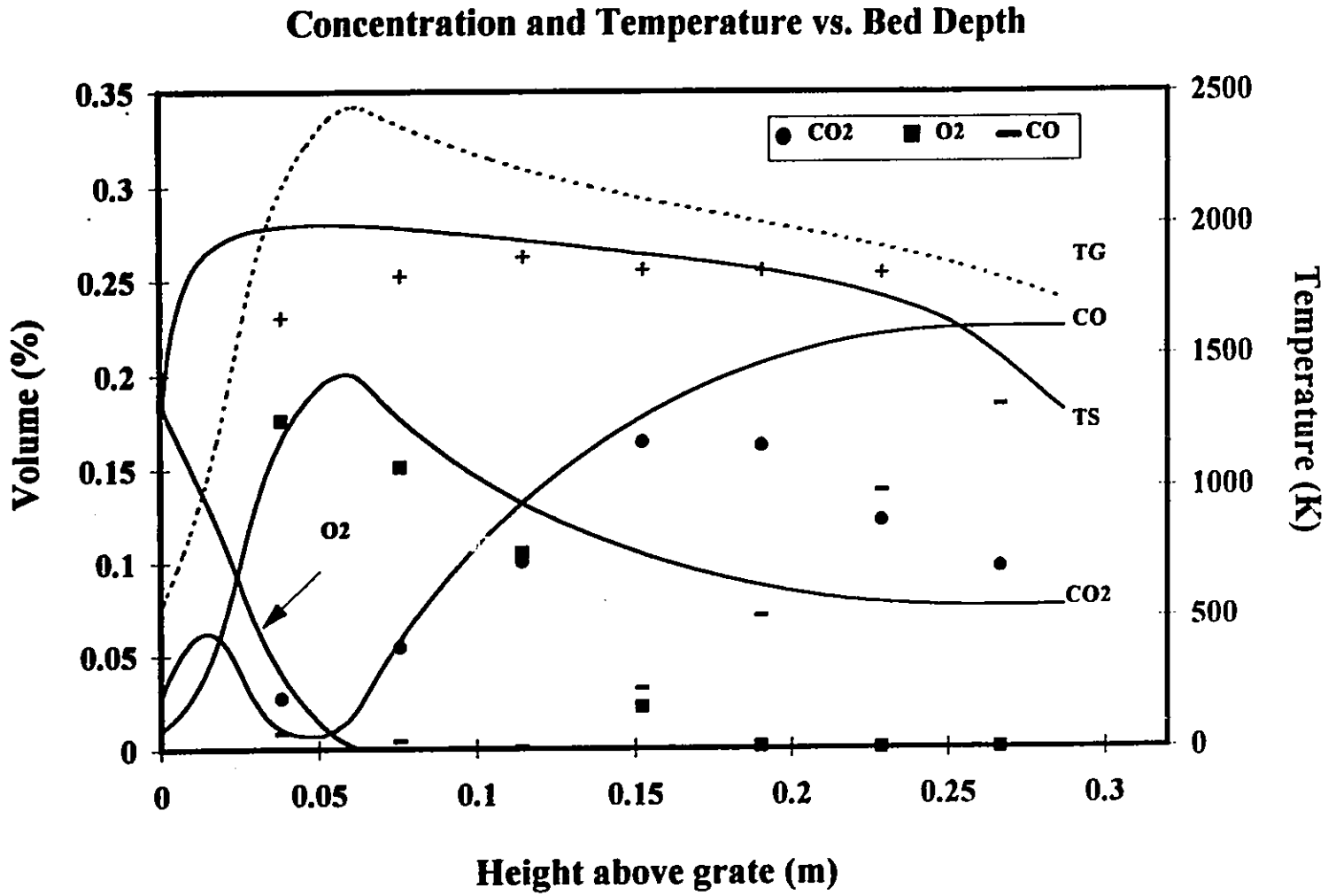

Figure 21: Predicted and experimental combustion profiles for the bed described in Fig. 18 except at air inlet velocities of 0.87 m/s (experimental data from Kreisinger, 1916)

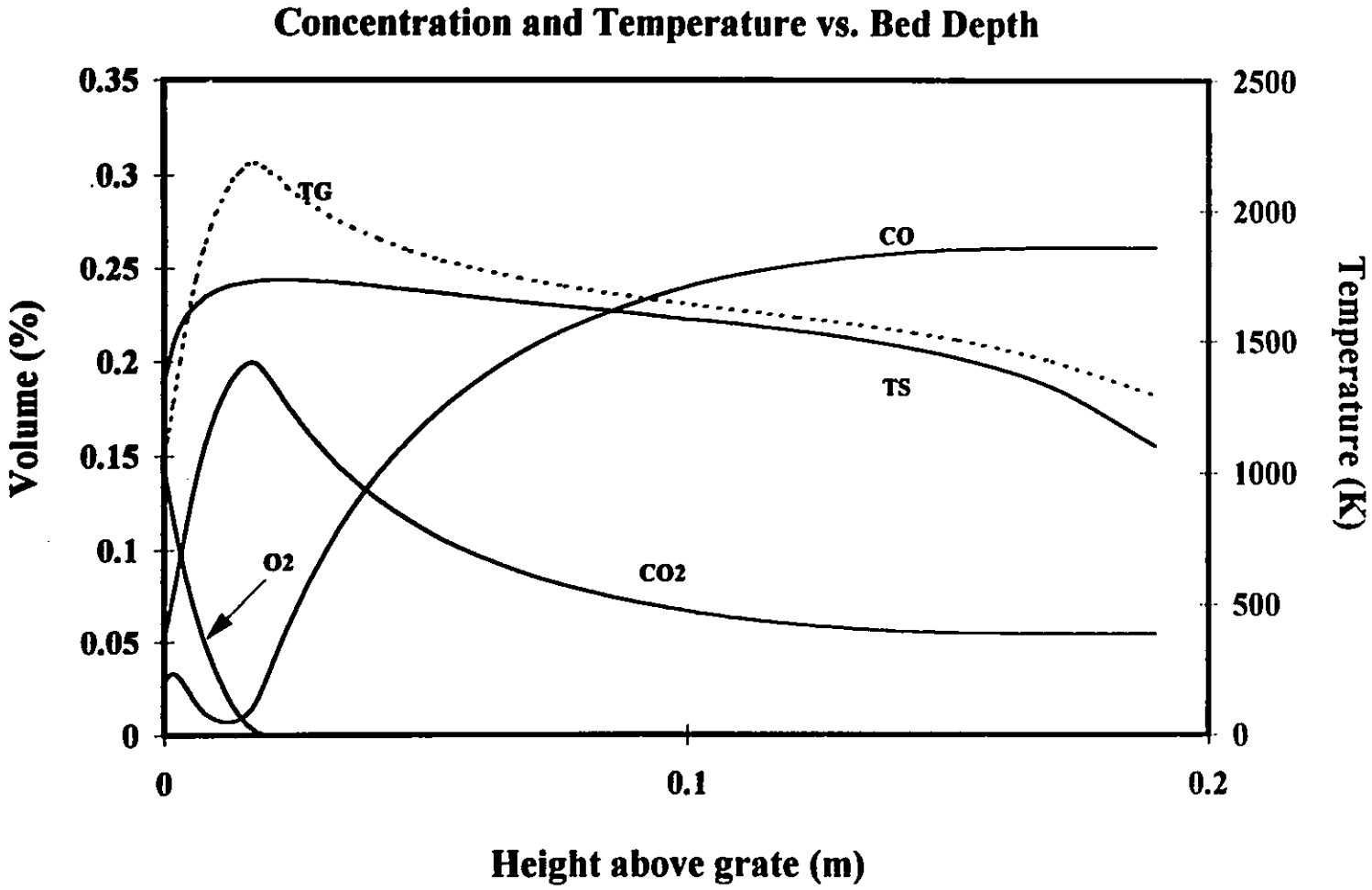

Figure 22: Predicted profiles for the combustion of 0.02 m particles in 0.2 m beds at air inlet velocity of 0.2 m/s (correlations as in Fig. 7)

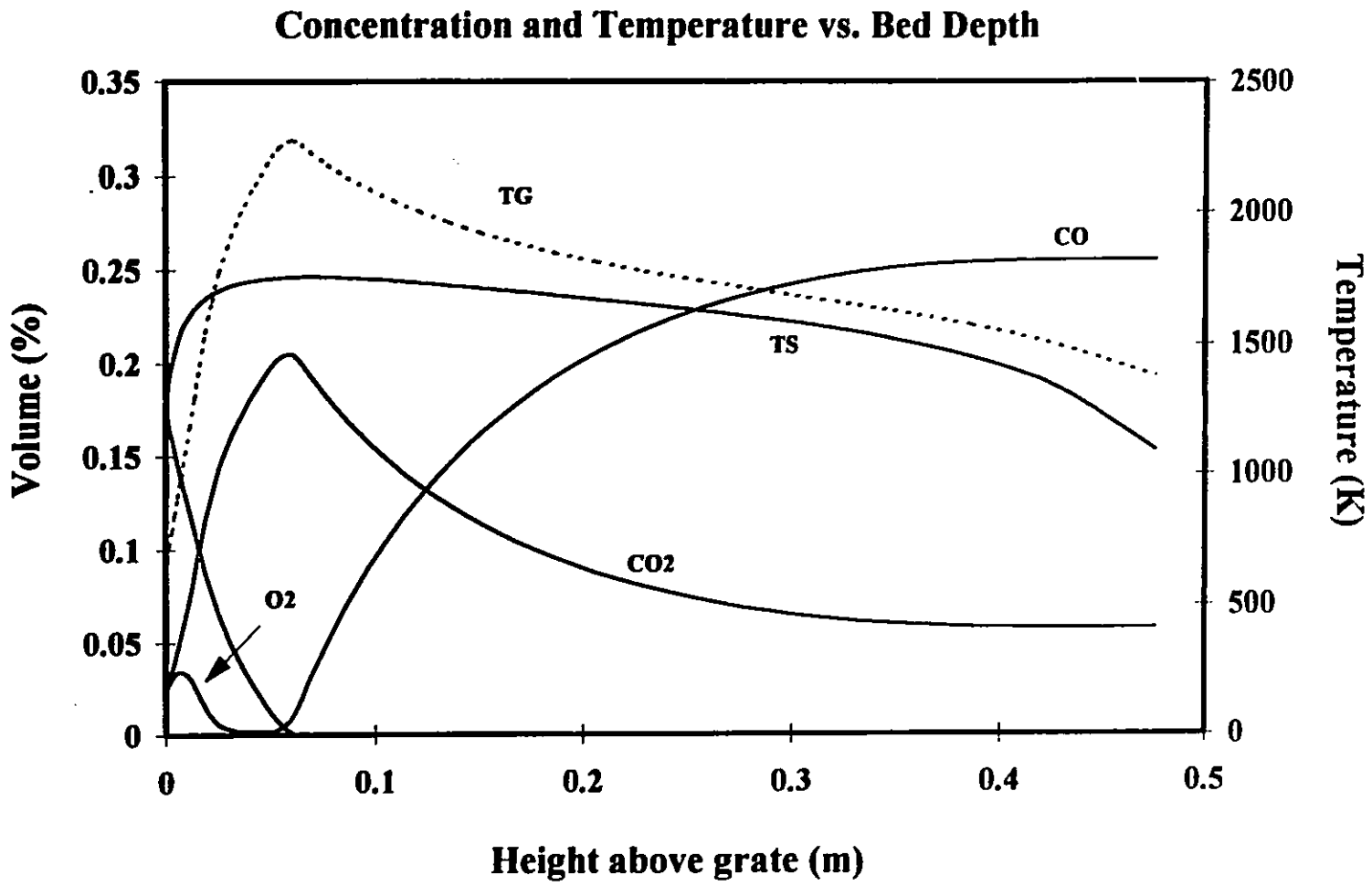

Figure 23: Predicted profiles for the combustion of 0.05 m particles in 0.5 m beds at air inlet velocity of 0.2 m/s (correlations as in Fig. 7)

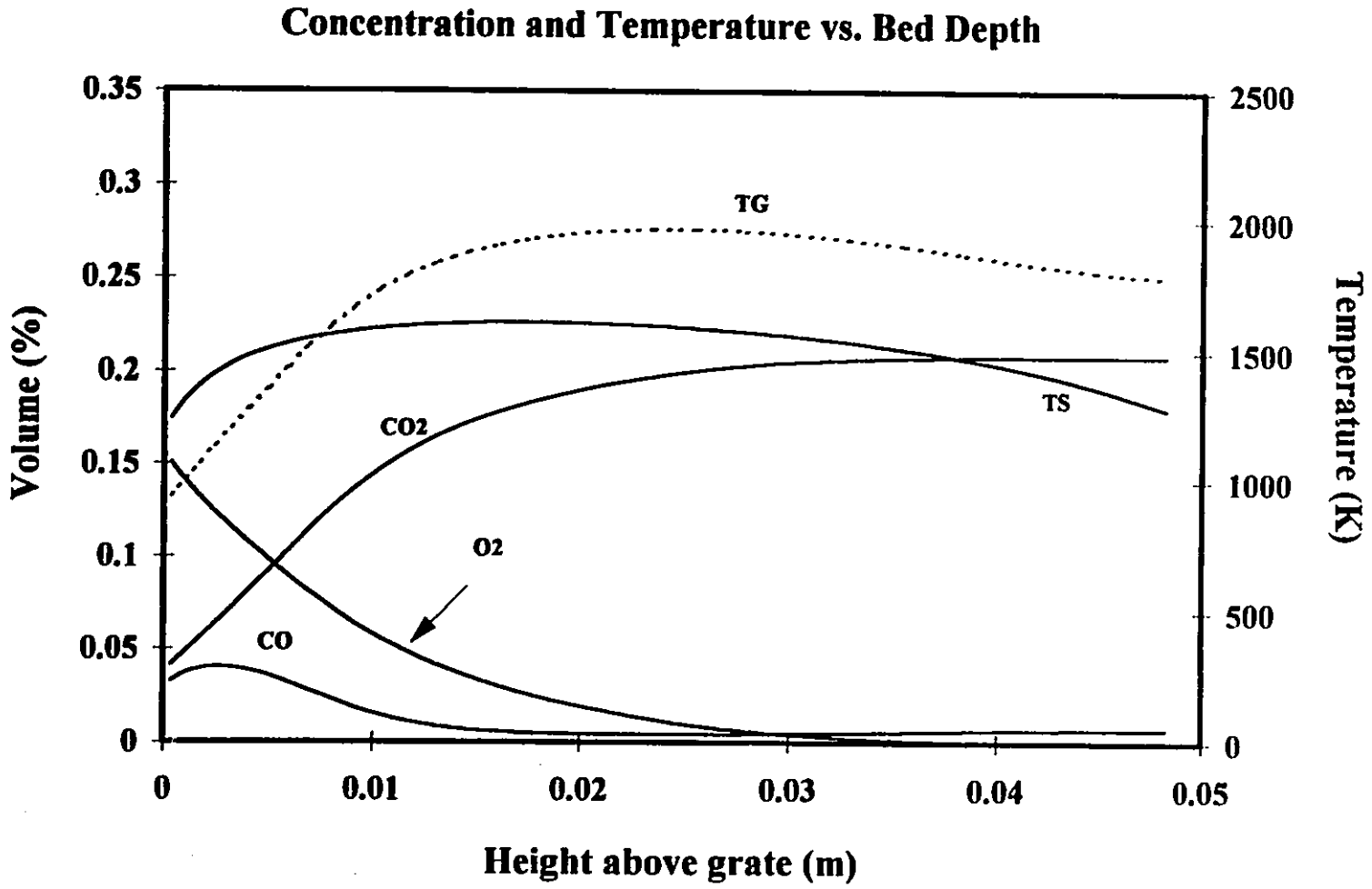

Figure 24: Predicted combustion profiles for 5 cm bed of 2 cm particles at an air inlet velocity of 0.2 m/s showing efficient combustion characteristic of thin beds (correlations as in Fig. 7)

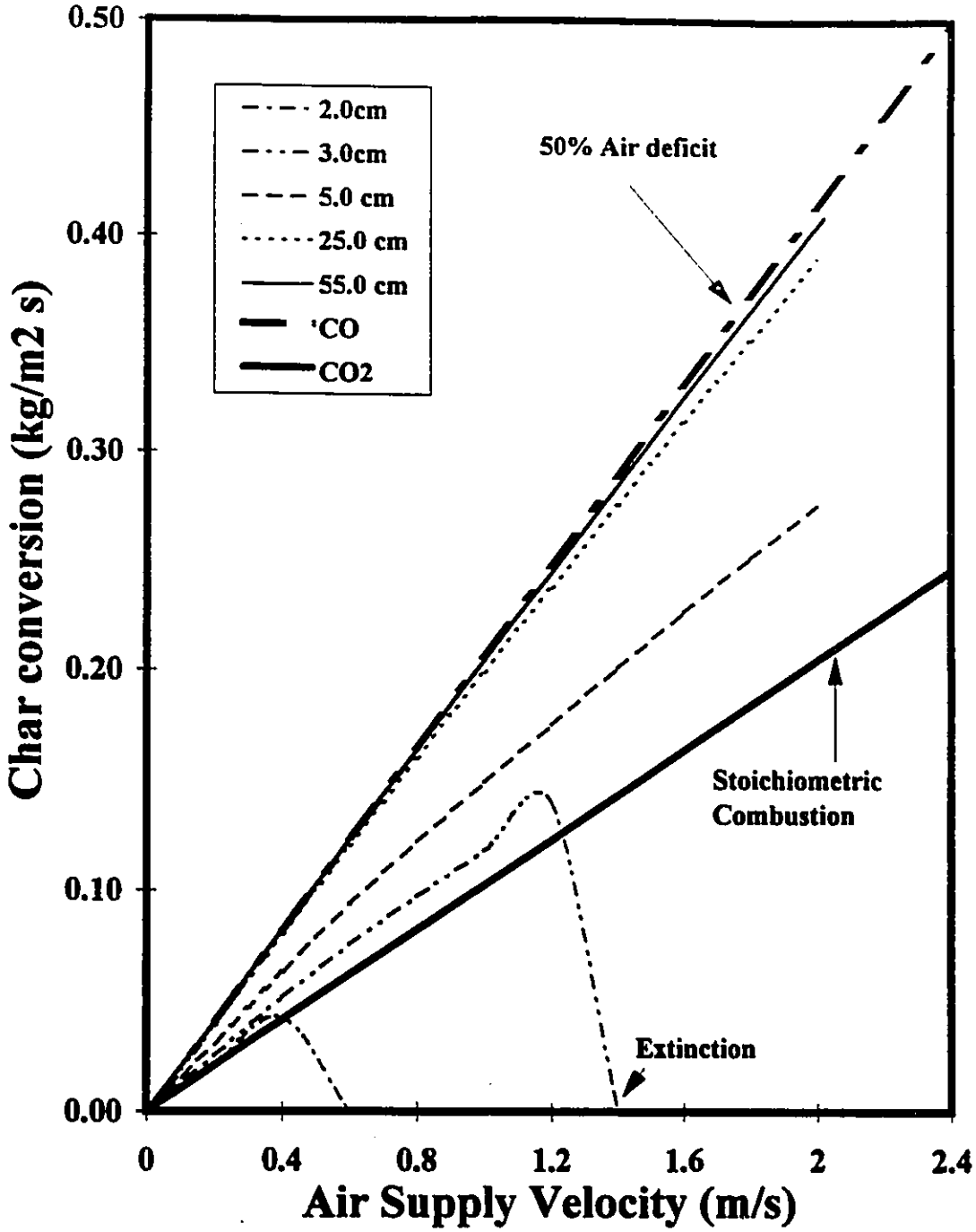

Figure 25: Predicted relationship between char conversion rate and air inlet velocity for 1 cm char particles in 2.0, 3.0, 5.0, 25.0 and 55.0 cm beds (air inlet at 300 K, correlations of Fig.7)

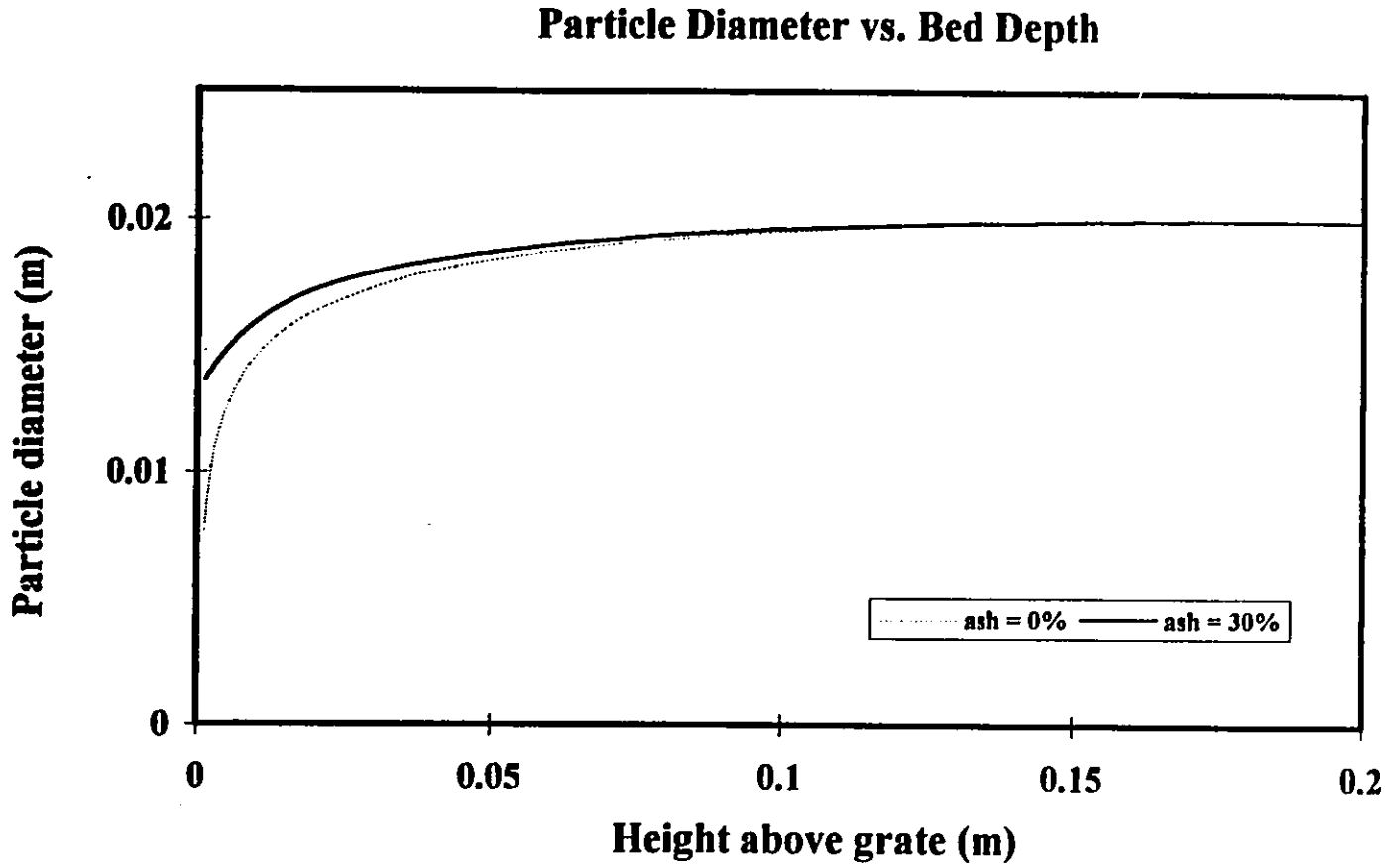

Figure 26: Comparison of predicted final steady state particle sizes for chars having 0% and 30% by weight ash (correlations of Fig. 7)

6.0 CONCLUSIONS

A Fortran program for the simulation of packed bed char combustion in beds of constant height was developed. The inputs of particle size, bed height, fuel ash content and air flow rate could be varied, allowing for the simulation of a variety of operating conditions. The program was able to predict transient and steady state temperature, concentration and particle size profiles for the combustion of 1.0-3.5 cm char particles. These predictions were compared to experimental data for air flow rates from 0.036 to approximately 0.5 m/s and bed thicknesses greater from 0.3 - 0.7 m and showed reasonable agreement. Most of the severe deviations could be attributed to sampling error in the experiments, or to other physical phenomena such as bed shrinkage and ash accumulation, which could not be reproduced by the simulation.

It is concluded that the simulation can be considered reliable enough for use in preliminary design calculations, such as the predictions of general trends and approximate combustion efficiencies from operating diagrams.

The concentration and temperature profiles obtained from the simulation were found to be most sensitive to the choice of particle-to-fluid transfer coefficients. High heat and mass transfer coefficients tended to accelerate processes in the bed, causing peak temperatures to occur closer to the grate, whereas low heat and mass transfer coefficients had the opposite effect. Both the oxidation and gasification zones were affected.

The rate of CO_2 reduction affected only the gasification zones of the beds, and a considerable change in the rate was necessary to evoke significant changes in the predicted

profiles. A factor of four reduction in the subbituminous coal char rate given by Goetz *et al.* (1982) seemed to give adequate predictions in most cases; however, since the original rate expression was developed for pulverized coal combustion, this change may have been insufficient to reflect the physical mechanism for the large particles that were studied.

Changes in the rate of CO oxidation, within the range of accepted expressions for this rate, had little effect on the predictions of the simulation. Significant changes in this rate, however, may exert a large influence on the shape of profiles in the oxidation zone and should be investigated.

Combustion efficiency (stoichiometry) was found to vary only with bed thickness. Thicker beds resulted in lower combustion efficiencies and thinner beds had high combustion efficiencies. Increasing the flow rate of air to the bed had no effect on combustion efficiency because it caused a proportional increase in char conversion rates; combustion beds are therefore self-regulating.

The behaviour of the bed in general approximated that predicted by simple mass transfer analyses of packed bed combustion in the literature, demonstrating the validity of some of the assumptions made in the simpler combustion models. Events in the bed generally scale with particle size, and beds of equal particle size to depth ratio exhibit very similar temperature and concentration profiles. The insensitivity of the current model's predictions to control volume size and timestep length appeared to indicate that gas phase transients do not greatly affect bed behaviour.

6.1 Recommendations

1.0. New packed-bed char combustion experiments concentrating on accurate sampling and temperature measurements should be conducted to enable a thorough statistical analysis of model adequacy.

2.0. Research should be conducted to examine the effects of high temperatures and chemical reaction on heat transfer, mass transfer and effective gas thermal conductivities. New correlations for these transport coefficients should be developed based on these findings to yield improved correlations of these coefficients for reactive flow situations.

3.0. More research on large-particle chemical kinetics is required to improve the kinetic submodels in the simulation, particularly that of the CO_2 reduction reaction, which is believed to be kinetically controlled to 1100 K .

4.0. An option to include transient collapse of the bed should be added to the simulation so that its transient performance can be tested

5.0. Research should be conducted on beds with non-monosized particles to examine the effects of particle size distributions on heat transfer, mass transfer and the particle surface reactions.

7.0 REFERENCES

Abdel-Hafez, A. H., "Simplified Overall rate Expression for Shrinking-Core Bituminous Char Combustion", Chemical Engineering Science **43**, p.839 (1988).

Amundson, A. and L. E. Arri, "Char Gasification in a Countercurrent Reactor", A.I.Ch.E. Journal **24**, p.87 (1978).

Arai, N. and M. Hasatani, "A mathematical model of simultaneous formation of volatile-NO and char-NO during the packed-bed combustion of coal-char particles under an NH_3 -O_2-Ar gas Stream", Fuel **66**, p.1418 (1987).

Argo, W. B. and J. M. Smith, "Heat Transfer in Packed Beds", Chemical Engineering Progress **49**, p.443 (1953).

Arthur, J. A. "Reactions between Oxygen and Carbon", Trans. Faraday Soc. **47**, p.164 (1951)

Balakrishnan, A. R. and D. C. T. Pei, "Heat Transfer in Gas-Solid Packed Bed Systems 1. A Critical Review", Ind. Eng. Chem. Process des. Dev. **18**, p.30 (1979).

Barker J. J. "Heat Transfer in Packed Beds", Ind. Eng. Chem. **57**, p.44 (1965).

Barriga, A., and R.H. Essenhigh, "A Mathematical Model of a Combustion Pot: Comparison of Theory and Experiment", ASME, Winter Annual Meeting, Heat Transfer Division, November 16-21, Chicago, Ill., p.1 (1980)

Bhattacharyya, D., and D. C. T. Pei, "Heat Transfer in Fixed-Bed Gas-Solid Systems", Chemical Engineering Science **30**, p.293 (1975).

Bhattacharyya, A., L. Salam, M. P. Dudukovic and B. Joseph, "Experimental and Modeling Studies in Fixed-Bed Char Gasification", Ind. Eng. Chem. Process Des. Dev. **25**, p.988 (1986).

Bird, R. B., W. E. Stewart and E. N. Lightfoot, "Transport Phenomena", John Wiley & Sons (1960).

Bischoff,. K. B., "Axial Thermal Conductivities in Packed Beds", Can. J. Chem. Eng. **40**, p.161 (1962).

Chu, J. C., J. Kalil and A. Wetteroth, "Mass Transfer in a Fluidized Bed", Chemical Engineering Progess **49**, p.141 (1953).

De Wasch, A. P. and G. F. Froment, "A two dimensional heterogeneous model for fixed bed catalytic reactors", Chemical Engineering Science **26**, p.629 (1971).

Dixon, A. G., and D. L. Cresswell, "Theoretical Prediction of Effective Heat Transfer Parameters in packed Beds", AIChE Journal **25**, p.663 (1979).

Dutta, S., C. Y. Wen, and R. J. Belt "Reactivity of Coal and Char.1. In Carbon Dioxide Atmosphere", Ind, Eng, Chem., Process Des, Dev. **16**, p.20 (1977).

Eapen, T., R. Blackadar, and R. H. Essenhigh, "Kinetics of Gasification in a Combustion Pot: Comparison of Theory and Experiment", 16th Symposium (International) on Combustion, the Combustion Institute, p.515 (1977).

Edwards, M. F., and J. F. Richardson, "Gas Dispersion in Packed Beds", Chemical Engineering Science **23**, p.109 (1968).

Field, M. A. "Rate of Combustion of Size-Graded Fractions of Char form a Low-Rank Coal between 1200-2000 K", Combust. Flame **13**, p.237 (1969).

Galloway, L. R., W. Komarnicky and N. Epstein, "Effect of Packing Configuration on Mass and Heat Transfer in Beds of Stacked Spheres", Can. J. Chem. Eng. **35**, p.139 (1957).

Goetz, J. G., N. Nsakala, R. L. Patel, and T. C. Lao, "Combustion and Gasification Kinetics of Chars from Four Commercially Significant Coals of Varying Rank", Proceedings of the 2nd Annual EPRI Contractor's Conference on Coal Gasification, Palo Alto, CA., October 20-21, p.571 (1982).

Goldman, J., D. Xieu, A. Oko, R. Milne and R. H. Essenhigh, "A Comparison of Prediction and Experiment in the Gasification of Anthracite in Air and Oxygen-Enriched/Steam Mixtures", 20th Symposium (International) on Combustion, The Combustion Institute, p.1365 (1984).

Gunn, D. J., "Axial and Radial Dispersion in Fixed Beds", Chemical Engineering Science **42**, p.363 (1987).

Hallett, W. L. H. Combustion Notes, University of Ottawa (1994).

Hautman, J.,F .L. Dryer, K. P. Schug, and I. Glassman, "A Multiple-step Overall Kinetic Mechanism for the Oxidation of Hydrocarbons", Combustion Science and Technology **25**, p.219 (1981).

Hobbs, M. L., P. T. Radulovic, and D.L. Smoot, "Modeling Fixed-Bed Gasifiers", AIChE Journal **38**, p.681 (1992).

Hobbs, M. L., P. T. Radulovic, and D.L. Smoot, "Combustion and Gasification of Coals in Fixed-Beds", Prog. Energy Combust. Sci. **19**, p.505 (1993).

Hobbs, M. L., P. T. Radulovic, and D.L. Smoot, "Prediction of Effluent Compositions for Fixed-Bed Coal Gasifiers", Fuel **71**, p.1177 (1992).

Howard, J. B.,G. C. Williams, and D.H. Fine, "Kinetics of Carbon Monoxide Oxidation in Postflame Gases", 14th Symposium (International) on Combustion, The Combustion Institute, p.975 (1973).

Katta, S., and D. L. Keairns, "Study of Kinetics of Carbon Gasification Reactions",Ind, Eng. Chem. Fundam. **20**, p.6 (1981).

Kreisinger, H., F. K. Ovitz, and C. E. Augustine, "Combustion in the Fuel Bed of Hand-Fired Furnaces", Fuel in Science and Practice **14**, p.271 (1935) (Reproduced from Bureau of Mines Technical Paper 137, 1916)

Kunii, D., and J. M. Smith, "Heat Transfer Characteristics of Porous Rocks",AIChE Journal **6**, p.71 (1960).

Kunii, D., and J. M. Smith, "Heat Transfer Characteristics of Porous Rocks II Thermal Conductivities of unconsolidated particles with flowing fluids",AIChE Journal 7, p.29 (1961).

Laurendeau, N., "Heterogeneous Kinetics of Coal Char Gasification and Combustion", Progress in Energy and Combustion Science **4**, p.221 (1978).

Lockwood, F. C. and A. P. Salooja, "The Prediction of Some Pulverized Bituminous Coal Flames in a Furnace", Combustion and Flame **54**, p.23 (1983).

Matsui, K.,H. Tsuji, and A. Makino, "A Further Study of the effects of Water Vapour Concentration on the Rate of Combustion of an Artificial Graphite in Humid Air Flow", Combustion and Flame **63**, p.415 (1986).

Mayers, M. A. "Temperature and Combustion Rates in Fuel Beds", Transactions of the ASME **59**, p.279 (1937).

McConnachie, J. T. L. and G. Thodos, "Transfer Processes in the Flow of Gases Through Packed and Distended Beds of Spheres", A.I.Ch.E. Journal **9**, p.60 (1963).

Merrick, D., "Mathematical Models of the Thermal Decomposition of Coal, 2. Specific heats of reaction", Fuel **62**, p.540 (1983).

Merrick, D. and B. Atkinson, "Mathematical Models of the Thermal Decomposition of Coal, 4. Heat transfer and temperature profiles in a coke oven charge", Fuel **62**, p.553 (1983).

Nichols, P., "Underfeed Combustion, Effect of Preheat, and Distribution of Ash in Fuel Beds", Fuel in Science and Practice **14**, p.205 (1935).

Ofuchi, K. and D. Kunii, "Heat transfer Characteristics of Packed Beds with Stagnant Fluids", Int, J. Heat Mass Transfer **8**, p.749 (1965).

Patankar, S. V., "Numerical Heat transfer and Fluid Flow", McGraw-Hill (1980).

Patel, M. M., D. T. Grow and B. C. Young, "Combustion Rates of Lignite char by TGA", Fuel **67**, p.165 (1988).

Pathengey, B. and S. Kovenklioglu, "Experimental Study of Particle to Gas Heat Transfer in Fixed-Bed Reactors", A.I.Ch.E. Journal **35**, p.104 (1989).

Radhakrishnan K. and D.T. Pratt, "Fast Algorithm for Calculating Chemical Kinetics in Turbulent Reacting Flow", Calculation of Turbulent Reactive Flows, ASME AMD **81** , p.313 (1986).

Schuler, R. W., V. P. Stallings and J. M. Smith, "Heat and Mass Transfer in Fixed-Bed Reactors", Chem. Eng. Progress Symposium Series **48**, p.19 (1952).

Sen Gupta, A., and G. Thodos, "Direct Analogy Between Heat and Mass Transfer to Beds of Spheres", A.I.Ch.E. Journal **9**, p.751 (1963).

Sen Gupta, A. and G. Thodos, "Mass and Heat transfer in The Flow of Fluids Through Fixed and Fluidized Beds of Spherical Particles", A.I.Ch.E. Journal **8**, p.608 (1962).

Silver, R. S., "Theoretical Treatment of Combustion in Fuel Beds I -Gas Composition and Heat Release", Fuel **32**, p.121 (1953).

Smoot, D. L., "Modeling of Coal Combustion Processes", Prog. Energy Combust. Sci. **10**, p.229 (1984).

Smoot, D. L. and P. J. Smith, "Coal Combustion and Gasification", Plenum Press, New York (1985).

Spalding, D.B. "Some Fundamantals of Combustion", Butterworths (1955).

Thring, M. W., "Physics of Fuel Bed Combustion", Fuel **31**, p.355 (1932).

Westbrook, C. K. and F. L. Dryer, "Simplified Reaction Mechanisms for the Oxidation of Hydrocarbon Fuels in Flames", Combustion Science and Technology **27**, p.31 (1981).

von Fredersdorff, C. G., and M. A. Elliot, "Chemistry of Coal Utilization, Supplementary Volume", H. H. Lewry, Ed., John Wiley & Sons, p.892 (1963).

Yagi, S. and D. Kunii, "Studies on Effective Thermal Conductivity in Packed Beds",AIChE Journal **3**, p.373 (1957)

Yagi, S., D. Kunii and N. Wakao, "Studies on Effective Thermal Conductivities in Packed Beds", AIChE Journal **6**, p.543 (1960).

Yetter, R.A. and F.L. Dryer, "Inhibition of Moist Carbon Monoxide Oxidation by Trace Amounts of Hydrocarbons", 24th Symposium (International) on Combustion, The Combustion Institute, p.757 (1992).

Yoshida, F., D. Ramaswami, and O.A. Hougen, " Temperatures and Partial Pressures at the Surfaces of Catalyst Particles", A.I.Ch.E. Journal **8**, p.5 (1962).

Yoon. H., J. Wen, and M. M. Denn, "A Model for Moving-Bed Coal Gasification Reactors", A.I.Ch.E. Journal **24**, p.885 (1978).

Yu, W., M. M. Denn, and J. Wei, "Radial Effects in Moving Bed Coal Gasifiers", Chemical Engineering Science **38**, p.1467 (1983).

8.0 APPENDICES

APPENDIX A: DISCRETIZED EQUATIONS

Listed below are the general coefficients for the discretized Patankar (1980) forms of the governing differential equations given by (3-2)-(3-6) and (3-12). The coefficients shown apply to each node P of the bed as shown in Fig. 4 of Section 4.1.3 for the general discretization equation:

$$a_P\phi_P = a_N\phi_N + a_S\phi_S + b \qquad \text{(A-1)}$$

where ϕ is the dependent variable being solved for and the subscripts S, N and P apply to the three bed nodes involved in the discretization equation (see Fig. 4).

A.1 Gas and solid mass balances

For the gas and solid mass balances, (3-2,3), $\phi = \rho v$ and the general coefficients for (A-1) applying to each node in the bed are given by:

$$\begin{aligned} a_P &= 1.0 \\ a_N &= 0.0 \\ a_S &= 1.0 \\ \textit{Gas:}\quad b &= G\Delta x a_B + \epsilon(\rho_G - \rho^o_P)\Delta x/\Delta t \\ \textit{Solid:}\quad b &= -G\Delta x a_B \end{aligned} \qquad \text{(A-2)}$$

where the subscript ^{o} refers to the value of a property or dependent variable at the beginning of the timestep being solved. (Note that the variables in the above equation are not indexed for the node number *i*, but that general coefficient above applies to each node of the bed in turn. Thus, unindexed quantities occur at *i*, or the central node P in (A-1), and quantities from nodes to either side of node *i* carry the subscripts *i+1*, and *i-1*. This convention will apply throughout the appendices.)

A.2 Particle number balance

In the particle number balance (see equation 3-12), the dependent variable ϕ in equation (A-1) is the particle diameter d_p, and the coefficients are given by:

$$\begin{aligned} a_P &= (1 - \epsilon)\Delta x - v_{S_{i-1}}\Delta t \\ a_N &= [\![0, -v_{S_i}\Delta t]\!] \\ a_S &= 0 \\ b &= (1 - \epsilon)\Delta x d^o_P - 8.0G(1 - \epsilon)\Delta t\Delta x/\rho_{S_i} \end{aligned} \qquad \text{(A-3)}$$

A.3 Species and energy balances

The coefficients a_N and a_S for the species and energy balances (equations 3-4,5 and 6) have the same form for each of these equations because all these equations involve conduction and convection of the dependent variable ϕ. In the discretization process, conduction and convection are handled by a power law scheme to give the best possible approximation to the differential equations upon (numerical) integration. The resulting general coefficients power law coefficients a_N and a_S are given by:

$$\begin{aligned} a_N &= D_n[\![0,\ 1-0.1|Pe_n|^5]\!] + [\![0,\ -F_n]\!] \\ a_S &= D_s[\![0,\ 1-0.1|Pe_s|^5]\!] + [\![0,\ F_s]\!] \end{aligned} \qquad \text{(A-4)}$$

where D represents diffusion of heat or chemical species across the interfaces between the control volumes (see the subscript conventions outlined in Fig. 4) and F represents species or energy convection. Pe is the Peclet number for the flow of species or heat and is a measure of the importance of convection with respect to diffusion.

A.3.1 Species Balances

For the species balance, the form of which is given by equation (3-4), the dependent variable ϕ is the species concentration Y. The discretized differential equation is defined by the general coefficients shown in (A-4) and the following:

$$\begin{aligned} a_P &= \epsilon \Delta x \rho_G + a_N + a_S + F_n + F_s - S_P \\ b &= \epsilon \Delta x \rho^o_G Y^o + S_C \\ D_n &= (\rho_{G_i} D_{eff_n} \Delta t)/\Delta x_n \\ F_n &= v_{G_i} \rho_{G_i} \Delta t \\ Pe_n &= F_n/D_n \\ D_s &= (\rho_{G_{i-1}} D_{eff_s} \Delta t)/\Delta x_s \\ F_s &= v_{G_{i-1}} \rho_{G_{i-1}} \Delta t \\ Pe_s &= F_s/D_s \end{aligned} \qquad \text{(A-5)}$$

where all variables are as defined previously. The S_C and S_P (see Appendix C) are respectively the ϕ-independent and ϕ-dependent parts of the overall reaction source terms S (as discussed in Section 4.3.) whereas $D_{eff\,n}$ and $D_{eff\,s}$ are the diffusivities at the interfaces of the control volumes. The latter are obtained from a weighted mean of the values in the control volumes sharing that interface by:

$$D_{eff_n} = f_e D_{eff_i} + (1 - f_e) D_{eff_{i+1}}$$
$$D_{eff_s} = f_e D_{eff_{i-1}} + (1 - f_e) D_{eff_i}$$

and f_e is a weighting factor based on the distance of adjacent nodes from their shared interface:

$$f_e = \frac{0.5\Delta x}{\Delta x_n}$$

A.3.2 Gas Phase Energy Balance

The gas phase energy balance is given by (3-6), and the dependent variable ϕ is the free stream gas temperature T_G. The discretized differential equation is defined by the general coefficients shown in (A-4) and the following:

$$\begin{aligned}
a_P &= \epsilon \Delta x \rho_G \overline{Cp}_G + a_N + a_S + F_n - F_s + ha^o_B \Delta x \Delta t \\
b &= \epsilon \Delta x \rho^o_G \overline{Cp}^o_G T^o_G + h a^o_B T^*_S \Delta x \Delta t + S_C \Delta H_R \\
D_n &= k_{Geff_n} \Delta t / \Delta x_n \\
F_n &= \rho_{G_i} v_{G_i} Cp_{G_i} \Delta t \\
Pe_n &= F_n / D_n \\
D_s &= k_{Geff_s} \Delta t / \Delta x_s \\
F_s &= \rho_{G_{i-1}} v_{G_{i-1}} Cp_{G_{i-1}} \Delta t \\
Pe_s &= F_s / D_s
\end{aligned} \qquad \text{(A-6)}$$

where ΔH_R is the heat release for CO oxidation, and

$$k_{Geff_n} = f_e k_{Geff_i} + (1 - f_e) k_{Geff_{i+1}}$$
$$k_{Geff_s} = f_e k_{Geff_{i-1}} + (1 - f_e) k_{Geff_i}$$

For the discretized differential equations given by (A-2-A-6), a boundary condition was required for the top node in the bed, because of the absence there of a north neighbour node (N). This boundary condition is given by:

$$a_P = a_N = 1$$
$$a_S = b = 0$$

and has the same effect as setting the value of ϕ_P at the top node equal to ϕ_S.

A.4 Solid Energy Balance

The solid phase energy balance is given by (3-5), and the dependent variable ϕ is the free stream gas temperature T_S. The discretized differential equation is defined by the general coefficients shown in (A-4) and the following:

$$a_P = (1 - \epsilon)\Delta x \rho_S \overline{Cp}_S + a_N + a_S + F_n - F_s - S_P$$
$$b = (1 - \epsilon)\Delta x \rho^o_S \overline{Cp}^o_S T^o_S + h a^o_B (T_G - T^*_S)\Delta x \Delta t + S_C$$
$$D_n = k_{Seff_n} \Delta t / \Delta x_n$$
$$F_n = \rho_{S_i} v_{S_i} Cp_{S_i} \Delta t$$
$$Pe_n = F_n / D_n$$
$$D_s = k_{Seff_s} \Delta t / \Delta x_s$$
$$F_s = \rho_{S_{i-1}} v_{S_{i-1}} Cp_{S_{i-1}} \Delta t$$
$$Pe_s = F_s / D_s$$

where $k_{Seff\,n}$ and $k_{Seff\,s}$ represent harmonic means of the effective conductivities at adjacent nodes, required because of a step-change in conductivity between the bed and the grate (Patankar, 1980):

$$k_{Seff_n} = \left(\frac{1 - f_e}{k_{Seff_i}} + \frac{f_e}{k_{Seff_{i+1}}} \right)^{-1}$$
$$k_{Seff_s} = \left(\frac{1 - f_e}{k_{Seff_{i-1}}} + \frac{f_e}{k_{Seff_i}} \right)^{-1}$$

The solid phase required boundary conditions for the top and bottom of the bed because it was discontinous at these locations. These boundary conditions involved radiative exchanges between the bottom of the bed and a surface at T_{B2} and between the top of the bed and another surface at T_{BN} :

$$a_S = \left(\frac{k_{Seff_i}\,\Delta t}{\Delta x/2}\right)\left(\frac{1}{1 + 2\,k_{Seff_i}/(\Delta x\, H_{R_2})}\right)$$

BOTTOM:

$$H_{R_2} = \sigma\,(T_{S_{i-1}}^2 + T_{B_2}^2)(T_{S_{i-1}} + T_{B_2})$$

$$T_{B_2} = \left(\frac{k_{Seff_i} T_{S_i}}{\Delta x/2} + H_{R_2}^{*}\, T_{S_{i-1}}\right)\left(\frac{k_{Seff_i}}{\Delta x/2} + H_{R_2}^{*}\right)^{-1}$$

where the subscript * refers to previous iteration values, and

$$a_N = \left(\frac{k_{Seff_i}\,\Delta t}{\Delta x/2}\right)\left(\frac{1}{1 + 2\,k_{Seff_i}/(\Delta x\, H_{R_N})}\right)$$

TOP:

$$H_{R_N} = \sigma\,(T_{S_{i+1}}^2 + T_{B_N}^2)(T_{S_{i+1}} + T_{B_N})$$

$$T_{B_N} = \left(\frac{k_{Seff_i} T_{S_i}}{\Delta x/2} + H_{R_N}^{*}\, T_{S_i}\right)\left(\frac{k_{Seff_i}}{\Delta x/2} + H_{R_N}^{*}\right)^{-1}$$

APPENDIX B: DEVELOPMENT OF SOURCE TERMS

B.1 Source Terms for Species Balances

The handling of the source terms for each of the three chemical species are given below, with reference to the ϕ-dependent and ϕ-independent parts discussed in Section 4., where:

$$S = S_C + S_P \phi_P$$

The subscript C refers to the ϕ-independent source terms, and the subscript P refers to ϕ-dependent source terms. The source treatment for each species is then as follows

O_2:

$$S_P = (-S_1 G_1 a_B^o \Delta x \Delta t - S_3 R_{CO} \epsilon \Delta x \Delta t) / Y^*_{O_2,\infty}$$

$$S_C = 0$$

and

CO_2:

$$S_P = \frac{-S_2 G_2 a^o_B \Delta x \Delta t}{Y^*_{CO_2,\infty}} - \frac{(1 + S_3) R_{CO} \epsilon \Delta x \Delta t}{\tilde{Y}_{CO_2,\infty} - Y^*_{CO_2,\infty}}$$

$$S_C = \chi(1 + S_1) G_1 a^o_B \Delta x \Delta t + \frac{(1 + S_3) R_{CO} \epsilon \Delta x \Delta t \tilde{Y}_{CO_2,\infty}}{\tilde{Y}_{CO_2,\infty} - Y^*_{CO_2,\infty}}$$

and

CO:

$$S_P = \frac{-\epsilon R_{CO} \Delta x \Delta t}{Y^*_{CO,\infty}}$$

$$S_C = [(1 - \chi)(1 + S_1) G_1 + (1 + S_2) G_2] a^o_B \Delta x \Delta t$$

where

$$\tilde{Y}_{CO_{2^\infty}} = (Y^*_{CO_{2^\infty}} + 1)/2$$

and the other variables are as defined previously. The term R_{CO} represents the rate expression for the CO oxidation reaction and is defined elsewhere (see Section 3.4). In the numerical analysis, this reaction rate was calculated based on previous iteration values of the gas species concentrations and the previous timestep value of T_G.

B.2 Gas Phase Energy Balance- Reaction Source Term

The gas phase energy balance terms were all contained in Sc because of the dependence of R_{CO} on the gas temperature from the previous timestep:

$$S_P = 0$$

$$S_C = R_{CO} \epsilon \Delta x \Delta t \Delta H_{R_{CO}}$$

where ΔH_{Rco} is the heat release from the CO oxidation reaction in J kg^{-1} CO^{-1}.

B.3 Solid Phase Energy Balance- Reaction Source Term

The reaction source term for the solid consisted of two terms, one for each of the solid surface reactions R3 and R4. The term for R3 was placed into S_P because it represented a negative temperature source (due to the endothermicity of this reaction):

$$S_P = G_2 \Delta H_3 \, a^\circ_B \Delta x \Delta t / T^*_S$$

$$S_C = \left(\frac{\Delta H_2 \chi \left(\frac{M_C}{M_{CO2}} \right) + \Delta H_1 (1 - \chi) \left(\frac{M_C}{M_{CO}} \right)}{\chi \left(\frac{M_C}{M_{CO2}} \right) + (1 - \chi) \left(\frac{M_C}{M_{CO}} \right)} \right) G_1 a^\circ_B \Delta x \Delta t$$

where the term in large parentheses represents a weighted average of ΔH_1 and ΔH_2 in J kg C^{-1} for the simultaneous surface reactions R1 and R2 respectively. This weighted average is

based on the CO to CO_2 product ratio. The heat of reaction ΔH_3 corresponds to the heat release of reaction R3.

APPENDIX C: ESTIMATE OF THE INTERDIFFUSION EFFECT ON HEAT TRANSFER

The effect of the interdiffusion term in the energy equation on heat transfer to/from the char surface will be estimated by evaluating this term for a spherical particle in quiescent surroundings. The energy equation for this situation is:

$$R^2 G Cp_G \frac{\partial T}{\partial r} = k_S \frac{\partial}{\partial r}\left(r^2 \frac{\partial T}{\partial r} \right) - \sum r^2 j_i Cp_i \frac{\partial T}{\partial r} \qquad \text{(C-1)}$$

where the first term represents energy convection away from the particle due to the net flux of product gases leaving the surface, the second term represents heat conduction to the particle, and the last term represents heat transport due to species interdiffusion and G is the total carbon consumption rate as previously defined. The diffusion fluxes can then be expressed in terms of the net flux and the convective flux of each species respectively:

$$\begin{aligned} r^2 j_i &= r^2 (\rho v)_i - r^2 (\rho v) Y_i \\ &= R^2 G_i - R^2 G Y_i \end{aligned}$$

Evaluating the individual species fluxes to and from the particle surface:

$$\begin{aligned} O_2: &\quad G_i = -G S_1 \\ CO: &\quad G_i = G(1 + S_1) \\ N_2: &\quad G_i = 0 \qquad (\textit{no surface penetration of } N_2) \end{aligned}$$

Then:

$$\begin{aligned} r^2 j_{O_2} &= R^2 G(-S_1 - Y_{O_2}) \\ r^2 j_{CO} &= R^2 G(1 + S_1 - Y_{CO}) \\ r^2 j_{N_2} &= R^2 G(-Y_{N_2}) \\ &= R^2 G(-1 + Y_{O_2} + Y_{CO}) \end{aligned}$$

Replacing the last term in equation (C-1)

$$\sum r^2 j_i Cp_i \frac{\partial T}{\partial r} = R^2 G[\, Cp_{O_2}(-S_1 - Y_{O_2}) + Cp_{CO}(1 + S_1 - Y_{CO}) + Cp_{N_2}(-1 + Y_{O_2} + Y_{CO})\,] \frac{\partial T}{\partial r}$$

Since $Cp = \sum Cp_i Y_i$, the term above can be rewritten as:

$$\sum r^2 j_i Cp_i \frac{\partial T}{\partial r} = R^2 G[\, -S_1 Cp_{O_2} + (1 + S_1) Cp_{CO} - Cp\,] \frac{\partial T}{\partial r} \qquad \text{(C-2)}$$

where Cp is the heat capacity of the gas mixture. Substituting (C-2) into (C-1) then gives:

$$0 = k \frac{\partial}{\partial r}\left(r^2 \frac{\partial T}{\partial r} \right) - R^2 G[\,(1 + S_1) Cp_{CO} - S_1 Cp_{O_2}\,] \frac{\partial T}{\partial r}$$

or:

$$k \frac{\partial}{\partial r}\left(r^2 \frac{\partial T}{\partial r} \right) = R^2 G\, Cp_{eff} \frac{\partial T}{\partial r}$$

where Cp_{eff} is an effective heat capacity for the gas mixture that corrects for the effect of interdiffusion. Substitution of the appropriate values demonstrates that $C_{peff} = C_p$ to within a few percent. Thus, the interdiffusion effect is virtually negligible.

APPENDIX D: PROGRAM CODE AND DATA

```
      PROGRAM CHAR
*
*     CALCULATES T AND CONC PROFILES FOR BURNING FIXED BED
*
      PARAMETER (N=50,M=1000)
      DIMENSION G(N),TG(N),TS(N),TGO(N),TSO(N),V(N),VS(N)
      DIMENSION Y8O2(N),Y8CO(N),Y8CO2(N),Y8N2(N),RHOG(N)
      DIMENSION YO2(N),YCO2(N),YCO(N),YN2(N),XB(N),DXN(N)
      DIMENSION G1(N),G2(N),G1O(N),G2O(N),X(N),S(N),CPG(N)
      DIMENSION AKY(N),AKG(N),H(N),CO2(N),CO(N),O2(N),RHOS(N)
      DIMENSION AKAG(N),DEFF(N),AKAS(N),TESTTS(N),TESTTG(N)
      DIMENSION PAO(N),RHO(N),D(N),DO(N),Y8O2P(N),Y8COP(N),Y8CO2P(N)
      DIMENSION Y8N2P(N),TP(N),TSI(N),DIAM(N),PA(N),RCO(N),SLAB(N)
        DIMENSION CPGREG(N),AMWG(N),AKS(N),FE(N)
*
      COMMON/PRIME/ Y8O2P,Y8COP,Y8CO2P,Y8N2P,TP
      COMMON/SYST/VOID,DIAM,E,SLAB,PA,AKS,CARB,ASH,DT,RHOS
      COMMON/INFO/WTN2,WTO2,WTCO2,WTCO,R,P,SIGMA,AMEGA,BETA,GAMMA,THI
      COMMON/STOIC/ SCO2,SCO,S3,S2,DH1,DH2,DH3,DH4
      COMMON/GE/ A,A1,ER,ER1,ALPHA1,ALPHA2,ALPHA3
      COMMON/CP/AO2,BO2,DO2,ACO,BCO,DCO,ACO2,BCO2,DCO2,AN2,BN2,DN2
      COMMON/ARRAY/V,VS,G,YO2,YCO2,YCO,Y8O2,Y8CO2,Y8CO,RHOG
      COMMON/EXTRA/Y8N2,YN2,CPEFF,CPGREG
      COMMON/TIME/IFLAG,ITIME,ITERNS,IREACT,TURNS,IB,IG
      COMMON/TEST/TESTTG,TESTTS,CRIT
      COMMON/REACT/ G1,G2,X,S
      COMMON/RAD/ TBN,HR2,HRN,BOLTZ,TCOAL
      COMMON/FLUXES/FO2,FC,FCO2,FTG,FTS
*
*     READ IN SYSTEM PARAMETERS
*
      OPEN (1,FILE='CHAR.DAT',STATUS='OLD')
      OPEN (3,FILE='TEMP.DAT', STATUS='OLD')
      OPEN (2,FILE='CHAR.OUT')

      IFLAG = 2
        IFLAG3 = 0
        ITIME= 0
        ITERNS= 0
        CRIT = 2.0
      CALL READER( HTTR,RXN,1,3,U,US,IEND,LIMIT,TG,TS,GRATE,HT)
      CALL SETUP( TG,TS,U,US,TB2,CPG,PAO,TSI,RHO,D,DO)
      CALL DIVIDE(FE,GRATE,HT,XB,DXN)
**    ****************************************************************
*     RECURSION OF MAIN TIME LOOP
**    ****************************************************************
```

```
66      IF((ITIME .EQ. LIMIT).AND.(IFLAG3.EQ.5)) THEN
        IFLAG=4
      CALL PRINT (2,TSI,CGONE,D,XB,AMWG)
      WRITE(2,*) 'END OF RUN, BUT ERROR CRITERION MAY NOT BE MET'
      WRITE(2,44) ERROR
        GO TO 111
        ENDIF
        IF(ITERNS .EQ. IEND) THEN
      WRITE(2,*) 'THE DAMN THING DNCV'
        GO TO 111
        ENDIF
        CALL STOICH(TS)

      CALL GEE(TG,G1O,G2O,CGONE,TSI,AMWG)
      CALL DEE(D,DO)
      CALL GPROP( HTTR,TG,CPG,AKG,AKY,H )
      CALL MFLUX(RHO,PAO)
      CALL SFLUX(2,ISTOP,PAO)
        IF(ISTOP.GT.0) THEN
        GO TO 111
        ENDIF
      CALL COND( GRATE,TG,TS,AKG,AKAS,AKAG,DEFF)
      CALL PCONC( CO2,O2,CO,AKY)
      CALL TDMACN(FE,RXN,DEFF,RHO,PAO,RCO,DXN)
        CALL TDMATG(FE,TG,TS,CPG,AKAG,RHO,PAO,H,TGO,RCO,DXN)
      CALL TDMATS(FE,PAO,TB2,TG,TS,H,TSO,AKAS,TSI,DXN)
      CALL STOCK( TG,TS,TSI,RHO,PAO,CGONE,TSO,TGO,D,DTEMP)
        IF (IFLAG.EQ. 2) THEN
*
*       NEED ANOTHER ITERATION
*
       ITERNS=ITERNS+1.0
       GO TO 66
         ENDIF
         IF (IFLAG.EQ. 3) THEN
*
*       PROCEED TO THE NEXT TIMESTEP, CHECK ERROR, PRINT IF AT S.S.
*
       ITIME = ITIME + 1
       CALL ENERGY(TB2,CPG,TG,TS,ERROR)
*          IF(ABS(DTEMP).LE.10.0*(IB+IG)) THEN
*            DT=10.
*          ENDIF

           IF( ABS(DTEMP).LE.0.001*(IB+IG) ) THEN

             IFLAG=4
         CALL PRINT (2, TSI,CGONE,D,XB,AMWG)
             WRITE(2,44) ERROR
             WRITE(2,43) ITIME*DT
```

```
          ELSE
            ITERNS=0
            IFLAG3 = 5
            GO TO 66
          ENDIF
        ENDIF
**    ***************************************************************
*       END OF MAIN TIME LOOP
**    ***************************************************************
43    FORMAT(/,'TIME ELAPSED IS :',F10.5)
44    FORMAT(/,'PERCENT ENERGY ERROR IS:',F10.6)
111    STOP
        END


    SUBROUTINE READER(HTTR,RXN,IN,INPUT,U,US,IEND,LIMIT,TG,TS,
   + GRATE,HT)
*
*     reads in all system boundaries and constants
*
        CHARACTER*72 TITLE
    PARAMETER (N=50,M=1000)
    DIMENSION G(N),TG(N),TS(N),Y8O2(N),Y8CO2(N),Y8CO(N)
    DIMENSION YO2(N),YCO(N),YCO2(N),V(N),VS(N),RHOG(N)
    DIMENSION RHOS(N),DIAM(N),PA(N),SLAB(N),AKS(N)
    COMMON/SYST/ VOID,DIAM,E,SLAB,PA,AKS,CARB,ASH,DT,RHOS
    COMMON/INFO/WTN2,WTO2,WTCO2,WTCO,R,P,SIGMA,AMEGA,BETA,GAMMA,THI
    COMMON/STOIC/ SCO2,SCO,S3,S2,DH1,DH2,DH3,DH4
    COMMON/GI:/ A,A1,ER,ER1,ALPHA1,ALPHA2,ALPHA3
    COMMON/CP/AO2,BO2,DO2,ACO,BCO,DCO,ACO2,BCO2,DCO2,AN2,BN2,DN2
    COMMON/ARRAY/V,VS,G,YO2,YCO2,YCO,Y8O2,Y8CO2,Y8CO,RHOG
    COMMON/TIME/IF1.AG,ITIME,ITERNS,IREACT,TURNS,IB,IG
    COMMON/RAD/ TBN,HR2,HRN,BOLTZ,TCOAL
    rewind in
    REWIND INPUT
    READ(INPUT,99) TITLE
    READ(INPUT,*) IB,IG,GRATE,HT,CARB,ASH,DT
    READ(INPUT,99) TITLE
    L= IG+IB
    READ(INPUT,*) DIAM(L),U,TG(1),A1,ER1,HTTR,RXN
    READ(IN,99) TITLE
    READ(IN,*) BOLTZ,TCOAL,VOID,E,RHOS(L),A,ER
    READ(IN,99) TITLE
    READ(IN,*) WTN2,WTO2,WTCO2,WTCO,R,P,SIGMA,AMEGA,BETA,GAMMA,THI
    READ(IN,99) TITLE
    READ(IN,*) AO2,BO2,DO2,ACO,BCO,DCO,ACO2
    READ(IN,99) TITLE
    READ(IN,*) BCO2,DCO2,AN2,BN2,DN2
    READ(IN,99) TITLE
    READ(IN,*) US,G(1),TS(1),Y8O2(1),Y8CO(1),Y8CO2(1)
```

```
      READ(IN,99) TITLE
      READ(IN,*) G(L),TG(L),TS(L),TS(L-1),Y8O2(L),Y8CO(L),Y8CO2(L)
      READ(IN,99) TITLE
      READ(IN,*) SCO,SCO2,S3,S2,IREACT,DH1,DH2,DH3,DH4
      READ(IN,99) TITLE
      READ(IN,*) LIMIT,IEND,ALPHA1,ALPHA2
98    FORMAT(7F14.6,1X)
99      FORMAT(A72)
100   FORMAT(I8)
        RETURN
        END


      SUBROUTINE SETUP(TG,TS,U,US,TB2,CPG,PAO,TSI,RHO,D,DO)
*
*       calculates initial profiles and boundaries
*
      PARAMETER (N=50,M=1000)
      DIMENSION G(N),Y8O2(N),Y8CO2(N),Y8CO(N),Y8N2(N),VS(N)
      DIMENSION YO2(N),YCO(N),YCO2(N),YN2(N),V(N),RHOG(N),CPG(N)
      DIMENSION G1(N),G2(N),X(N),S(N),D(N),DO(N),SLAB(N)
      DIMENSION TS(N),TG(N),RHOS(N),DIAM(N),PA(N),PAO(N),Y8O2P(N)
      DIMENSION Y8N2P(N),Y8COP(N),Y8CO2P(N),TP(N),TSI(N),RHO(N)
      DIMENSION CPGREG(N),AKS(N)
      COMMON/PRIME/ Y8O2P,Y8COP,Y8CO2P,Y8N2P,TP
      COMMON/REACT/ G1,G2,X,S
      COMMON/SYST/ VOID,DIAM,E,SLAB,PA,AKS,CARB,ASH,DT,RHOS
      COMMON/INFO/WTN2,WTO2,WTCO2,WTCO,R,P,SIGMA,AMEGA,BETA,GAMMA,THI
      COMMON/ARRAY/V,VS,G,YO2,YCO2,YCO,Y8O2,Y8CO2,Y8CO,RHOG
      COMMON/EXTRA/Y8N2,YN2,CPEFF,CPGREG
      COMMON/TIME/IFLAG,ITIME,ITERNS,IREACT,TURNS,IB,IG
      COMMON/RAD/ TBN,HR2,HRN,BOLTZ,TCOAL
      IT = IB + IG
      DO 11  I = 2, IT-1
        TS(I) = TS(IT-1)
        TG(I) = TG(1)
        Y8O2(I) = Y8O2(1)
        Y8CO2(I)= Y8CO2(1)
        Y8CO(I) = Y8CO(1)
11    CONTINUE
      DO 22 I=1,IT
        RHOS(I) = RHOS(IT)
        RHOG(I)=DENS(TG(I),I)
        G1(I) = G(IT)
        G2(I) = G(IT)
        YO2(I) = Y8O2(I)
        YCO2(I) = Y8CO2(I)
        YCO(I) = Y8CO(I)
        YN2(I) = 1.0-YO2(I)-YCO2(I)-YCO(I)
```

```
      TP(I) = TG(I)
      TSI(I) = TS(I)
      Y8O2P(I) = Y8O2(I)
      Y8CO2P(I) = Y8CO2(I)
      Y8COP(I) = Y8CO(I)
      DIAM(I) = DIAM(IT)
      PA(I) = 6.0*(1.0-VOID)/DIAM(I)
      DO(I) = DIAM(IT)
      D(I) = DIAM(IT)
      PAO(I) = PA(I)
      RHO(I) = RHOG(I)
      CPG(I) = CPGBAR(TG(I),I)
      VS(I) = US*RHOS(1)*ASH
      V(I) = U*RHOG(1)
22    CONTINUE
        TB2=( TS(1)+TS(2) )/2.0
        TBN=( TS(IT)+TS(IT-1) )/2.0
        HR2 = BOLTZ*( TS(1)*TS(1) + TB2*TB2 )
        HR2 = HR2*( TS(1) +  TB2 )
        HRN = BOLTZ*( TS(IT)*TS(IT) + TBN*TBN )
        HRN = HRN*( TS(IT) + TBN )
        RETURN
        END


      SUBROUTINE DIVIDE(FE,GRATE,HT,XB,DXN)
      PARAMETER (N=50,M=1000)
          DIMENSION DIAM(N),SLAB(N),PA(N),RHOS(N),XB(N),DXN(N),AKS(N)
          DIMENSION FE(N)
      COMMON/TIME/IFLAG,ITIME,ITERNS,IREACT,TURNS,IB,IG
      COMMON/SYST/ VOID,DIAM,E,SLAB,PA,AKS,CARB,ASH,DT,RHOS
      DEL1 = LOG(HT+1.0)/(IB-1)
      DEL2 = LOG(GRATE+1.0)/(IG-1)
      DO 11 I=IG+1,IB+IG
       XB(I) = ( EXP( (I-IG)*DEL1 ) - 1.0)* .01
11    CONTINUE
      DO 22 I=1,IG
       XB(IG-I+1) = -(EXP( (I-1)*DEL2) - 1.0)* .001
22    CONTINUE
      DO 33 I=1,IB+IG
       IF(I.EQ.1) THEN
        SLAB(I) = ABS(XB(I+1)-XB(I))
       ELSE
        SLAB(I) = ABS( XB(I) - XB(I-1))
       ENDIF
33    CONTINUE
      DO 44 I=1,IB+IG-1
           DXN(I) = ABS(SLAB(I) + SLAB(I+1))/2.0
       FE(I) = 0.5*SLAB(I)/DXN(I)
44    CONTINUE
```

```
      RETURN
         END


         SUBROUTINE STOICH(TS)
*
*        calculates co/co2 ratio and mass c burned per co+co2 product
*
      PARAMETER (N=50,M=1000)
         DIMENSION X(N),TS(N),S(N),V(N),G(N),YO2(N),YCO2(N),YCO(N)
      DIMENSION Y8O2(N),Y8CO2(N),Y8CO(N),G1(N),G2(N),RHOG(N),VS(N)
      COMMON/REACT/ G1,G2,X,S
      COMMON/STOIC/ SCO2,SCO,S3,S2,DH1,DH2,DH3,DH4
      COMMON/ARRAY/V,VS,G,YO2,YCO2,YCO,Y8O2,Y8CO2,Y8CO,RHOG
      COMMON/INFO/WTN2,WTO2,WTCO2,WTCO,R,P,SIGMA,AMEGA,BETA,GAMMA,THI
      COMMON/TIME/IFLAG,ITIME,ITERNS,IREACT,TURNS,IB,IG
         S(1) = 0.0
         X(1) = 0.0
      DO  22    I=2,IG+IB-1
        X(I) = 2500*EXP(-6240.0/TS(I))*WTCO/WTCO2
        X(I) = 1.0/(1.0+X(I))
        S(I) = (1.0 + SCO2)*(1.0 + SCO)
        S(I) = S(I)/( X(I)*(1.0 + SCO) + ( 1.0-X(I) )*(1.0 + SCO2 ))
        S(I) = S(I)-1.0
22    CONTINUE
         S(IB+IG) = 0.0
         X(IB+IG) = 0.0
         RETURN
         END
CC       CCCCCC
      SUBROUTINE DEE(D,DO)
      PARAMETER (N=50,M=1000)
      DIMENSION RHOS(N),V(N),VS(N),G(N),YO2(N),YCO(N),Y8O2(N),Y8CO(N)
      DIMENSION YCO2(N),Y8CO2(N),RHOG(N),PD(N),QD(N)
      DIMENSION DIAM(N),PA(N),D(N),DO(N),SLAB(N),AKS(N)
      COMMON/SYST/ VOID,DIAM,E,SLAB,PA,AKS,CARB,ASH,DT,RHOS
      COMMON/ARRAY/V,VS,G,YO2,YCO2,YCO,Y8O2,Y8CO2,Y8CO,RHOG
      COMMON/TIME/IFLAG,ITIME,ITERNS,IREACT,TURNS,IB,IG
      COMMON/GE/ A,A1,ER,ER1,ALPHA1,ALPHA2,ALPHA3
         AD = 1.0
         BD = 0.0
         CD = 0.0
         DD = DIAM(IB+IG)
         PD(IB+IG) = BD/AD
         QD(IB+IG) = DD/AD
      DO   10   I=IB+IG-1,IG+1,-1
        DO(I) = DIAM(I)
        BD = AMAX1( 0.0,-VS(I)*DT/RHOS(I) )
        CD = 0.0
        AD = (1.0-VOID)*SLAB(I) - VS(I-1)*DT/RHOS(I)
```

```
      DD = (1.0-VOID)*SLAB(I)*D(I)
      DD = DD - 8.0*G(I)*(1.0-VOID)*DT*SLAB(I)/RHOS(I)
      PD(I) = CD/( AD - BD*PD(I+1) )
      QD(I) = (BD*QD(I+1) +DD) / ( AD-BD*PD(I+1) )
10      CONTINUE
        DIAM(IG+1) = QD(IG+1)
        PA(IG+1) = 6.0*(1.0-VOID)/DIAM(IG+1)

      DO   11  I=IG+2,IG+IB-1
        DIAM(I) = PD(I)*DIAM(I-1) + QD(I)
        PA(I) = 6.0*(1.0-VOID)/DIAM(I)
11      CONTINUE
        RETURN
        END



      SUBROUTINE GEE(TG,G1O,G2O,CGONE,TSI,AMWG)
*
*       calculate carbon consumption rates
*
      PARAMETER (N=50,M=1000)
      DIMENSION YO2(N),YCO(N),YCO2(N),G1O(N),TG(N),RHOG(N),G2O(N)
      DIMENSION G1(N),G2(N),G(N),V(N),VS(N),Y8O2(N),Y8CO2(N),Y8CO(N)
      DIMENSION X(N),S(N),TSI(N),RHOS(N),DIAM(N),PA(N),SLAB(N)
      DIMENSION AMWG(N),AKS(N)
      COMMON/REACT/ G1,G2,X,S
      COMMON/SYST/ VOID,DIAM,E,SLAB,PA,AKS,CARB,ASH,DT,RHOS
      COMMON/INFO/WTN2,WTO2,WTCO2,WTCO,R,P,SIGMA,AMEGA,BETA,GAMMA,THI
      COMMON/GE/  A,A1,ER,ER1,ALPHA1,ALPHA2,ALPHA3
      COMMON/ARRAY/V,VS,G,YO2,YCO2,YCO,Y8O2,Y8CO2,Y8CO,RHOG
      COMMON/TIME/IFLAG,ITIME,ITERNS,IREACT,TURNS,IB,IG
      COMMON/RAD/ TBN,HR2,HRN,BOLTZ,TCOAL
        CGONE = 0.0
        G1(1) = 0.0
        G2(1) = 0.0
      DO 11 I=2,IG
        G(I) = 0.0
        G1(I) = 0.0
        G2(I)= 0.0
11    CONTINUE
      DO 22 I=1,IB+IG-1
        AMWG(I) = RHOG(I)*R*TG(I)/P
22    CONTINUE
      DO  33    I=IG+1,IB+IG-1
        G1O(I) = G1(I)
        G2O(I) = G2(I)
        IF(IREACT.GT.0) THEN
*
*       SET PARTIAL PRESSURES OF GASES IN THE BED SLABS ( IN KPA )
```

```
*
      PO2 = ( P/1000.)*YO2(I)*AMWG(I)/WTO2
      PCO = ( P/1000.)*YCO(I)*AMWG(I)/WTCO
      PCO2 = ( P/1000.)*YCO2(I)*AMWG(I)/WTCO2
*
*       SET ARRHENIUS RATE CONSTANTS FOR THE C+CO2-CO RXN
*
      AK1 = A1*EXP(-ER1/TSI(I))
*
* FIND THE CARBON CONSUMPTION RATES FOR RXNS AND THE TOTAL CONSUMPTION
*
      G1(I) = A*EXP(-ER/TSI(I))*PO2
      G2(I) = 0.0
      IF (IREACT.GT.1) THEN
            G2(I) = AK1*PCO2/101.3
      ENDIF
      IF(DIAM(I).LT.DIAM(IG+IB)/1000.) THEN
        G1(I) = 0.0
        G2(I) = 0.0

      ENDIF
      G(I) = G1(I)+G2(I)
     ELSE
      G1(I) = 0.0
      G2(I) = 0.0
      G(I) = G1(I)+G2(I)
     ENDIF

33    CONTINUE
        G1(IB+IG) = 0.0
        G2(IB+IG) = 0.0
        RETURN
    END

*
    SUBROUTINE GPROP( HTTR,TG,CPG,AKG,AKY,H)
    PARAMETER (N=50,M=1000)
    DIMENSION CPG(N),AKG(N),AKY(N),H(N),TG(N),SLAB(N)
    DIMENSION V(N),VS(N),Y8O2(N),Y8N2(N),Y8CO(N),Y8CO2(N),G(N)
    DIMENSION YO2(N),YCO2(N),YCO(N),YN2(N),RHOS(N),DIAM(N),PA(N)
        DIMENSION CPGREG(N),AMWG(N),AKS(N),RHOG(N)

        COMMON/SYST/ VOID,DIAM,E, SLAB,PA,AKS,CARB,ASH,DT,RHOS
    COMMON/INFO/WTN2,WTO2,WTCO2,WTCO,R,P,SIGMA,AMEGA,BETA,GAMMA,THI
    COMMON/STOIC/ SCO2,SCO,S3,S2,DH1,DH2,DH3,DH4
    COMMON/CP/AO2,BO2,DO2,ACO,BCO,DCO,ACO2,BCO2,DCO2,AN2,BN2,DN2
    COMMON/ARRAY/V,VS,G,YO2,YCO2,YCO,Y8O2,Y8CO2,Y8CO,RHOG
    COMMON/EXTRA/Y8N2,YN2,CPEFF,CPGREG
    COMMON/TIME/IFLAG,ITIME,ITERNS,IREACT,TURNS,IB,IG
```

```
      DO 5 I=1,IB+IG
       CPG(I) = CPGBAR(TG(I),I)
       AMU = 2.6693E-06*SQRT(WTN2*TG(I)*1000.)/((SIGMA**2)*AMEGA)
       AMWG(I)=RHOG(I)*TG(I)*R/P
       AKG(I) = ( CPGREG(I) + (5.0/4.0)*(R/(AMWG(I)*1000) )*AMU
       ALEFF =1.0
       BM = ( Y8O2(I) - YO2(I) ) / ( SCO + YO2(I) )
       IF(ABS(BM).LE.1.0E-3) THEN
        CORRKY = 1.0
       ELSE
        CORRKY = (LOG( 1.0 + BM ))/BM
       ENDIF
       BT = (( 1.0 + BM)**ALEFF) - 1.0
       IF((BT.LE.1.0E-3).OR.(ABS(BM).LT.1.0E-3) ) THEN
        CORRH = 1.0
       ELSE
        CORRH = (LOG( 1.0 + BT ))/BT
       ENDIF
       RE= V(I)/( AMU*PA(I) )
       AR=(DIAM(I)**(3))*9.8*RHOG(I)*( RHOS(I)-RHOG(I) )/(AMU**2)
       PR = AMU*CPGREG(I) / AKG(I)
       if(ITIME.eq.2000) then
       test = ar/(re*re*36)
       write(2,*) float(i),re,test
       endif
       IF(HTTR.EQ.1970) THEN
*
*        BRATTACHARYA AND PEI HEAT TR OPTION
*
        AJH =  0.018*( AR/(RE*RE*36.) )**(0.25)
       ENDIF
       IF(HTTR.EQ.1960) THEN
*
*        YOSHIDA AND WEN OPTION
*
        IF(RE.LT.50.0) THEN
         AJH = 0.91*(RE**(-0.51))
        ELSE
         AJH = 0.61*(RE**(-0.41))
        ENDIF
       ENDIF

       IF (HTTR.EQ.1950) THEN
*
*        CHU OPTION
*
        AJH = 1.77*(RE*6.)**(-0.44)
        AJD = 5.7*(RE*6.)**(-0.78)
       ELSE
        AJD = AJH
```

```
      ENDIF
      IF((I.EQ.1).OR.(I.EQ.IB+IG)) THEN
        AKY(I) = 0.0
        H(I) = 0.0
      ELSE
        AKY(I) = (AJH*V(I)/( PR**(0.66) ))*CORRKY
        H(I) = AJH*CORRH*CPGREG(I)*V(I)/( PR**(0.66) )
      ENDIF
5       CONTINUE
        RETURN
      END


      SUBROUTINE MFLUX(RHO,PAO)
*
*       CALCULATE MASS VELOCITIES THROUGH THE BED SLABS
*
      PARAMETER (N=50,M=1000)
      DIMENSION V(N),VS(N),G(N),RHOS(N),RHOG(N)
      DIMENSION YO2(N),YCO2(N),YCO(N),Y8O2(N),Y8CO2(N),Y8CO(N)
      DIMENSION RHO(N),DIAM(N),PA(N),PAO(N),SLAB(N),AKS(N)
      COMMON/SYST/ VOID,DIAM,E,SLAB,PA,AKS,CARB,ASH,DT,RHOS
      COMMON/ARRAY/V,VS,G,YO2,YCO2,YCO,Y8O2,Y8CO2,Y8CO,RHOG
      COMMON/TIME/IFLAG,ITIME,ITERNS,IREACT,TURNS,IB,IG
*
      DO 7  I = 2, IB+IG-1
        V(I) = G(I)*SLAB(I)*PAO(I)+VOID*(RHOG(I)-RHO(I))*SLAB(I)/DT
        V(I) = V(I) + V(I-1)
7       CONTINUE
      V(IB+IG) = V(IB+IG-1)
        RETURN
        END
CC      CCCCC


      SUBROUTINE SFLUX(IO,ISTOP,PAO)
*
*       CALCULATE MASS VELOCITIES THROUGH THE BED SLABS
*
      PARAMETER (N=50,M=1000)
      DIMENSION V(N),VS(N),G(N),VSOLD(N),RHOG(N)
      DIMENSION YO2(N),YCO2(N),YCO(N),Y8O2(N),Y8CO2(N),Y8CO(N)
      DIMENSION RHOS(N),DIAM(N),PA(N),PAO(N),SLAB(N),AKS(N)

      COMMON/SYST/ VOID,DIAM,E,SLAB,PA,AKS,CARB,ASH,DT,RHOS
      COMMON/ARRAY/V,VS,G,YO2,YCO2,YCO,Y8O2,Y8CO2,Y8CO,RHOG
      COMMON/TIME/IFLAG,ITIME,ITERNS,IREACT,TURNS,IB,IG
*
        ISTOP = 0
        ICOUNT = 0
```

```
*
*       RESET A GUESS FUEL INLET MASS VELOCITY UNTIL CONVERGENCE
*
333   DO 7  I = 2,IB+IG-1
      VSOLD(I) = VS(I)
      VS(I) = -G(I)*SLAB(I)*PAO(I)
      VS(I) = VS(I) + VS(I-1)
7       CONTINUE
        IF(ASH.GT.0.0)THEN
      VS(IB+IG) = VS(1)/ASH
        ELSE
      VS(IB+IG) = VS(IG+IB-1)
        ENDIF
        VCHK = ABS( VS(IB+IG)-VS(IB+IG-1) )
        IF(VCHK.GT.1.0E-04) THEN
      VS(1) = VS(IB+IG-1)*ASH
      ICOUNT = ICOUNT+1
      IF(ICOUNT.GT.100) THEN
        WRITE(IO,*) 'RESULTS INVALID VS DNCNV'
        WRITE(IO,*) VCHK
        ISTOP = 1
        GO TO 33
      ENDIF
      GO TO 333
    ENDIF
33      RETURN
        END



        SUBROUTINE COND( GRATE,TG,TS,AKG,AKAS,AKAG,DEFF)
*
*       calculates effective conds of gas and solid phases
*
   PARAMETER  (N=50,M=1000)
   DIMENSION TG(N),TS(N),AKAS(N),AKAG(N),V(N),VS(N),AKG(N)
   DIMENSION G(N),YO2(N),YCO2(N),YCO(N),Y8O2(N),Y8CO2(N),Y8CO(N)
   DIMENSION DEFF(N),RHOG(N),RHOS(N),DIAM(N),PA(N),SLAB(N)
   DIMENSION Y8N2(N),YN2(N),AKS(N),CPGREG(N)
   COMMON/SYST/ VOID,DIAM,E,SLAB,PA,AKS,CARB,ASH,DT,RHOS
   COMMON/INFO/WTN2,WTO2,WTCO2,WTCO,R,P,SIGMA,AMEGA,BETA,GAMMA,THI
   COMMON/ARRAY/V,VS,G,YO2,YCO2,YCO,Y8O2,Y8CO2,Y8CO,RHOG
   COMMON/TIME/IFLAG,ITIME,ITERNS,IREACT,TURNS,IB,IG
   COMMON/EXTRA/Y8N2,YN2,CPEFF,CPGREG
   DO  9   I=1,IG+IB
     TM = ( TS(I) + TG(I) ) / 2.0
     HRV = 0.2268/( 1.0 + (0.5*VOID/(1.0-VOID)) * ((1-E)/E) )
     HRV = HRV*(( TM/100.0 )**(3))
     HRS = 0.2268*( E/(2-E) )*(( TM/100.0 )**(3))
     AKS(I) = ((RHOS(I)/4511.)**3.5)*TS(I)**0.5
```

```
      AKAS(I) =(GAMMA/AKS(I)) + ((AKG(I)/THI + HRS*DIAM(I) )**(-1))
      AKAS(I)= ( BETA*(1.0-VOID)/AKAS(I) ) + VOID*BETA*DIAM(I)*HRV
      AKAG(I) = 1.0 + (9.7*VOID*AKG(I)/(V(I)*DIAM(I)*CPGREG(I)))
          AKAG(I) = 0.73*VOID*AKG(I) + 0.5*V(I)*DIAM(I)*CPGREG(I)/AKAG(I)
      DEFF(I) = AKAG(I)/( CPGREG(I)*RHOG(I) )
9     CONTINUE
      DO 88 I=1,IG
        AKAS(I) =(GAMMA/35.) + ((AKG(I)/THI + HRS*DIAM(I) )**(-1))
        AKAS(I)= ( BETA*(1.0-VOID)/AKAS(I) ) + VOID*BETA*DIAM(I)*HRV
88    CONTINUE
      RETURN
      END


      SUBROUTINE PCONC( CO2,O2,CO,AKY)
*
*     calculates gas concn's at particle surface
*
      PARAMETER (N=50,M=1000)
      DIMENSION G(N),G1(N),G2(N),AKY(N),S(N),X(N),O2(N),CO(N),CO2(N)
      DIMENSION Y8O2(N),Y8CO(N),Y8CO2(N),YO2(N),YCO(N),YCO2(N)
      DIMENSION V(N),VS(N),RHOG(N)
      COMMON/STOIC/ SCO2,SCO,S3,S2,DH1,DH2,DH3,DH4
      COMMON/ARRAY/V,VS,G,YO2,YCO2,YCO,Y8O2,Y8CO2,Y8CO,RHOG
      COMMON/TIME/IFLAG,ITIME,ITERNS,IREACT,TURNS,IB,IG
      COMMON/REACT/ G1,G2,X,S
      DO 6 I=2,IG+IB-1
        CO2(I)=YCO2(I)
        O2(I)=YO2(I)
        CO(I)=YCO(I)
        FACTOR = G(I) + (S(I)*G1(I))/O2(I)
        YO2(I) = Y8O2(I)/( 1.0 + (1.0/AKY(I)) * FACTOR )
        YCO2(I) = X(I)*(1.0+S(I))*G1(I)/AKY(I) + Y8CO2(I)
        YCO2(I) = YCO2(I)/( 1.0+(1.0/AKY(I))*(G(I) +S2*G2(I)/CO2(I)))
        ADD = (1.0-X(I))*(1.0+S(I))*G1(I) + AKY(I)*Y8CO(I)
        YCO(I) = ((1.0+S2)*G2(I) + ADD)/(G(I)+AKY(I))
        IF(YCO(I).LE.1.0E-40) THEN
          YCO(I) = 1.0E-40
        ENDIF
        IF(YO2(I).LE.1.0E-40) THEN
          YO2(I) = 1.0E-40
        ENDIF
        IF(YCO2(I).LE.1.0E-40) THEN
          YCO2(I) = 1.0E-40
        ENDIF
6     CONTINUE
      RETURN
      END
```

```
      SUBROUTINE TDMACN(FE,RXN,DEFF,RHO,PAO,RCO,DXN)
*
      PARAMETER (N=50,M=1000)
      DIMENSION V(N),VS(N),S(N),CO28(N),O28(N),CO8(N),Y8O2(N),Y8CO(N)
      DIMENSION Y8CO2(N),Y8N2(N),G1(N),G2(N),G(N),RHOG(N),X(N)
      DIMENSION YO2(N),YCO2(N),YCO(N),YN2(N),Y8O2P(N),Y8CO2P(N)
      DIMENSION Y8COP(N),TP(N),PAO(N),RHO(N),AC(N),CC(N),QC(N),PC(N)
      DIMENSION CONC(N),DIAM(N),PA(N),Y8N2P(N),RCO(N),DEFF(N)
      DIMENSION FN(N),DN(N),FS(N),DS(N),PEN(N),PES(N),RHOS(N),DXN(N)
      DIMENSION SPO2(N),SPCO(N),SCCO(N),SPCO2(N),SCCO2(N),SLAB(N)
        DIMENSION CPGREG(N),AKS(N),FE(N)

      COMMON/PRIME/ Y8O2P,Y8COP,Y8CO2P,Y8N2P,TP
      COMMON/RAD/ TBN,HR2,HRN,BOLTZ,TCOAL
      COMMON/REACT/ G1,G2,X,S
      COMMON/INFO/WTN2,WTO2,WTCO2,WTCO,R,P,SIGMA,AMEGA,BETA,GAMMA,THI
      COMMON/SYST/ VOID,DIAM,E,SLAB,PA,AKS,CARB,ASH,DT,RHOS
      COMMON/STOIC/ SCO2,SCO,S3,S2,DH1,DH2,DH3,DH4
      COMMON/ARRAY/V,VS,G,YO2,YCO2,YCO,Y8O2,Y8CO2,Y8CO,RHOG
      COMMON/EXTRA/Y8N2,YN2,CPEFF,CPGREG
      COMMON/TIME/IFLAG,ITIME,ITERNS,IREACT,TURNS,IB,IG
      COMMON/FLUXES/FO2,FC,FCO2,FTG,FTS
      DO 14   I = 2,IB+IG-1
        O28(I) = Y8O2(I)
        CO28(I) = Y8CO2(I)
        CO8(I) = Y8CO(I)
        IF(CO28(I).LE.1.0E-40) THEN
          CO28(I) = 1.0E-40
        ENDIF
        IF(O28(I).LE.1.0E-40) THEN
         O28(I) = 1.0E-40
        ENDIF
        FN(I) = V(I)*DT
        FS(I) = V(I-1)*DT
            DN(I) = FE(I)*DEFF(I) + (1.0-FE(I))*DEFF(I+1)
            DN(I) = RHOG(I)*DN(I)*DT/DXN(I)
            DS(I) = FE(I-1)*DEFF(I-1) + (1.0-FE(I-1))*DEFF(I)
            DS(I) = RHOG(I-1)*DS(I)*DT/DXN(I-1)
        PEN(I) = FN(I)/DN(I)
        PES(I) = FS(I)/DS(I)
        IF(RXN.EQ.1980) THEN
*
*         WESTBROOK AND DRYER CO KINETICS OPTION
*
          IF((IREACT.LT.3))THEN
            RCO(I) = 0.0
          ELSE
                  RCO(I) = (O28(I)**0.25)*(1.8562E+10)*EXP(-20130./TP(I))
           RCO(I) = RCO(I)*(RHOG(I)**1.75)*CO8(I)*VOID*SLAB(I)*DT
          ENDIF
```

```
      ENDIF

      IF(RXN.EQ.1970) THEN
*
*       HOWARD AND FINE CO KINETICS OPTION
*
        IF((IREACT.LT.3))THEN
         RCO(I) = 0.0
        ELSE
                RCO(I) = (O28(I)**0.5)*(4.5319E+8)*EXP(-15098./TP(I))
                RCO(I) = RCO(I)*(RHOG(I)**2.0)*CO8(I)*VOID*SLAB(I)*DT
        ENDIF
      ENDIF
      ECO2 = (CO28(I) + 1.0)/2.0
      SPCO2(I) = -S2*G2(I)*PAO(I)*SLAB(I)*DT/CO28(I)
      SPCO2(I) = SPCO2(I) - RCO(I)*(1.0+S3)*(ECO2-CO28(I))
      SCCO2(I) = X(I)*( 1.0+S(I) )*G1(I)*PAO(I)*SLAB(I)*DT
      SCCO2(I) = SCCO2(I) + (1.0+S3)*RCO(I)*ECO2/(ECO2-CO28(I))
      SPO2(I) = (-S(I)*G1(I)*PAO(I)*SLAB(I)*DT - S3*RCO(I))/O28(I)
      SPCO(I) = -RCO(I)/CO8(I)
      SCCO(I) = ( 1.0-X(I) )*( 1.0+S(I) )*G1(I)
      SCCO(I) = ( SCCO(I)+(1.0+S2)*G2(I) ) *PAO(I)*SLAB(I)*DT

14      CONTINUE
*
        IF(IREACT.GT.0) THEN
      DO 15 IGAS=1,3
        DO 16 I=2,IB+IG-1
          AC(I) = 1.0
          PC(I) = 0.0
          BC = DN(I)*AMAX1( 0.0,( 1.0 - 0.1*ABS(PEN(I)) )**5 )
          BC = BC + AMAX1(0.0,-FN(I))
          IF(I.EQ.IB+IG-1) THEN
           BC = 0.0
          ENDIF
          CC(I) = DS(I)*AMAX1( 0.0,( 1.0 - 0.1*ABS(PES(I)) )**5)
          CC(I) = CC(I) + AMAX1(0.0,FS(I))
          AC(I) =  VOID*SLAB(I)*RHOG(I) +BC +CC(I) +FN(I)-FS(I)
          IF(IGAS.EQ.1) THEN
            AC(I) = AC(I) - SPO2(I)
            DDC = Y8O2(1)
            DC = VOID*SLAB(I)*RHO(I)*Y8O2P(I)
          ENDIF
          IF(IGAS.EQ.2) THEN
            AC(I) = AC(I) - SPCO2(I)
            DDC = Y8CO2(1)
            DC = VOID*SLAB(I)*RHO(I)*Y8CO2P(I) + SCCO2(I)
          ENDIF
          IF(IGAS.EQ.3) THEN
            AC(I) = AC(I) - SPCO(I)
```

```
          DDC = Y8CO(1)
          DC =  VOID*SLAB(I)*RHO(I)*Y8COP(I) + SCCO(I)
        ENDIF
        QC(1) = DDC/AC(1)
        PC(I) = BC/( AC(I) - CC(I)*PC(I-1) )
        QC(I) =(CC(I)*QC(I-1) + DC)/( AC(I) - CC(I)*PC(I-1))
16      CONTINUE
      PC(IB+IG) = 0.0
      QC(IB+IG) = QC(IG+IB-1)/( 1.0-PC(IG+IB-1) )
      CONC(IB+IG) = QC(IB+IG)
*
      DO 17 I=IB+IG-1,2,-1
        CONC(I) = CONC(I+1)*PC(I) + QC(I)
        IF(IGAS.EQ.1) THEN
          Y8O2(IB+IG) = CONC(IB+IG)
          Y8O2(I) = CONC(I)
        ENDIF
        IF(IGAS.EQ.2) THEN
          Y8CO2(IB+IG) = CONC(IB+IG)
          Y8CO2(I) = CONC(I)
        ENDIF
        IF(IGAS.EQ.3) THEN
          Y8CO(IB+IG) = CONC(IB+IG)
          Y8CO(I) = CONC(I)
        ENDIF

17      CONTINUE
15       CONTINUE
         FLUXB = CC(2)
      FLUXA = CC(2) - AMAX1(FS(2),0.0) + AMAX1(-FS(2),0.0)
         FO2 = (FLUXB*Y8O2(1) - FLUXA*Y8O2(2))/DT
         FCO2 = (FLUXB*Y8CO2(1) - FLUXA*Y8CO2(2))/DT
         FC = (FLUXB*Y8CO(1) - FLUXA*Y8CO(2))/DT
         ENDIF
         RETURN
         END


     SUBROUTINE TDMATG(FE,TG,TS,CPG,AKAG,RHO,PAO,H,TGO,RCO,DXN)
     PARAMETER (N=50,M=1000)
     DIMENSION TG(N),TGO(N),TS(N),AKAG(N),H(N),RHOG(N),V(N),VS(N)
     DIMENSION CPG(N),FS(N),CGT(N),PGT(N),QGT(N),RHO(N),RHOS(N)
     DIMENSION G(N),YO2(N),YCO2(N),YCO(N),TP(N)
     DIMENSION Y8O2(N),Y8CO2(N),Y8CO(N),S(N),TESTTG(N),TESTTS(N)
     DIMENSION G1(N),G2(N),X(N),PAO(N),DIAM(N),RCO(N),DXN(N)
     DIMENSION  PA(N),Y8O2P(N),Y8COP(N),Y8CO2P(N),Y8N2P(N),SLAB(N)
         DIMENSION AKS(N),FE(N)
     COMMON/SYST/ VOID,DIAM,E,SLAB,PA,AKS,CARB,ASH,DT,RHOS
     COMMON/INFO/WTN2,WTO2,WTCO2,WTCO,R,P,SIGMA,AMEGA,BETA,GAMMA,THI
```

```
      COMMON/ARRAY/V,VS,G,YO2,YCO2,YCO,Y8O2,Y8CO2,Y8CO,RHOG
      COMMON/TEST/TESTTG,TESTTS,CRIT
      COMMON/TIME/IFLAG,ITIME,ITERNS,IREACT,TURNS,IB,IG
      COMMON/STOIC/ SCO2,SCO,S3,S2,DH1,DH2,DH3,DH4
      COMMON/REACT/ G1,G2,X,S
      COMMON/RAD/ TBN,HR2,HRN,BOLTZ,TCOAL
      COMMON/FLUXES/FO2,FC,FCO2,FTG,FTS
      COMMON/PRIME/ Y8O2P,Y8COP,Y8CO2P,Y8N2P,TP
          AGT = 1.0
          BGT = 0.0
          DGT = TG(1)
          PGT(1) = BGT/AGT
          QGT(1) = DGT/AGT
      DO   10   I=2,IB+IG-1
        TGO(I) = TG(I)
        FN = V(I)*CPG(I)*DT
        FS(I) = V(I-1)*CPG(I-1)*DT
            DN = ( FE(I)*AKAG(I) + (1.0-FE(I))*AKAG(I+1) )*DT/DXN(I)
            DS = ( FE(I-1)*AKAG(I-1) + (1.0-FE(I-1))*AKAG(I) )*DT/DXN(I-1)
        PEN = FN/DN
        PES = FS(I)/DS
        BGT = DN*AMAX1(0.0,( 1.0 - 0.1*ABS(PEN) )**5 )
        BGT = ( BGT + AMAX1(0.0,-FN) )
        IF (I.EQ. IG+IB-1) THEN
         BGT = 0.0
        ENDIF
        CGT(I) = DS*AMAX1( 0.0, ( 1.0 - 0.1*ABS(PES) )**5 )
        CGT(I) = ( CGT(I) + AMAX1(0.0, FS(I)) )
        AGT = VOID*SLAB(I)*RHOG(I)*CPG(I) + BGT + CGT(I)
        AGT = AGT + (FN - FS(I)) + H(I)*PAO(I)*SLAB(I)*DT
        DGT = VOID*SLAB(I)*RHO(I)*CPGBAR(TP(I),I)*TP(I)
        DGT = DGT + H(I)*PAO(I)*TS(I)*SLAB(I)*DT + RCO(I)*DH4
        PGT(I) = BGT/( AGT - CGT(I)*PGT(I-1) )
        QGT(I) = CGT(I)*QGT(I-1) + DGT
        QGT(I) = QGT(I) / ( AGT - CGT(I)*PGT(I-1) )
10        CONTINUE
          CGT(IB+IG)=0.0
          PGT(IG+IB) = 0.0
          QGT(IG+IB) = QGT(IG+IB-1)/(1.0-PGT(IB+IG-1))
          TG(IB+IG) = QGT(IB+IG)
      DO   11  I=IB+IG-1,2,-1
        TG(I) = PGT(I)*TG(I+1) + QGT(I)
        TESTTG(I) = ABS( TG(I)-TGO(I))
11        CONTINUE
          FLUXB = CGT(2)/DT
      FLUXA = CGT(2)/DT - AMAX1(FS(2),0.0)/DT + AMAX1(-FS(2),0.0)/DT
          FTG = FLUXB*TG(1) - FLUXA*TG(2)
          RETURN
          END
```

```
      SUBROUTINE TDMATS(FE,PAO,TB2,TG,TS,H,TSO,AKAS,TSI,DXN)
*
*         calculates the solid temperature profile
*
      PARAMETER (N=50,M=1000)
      DIMENSION H(N),TG(N),TSO(N),AKAS(N),TSI(N),TP(N),RHOG(N)
      DIMENSION Y8O2P(N),Y8COP(N),Y8CO2P(N),Y8N2P(N),PST(N),QST(N)
      DIMENSION TS(N),TESTTS(N),TESTTG(N),V(N),VS(N),G(N),YO2(N)
      DIMENSION YCO2(N),YCO(N),Y8O2(N),Y8CO2(N),Y8CO(N),SLAB(N)
      DIMENSION G1(N),G2(N),X(N),S(N),PA(N),PAO(N),DIAM(N),RHOS(N)
         DIMENSION DXN(N),AKS(N),FE(N)
      COMMON/SYST/ VOID,DIAM,E,SLAB,PA,AKS,CARB,ASH,DT,RHOS
      COMMON/STOIC/ SCO2,SCO,S3,S2,DH1,DH2,DH3,DH4
      COMMON/REACT/ G1,G2,X,S
      COMMON/INFO/WTN2,WTO2,WTCO2,WTCO,R,P,SIGMA,AMEGA,BETA,GAMMA,THI
      COMMON/ARRAY/V,VS,G,YO2,YCO2,YCO,Y8O2,Y8CO2,Y8CO,RHOG
      COMMON/TEST/TESTTG,TESTTS,CRIT
      COMMON/TIME/IFLAG,ITIME,ITERNS,IREACT,TURNS,IB,IG
      COMMON/RAD/ TBN,HR2,HRN,BOLTZ,TCOAL
      COMMON/FLUXES/FO2,FC,FCO2,FTG,FTS
      COMMON/PRIME/ Y8O2P,Y8COP,Y8CO2P,Y8N2P,TP
         IT = IB+IG
         AST = 1.0
         BST = 0.0
         CST = 0.0
         DST = TS(1)
         EST = 0.0
         PST(1) = BST / AST
         QST(1) = DST / AST
      TB2 = (2.0*AKAS(2)/SLAB(2))*TS(2) + HR2*TS(1)
      TB2 = TB2/( 2.0*AKAS(2)/SLAB(2)  + HR2 )
      TBN = (2.0*AKAS(IT-1)/SLAB(IT-1))*TS(IT-1) + HRN*TS(IT)
      TBN = TBN/( 2.0*AKAS(IT-1)/SLAB(IT-1)  + HRN )
         HR2 = BOLTZ*( TS(1)*TS(1) + TB2*TB2 )
         HR2 = HR2*( TS(1) +  TB2 )
         HRN = BOLTZ*( TS(IT)*TS(IT) + TBN*TBN )
         HRN = HRN*( TS(IT) + TBN )
      DO   12 I=2,IT-1
        TSO(I) = TS(I)
        FN = VS(I)*CPS(TS(I+1))*DT
        FS = VS(I-1)*CPS(TS(I))*DT
        IF(I.EQ.2) THEN
          FS = VS(I-1)*CPS(TB2)*DT
        ENDIF
        IF(I.EQ.IT-1) THEN
          T=TCOAL
          FN = VS(I)*CPS(T)*DT
        ENDIF
```

```
          DN = ( (1.0-FE(I))/AKAS(I) + FE(I)/AKAS(I+1) )**(-1)
          DN = DN*DT/DXN(I)
          DS = ( (1.0-FE(I-1))/AKAS(I-1) + FE(I-1)/AKAS(I) )**(-1)
          DS = DS*DT/DXN(I-1)
        PEN = FN/DN
        PES = FS/DS
        BST = DN*AMAX1(0.0,( 1.0-0.1*ABS(PEN) )**5)
        BST = (BST + AMAX1(0.0,-FN))
        IF (I.EQ.IT-1) THEN
          BST = (AKAS(I)*DT)/(SLAB(I)/2.0)
          BST = BST*(1.0/( 1.0 + 2.0*AKAS(I)/(SLAB(I)*HRN)))
        ENDIF
        CST = DS*AMAX1(0.0,( 1.0 - 0.1*ABS(PES) )**5)
        CST = (CST + AMAX1(0.0,FS))
        IF (I.EQ.2) THEN
          CST= (AKAS(I)*DT)/(SLAB(2)/2.0)
          CST = CST*(1.0/( 1.0 + 2.0*AKAS(I)/(SLAB(2)*HR2) ))
        ENDIF
        DENOM= X(I)*12./44. + (1.0-X(I))*12./28.
        SC =  ( DH1*X(I)*12./44. )/DENOM
        SC = SC + ( DH2*(1.0-X(I))*12./28. )/DENOM
        SC=  ( G1(I)*SC )*PAO(I)*SLAB(I)*DT
        DST = (1.0-VOID)*SLAB(I)*RHOS(I)*CPS(TSI(I))*TSI(I)
        DST = DST + H(I)*PAO(I)*( TG(I)- TSO(I) )*SLAB(I)*DT + SC
        AST = (1.0-VOID)*RHOS(I)*SLAB(I)*CPS(TS(I))
        SP = G2(I)*DH3*PAO(I)*SLAB(I)*DT
        IF((I.NE.IT-1).AND.(I.NE.2)) THEN
          AST = AST + BST + CST + FN-FS - SP/TSO(I)
        ENDIF
        IF(I.EQ.IT-1) THEN
          AST = AST + BST + CST - FS -SP/TSO(I)
          DST = DST - FN*TCOAL
        ENDIF
        IF(I.EQ.2) THEN
          AST = AST + BST + CST + FN  -SP/TSO(I)
          DST = DST + FS*TB2
        ENDIF
        PST(I) = BST / ( AST - CST*PST(I-1) )
        QST(I) = CST*QST(I-1) + DST
        QST(I) = QST(I) / ( AST - CST*PST(I-1) )
12      CONTINUE
      DO  13 I=IT-1,2,-1
        TS(I) = PST(I)*TS(I+1) + QST(I)
        TESTTS(I)=ABS(TS(I)-TSO(I))
13    CONTINUE
        RETURN
      END
```

```
      SUBROUTINE PRINT (IO,TSI,CGONE,D,XB,AMWG)
      PARAMETER (N=50,M=1000)
      DIMENSION Y8O2(N),Y8CO2(N),Y8CO(N),YO2(N),YCO(N),RHOG(N)
      DIMENSION YCO2(N),G(N),V(N),VS(N),TESTTG(N),TESTTS(N)
      DIMENSION TSI(N),G1(N),G2(N),X(N),S(N),RHOS(N),DIAM(N),D(N)
      DIMENSION PA(N),Y8O2P(N),Y8COP(N),Y8CO2P(N),Y8N2P(N),TP(N)
      DIMENSION SLAB(N),XB(N),AMWG(N),AKS(N)

      COMMON/INFO/WTN2,WTO2,WTCO2,WTCO,R,P,SIGMA,AMEGA,BETA,GAMMA,THI
      COMMON/FLUXES/FO2,FC,FCO2,FTG,FTS
      COMMON/SYST/ VOID,DIAM,E,SLAB,PA,AKS,CARB,ASH,DT,RHOS
      COMMON/TIME/IFLAG,ITIME,ITERNS,IREACT,TURNS,IB,IG
      COMMON/ARRAY/V,VS,G,YO2,YCO2,YCO,Y8O2,Y8CO2,Y8CO,RHOG
      COMMON/TEST/TESTTG,TESTTS,CRIT
      COMMON/RAD/ TBN,HR2,HRN,BOLTZ,TCOAL
      COMMON/REACT/ G1,G2,X,S
      COMMON/PRIME/ Y8O2P,Y8COP,Y8CO2P,Y8N2P,TP
      WRITE(IO,130)
      DO 18  J=1,IB+IG
        XB(J) = XB(J) - 0.5*SLAB(J)
        IF(IFLAG.EQ.4) THEN
          Y8O2P(J)=Y8O2P(J)*AMWG(J)/WTO2
          Y8CO2P(J)=Y8CO2(J)*AMWG(J)/WTCO2
          Y8COP(J)=Y8CO(J)*AMWG(J)/WTCO
        ENDIF
        WRITE(IO,135) XB(J),Y8O2P(J),Y8CO2P(J),Y8COP(J),
     +    V(J),VS(J),G(J),TP(J),TSI(J),TURNS,
     +    CPGBAR(TP(J),J),CPS(TSI(J)),D(J)
18    CONTINUE
*         WRITE(IO,*) CGONE
130       FORMAT(/,2X,'X',5X,'O2',5X,'CO2',5X,'CO',5X,'V',9X,'VS',7X,
     +    'G',9X,'TG',7X,'TS',5X,'ITNS',5X,
     +       'CPG',6X,'CPS',7X,'DIAM',/)
135   FORMAT(1F7.5,1X,1F6.5,1X,1F6.5,1X,1F6.5,1X,1F8.5,1X,1F8.5,1X,
     +    1F8.5,1X,2F9.2,1X,1F5.1,1X,F9.3,1X,F9.3,1X,
     +       F10.7)
      RETURN
      END

      SUBROUTINE ENERGY(TB2,CPG,TG,TS,ERROR)
      PARAMETER (N=50,M=1000)
      DIMENSION V(N),VS(N),G(N),YO2(N),YCO2(N),YCO(N),CPG(N)
      DIMENSION Y8O2(N),Y8CO(N),Y8CO2(N),RHOG(N),TG(N),TS(N)
      COMMON/TIME/IFLAG,ITIME,ITERNS,IREACT,TURNS,IB,IG
      COMMON/ARRAY/V,VS,G,YO2,YCO2,YCO,Y8O2,Y8CO2,Y8CO,RHOG
      COMMON/RAD/ TBN,HR2,HRN,BOLTZ,TCOAL
      COMMON/FLUXES/FO2,FC,FCO2,FTG,FTS
          IT = IB+IG
          T = TCOAL
          ENIN = FTG + BOLTZ*(TS(1)**4 - TB2**4)
```

```
      IF(VS(1).LT.0.0) THEN
     ENIN = ENIN + VS(1)*TB2*CPS(TB2)
      ENDIF
      ENOUT = V(IT)*CPG(IT)*TG(IT) + BOLTZ*(TBN**4 - TS(IT)**4)
      ENOUT = ENOUT + VS(IT)*TCOAL*CPS(T)
      ENB = ENOUT - ENIN
      ENR = (V(IT)*Y8CO(IT) - FC)*9.3E06*12./28.
      ENR = ENR + (V(IT)*Y8CO2(IT) - FCO2)*32.8E06*12./44.
    ERROR = 100.*(ENB - ENR)/AMIN1(ENB,ENR)
      RETURN
      END


    SUBROUTINE STOCK(TG,TS,TSI,RHO,PAO,
   + CGONE,TSO,TGO,D,DTEMP)
    PARAMETER (N=50,M=1000)
    DIMENSION V(N),VS(N),G(N),YO2(N),YCO2(N),YCO(N),YN2(N)
    DIMENSION TG(N),TGO(N),TS(N),TSO(N),G1(N),G2(N),RHOG(N)
    DIMENSION S(N),X(N),Y8O2(N),Y8CO(N),Y8CO2(N),Y8N2(N)
    DIMENSION Y8O2P(N),Y8CO2P(N),Y8COP(N),Y8N2P(N),TP(N),TSI(N)
    DIMENSION RHO(N),D(N),RHOS(N),DIAM(N),PA(N),PAO(N)
    DIMENSION TESTTS(N),TESTTG(N),SLAB(N),CPGREG(N),AKS(N)
    COMMON/REACT/ G1,G2,X,S
    COMMON/TIME/IFLAG,ITIME,ITERNS,IREACT,TURNS,IB,IG
    COMMON/INFO/WTN2,WTO2,WTCO2,WTCO,R,P,SIGMA,AMEGA,BETA,GAMMA,THI
    COMMON/ARRAY/V,VS,G,YO2,YCO2,YCO,Y8O2,Y8CO2,Y8CO,RHOG
    COMMON/EXTRA/Y8N2,YN2,CPEFF,CPGREG
    COMMON/TEST/TESTTG,TESTTS,CRIT
    COMMON/RAD/ TBN,HR2,HRN,BOLTZ,TCOAL
    COMMON/GE/ A,A1,ER,ER1,ALPHA1,ALPHA2,ALPHA3
    COMMON/SYST/ VOID,DIAM,E,SLAB,PA,AKS,CARB,ASH,DT,RHOS
    COMMON/PRIME/ Y8O2P,Y8COP,Y8CO2P,Y8N2P,TP
    IFLAG=3
    DO  22    I=2,IG+IB-1
      CRIT=AMAX1(TESTTS(I),TESTTG(I) )
      IF(CRIT.GT.0.1) THEN
        IFLAG=2
      ENDIF
22      CONTINUE

        IF((IFLAG .EQ.3).OR.(IFLAG.EQ.4)) THEN
      TURNS=ITERNS
      DTEMP = 0.0
      DO   23  I=1,IG+IB
        ANODE = FLOAT(I)
        PAO(I) = PA(I)
        DTEMP = DTEMP + ABS(TG(I)-TP(I))
        TP(I)=TG(I)
        Y8O2P(I)=Y8O2(I)
        Y8CO2P(I)=Y8CO2(I)
```

```
        Y8COP(I)=Y8CO(I)
        RHO(I) = RHOG(I)
        D(I) = DIAM(I)
        CGONE = CGONE+G(I)*SLAB(I)*PA(I)
23      CONTINUE
      DO  24  I=2,IG+IB-1
        TSI(I)=TS(I)
24      CONTINUE
        ELSE
      DO 25 I=2,IG+IB-1
        TG(I) = ALPHA1*TG(I)+(1.0-ALPHA1)*TGO(I)
        TS(I)=ALPHA2*TS(I)+(1.0-ALPHA2)*TSO(I)
25      CONTINUE
      IFLAG=2
        ENDIF
    DO 29 I=2,IG+IB
*
*       UPDATE DENSITY
*
      RHOG(I)=DENS(TG(I),I)
29    CONTINUE
    RETURN
        END

    REAL FUNCTION DENS(T,I)
    PARAMETER (N=50,M=1000)
    DIMENSION V(N),VS(N),G(N),YO2(N),YCO2(N),YCO(N),Y8O2(N)
    DIMENSION Y8CO2(N),Y8CO(N),RHOG(N),YN2(N),Y8N2(N),CPGREG(N)
    COMMON/INFO/WTN2,WTO2,WTCO2,WTCO,R,P,SIGMA,AMEGA,BETA,GAMMA,THI
    COMMON/ARRAY/V,VS,G,YO2,YCO2,YCO,Y8O2,Y8CO2,Y8CO,RHOG
    COMMON/EXTRA/Y8N2,YN2,CPEFF,CPGREG
        Y8N2(I) = 1.0 - Y8CO(I) - Y8O2(I) - Y8CO2(I)
        STORE = (Y8O2(I)/WTO2) + (Y8CO(I)/WTCO) + (Y8CO2(I)/WTCO2)
        STORE = 1.0/( STORE + (Y8N2(I)/WTN2) )
        DENS = P*STORE/(R*T)
        RETURN
        END

        REAL FUNCTION CPS(T)
*
*       CALCULATES SOLID HEAT CAP.
*
    PARAMETER (N=50,M=1000)
    COMMON/INFO/WTN2,WTO2,WTCO2,WTCO,R,P,SIGMA,AMEGA,BETA,GAMMA,THI
    COMMON/RAD/ TBN,HR2,HRN,BOLTZ,TCOAL
    COMMON/SYST/VOID,DIAM,E,SLAB,PA,AKS,CARB,ASH,DT,RHOS
    DIMENSION DIAM(N),SLAB(N),PA(N),AKS(N),RHOS(N)
    A = 1/12.0
        X1 = 380.0/T
        X1 = 1.0/(EXP(X1)-1.0)
```

```
      X2 = 1800.0/T
      X2 =  1.0/(EXP(X2)-1.0)
      CPS = (1000.0/T)*(R*A)*(380*X1 + 3600.*X2 )
CPS = CARB*CPS + ASH*(754. + .293*T )
RETURN
END


REAL FUNCTION CPGBAR(T,I)
PARAMETER (N=50,M=1000)
DIMENSION V(N),VS(N),G(N),YO2(N),YCO2(N),YCO(N),Y8O2(N)
DIMENSION Y8CO(N),RHOG(N),Y8N2(N),YN2(N),Y8O2P(N),Y8CO2P(N)
DIMENSION  Y8COP(N),Y8N2P(N),TP(N),CPGREG(N),Y8CO2(N)
      DIMENSION X(N),S(N),G1(N),G2(N)
      COMMON/INFO/WTN2,WTO2,WTCO2,WTCO,R,P,SIGMA,AMEGA,BETA,GAMMA,THI
COMMON/CP/AO2,BO2,DO2,ACO,BCO,DCO,ACO2,BCO2,DCO2,AN2,BN2,DN2
COMMON/ARRAY/V,VS,G,YO2,YCO2,YCO,Y8O2,Y8CO2,Y8CO,RHOG
COMMON/EXTRA/Y8N2,YN2,CPEFF,CPGREG
COMMON/PRIME/ Y8O2P,Y8COP,Y8CO2P,Y8N2P,TP
      COMMON/REACT/ G1,G2,X,S
      COMMON/STOIC/ SCO2,SCO,S3,S2,DH1,DH2,DH3,DH4
      Y8N2(I) = 1.0-Y8O2(I)-Y8CO(I)-Y8CO2(I)
      CPO2B = AO2 + BO2*T/2.0 - DO2*(T**(-2))
      CPO2B = (R/WTO2)*CPO2B
      CPCOB = ACO + BCO*T/2.0 - DCO*( T**(-2) )
      CPCOB = (R/WTCO)*CPCOB
      CPCO2B = ACO2 + BCO2*T/2.0 - DCO2*( T**(-2) )
      CPCO2B = (R/WTCO2)*CPCO2B
      CPN2B = AN2 + BN2*T/2.0 - DN2*( T**(-2) )
      CPN2B = (R/WTN2)*CPN2B

      CPO2 = AO2 + BO2*T + DO2*(T**(-2))
      CPO2 = (R/WTO2)*CPO2
      CPCO = ACO + BCO*T + DCO*( T**(-2) )
      CPCO = (R/WTCO)*CPCO
      CPCO2 = ACO2 + BCO2*T + DCO2*( T**(-2) )
      CPCO2 = (R/WTCO2)*CPCO2
      CPN2 = AN2 + BN2*T + DN2*( T**(-2) )
      CPN2 = (R/WTN2)*CPN2
      CPEFF = (1.0 + S(I) )*CPCO - S(I)*CPO2
      CPGBAR = Y8O2(I)*CPO2B + Y8CO2(I)*CPCO2B
      CPGBAR = CPGBAR + Y8N2(I)*CPN2B + Y8CO(I)*CPCOB
      CPGREG(I) = Y8O2(I)*CPO2 + Y8CO2(I)*CPCO2
      CPGREG(I) = CPGREG(I) + Y8N2(I)*CPN2 + Y8CO(I)*CPCO
      RETURN
      END
```

PROGRAM DATAFILE #1

BOLTZ	TCOAL	VOID	E	RHOS(N)	A	ER
5.67E-08	300.	0.33	0.8	1500.0	860.	18000.

WTN2	WTO2	WTCO2	WTCO	R	P(PA)	SIGMA	AMEGA	BETA	GAMMA	THI
.028	.032	.044	.028	8.314	101325.	3.681	0.799	1.0	1.0	.050

AO2	BO2	DO2	ACO	BCO	DCO	ACO2
3.639	5.06e-04	-2.27e04	3.376	5.57e-04	-3.1e03	5.457

BCO2	DCO2	AN2	BN2	DN2
1.045E-03	-1.157E05	3.2800	5.93E-04	-4.0E03

US(1)	G(1)	TS(1)	Y8O2(1)	Y8CO(1)	Y8CO2(1)
-.0011	0.0	350.	.232	.001	.003

G(N)	TG(N)	TS(N)	TS(N-1)	Y8O2(N)	Y8CO(N)	Y8CO2(N)
0.0	350.	350.	1500.	.232	.001	.003

SCO	SCO2	S3	S2	IREACT	DH1	DH2	DH3	DH4
1.3333	2.66667	0.571	3.667	3	32.8E06	9.3E06	-14.2E06	10.1E06

LIMIT	IEND	ALPHA1	ALPHA2
2001	1000	0.5	0.5

PROGRAM DATAFILE #2

IB	IG	GRATE(MM)	HT(CM-ACTIVE)	CARB	ASH	DT
30	7	20.00	60.96	.90	.10	5.

DIAM(N)	U(1)	TG(1)	A1	ER1	HTTR	RXN
0.03258	0.177	300.	3500.	21373.	1960	1970